An Interferometer for Atoms

by

David William Keith

B.Sc Physics, University of Toronto (Nov, 1986)

Submitted to the Department of Physics in
partial fulfillment of the requirements
for the degree of

Doctor of Philosophy

at the

MASSACHUSETTS INSTITUTE OF TECHNOLOGY

May, 1991

Signature of the Author
_____
Department of Physics
May , 1991

Certified by
_____
David E. Pritchard
Professor of Physics
Thesis Supervisor

Accepted by
_____
George F. Koster, Chairman,
Department Committee on Graduate Studies

An Interferometer for Atoms

by

David William Keith

Submitted to the Department of Physics in
partial fulfillment of the requirements
for the degree of Doctor of Philosophy

Abstract

We have demonstrated an interferometer for atoms. A three grating geometry is used, resulting in an interferometer of the "amplitude division " type. We used a highly collimated beam of sodium atoms with a de Broglie wavelength of 16 pm and high-quality 0.4 μm-period free-standing gratings. The interference signal is 70 Hz, which allows us to determine the phase to 0.1 rad in 1 min. This is the first atom interferometer in the sense that it simultaneously and distinctly separates the atoms in position and momentum.

In order to make the gratings for our interferometer, we have developed a novel method for fabricating free-standing micro-structures. Using this method we have made high-quality 0.2 and 0.4-μm period gratings, as well as the first zone plate lenses to be used for atoms. We have previously reported the first observation of the diffraction of atoms from a fabricated periodic structure.

We have developed a numerical procedure for modeling the behavior of our interferometer. The method allows us to compute the interference pattern formed by a system of perforated screens in O(Nlog(N)) time where N is the transverse resolution.

In addition, we have proposed a novel interferometer for atoms using diffraction gratings which work by grazing incidence reflection. We also suggest the possibility of doing two particle correlation experiments with atoms.

We discuss the possibility for measuring the phase shift due to the gravitational field acting on our interferometer.

Thesis: Supervisor: Dr. David E. Pritchard
Title: Professor of Physics

Table of Contents

0 Introduction

"the—well-planned—building of pigeon holes must proceed faster
than the recording of facts to be housed in them"
(Lakatos 1970)

Quantum mechanics was initially constructed to apply to the internal degrees of freedom of atomic systems. De Broglie (1924) began applying quantum mechanics (in the form of "phase waves") to the external degrees of freedom of photons and electrons. This generalization raised the problem of measurement: when are the dynamics of a particle governed by the phase wave? The easy answer is, of course, when you do not measure its position. But this answer does not consistently resolve the question of what constitutes a measurement.

De Broglie's ideas have been gradually extended so that it is now generally believed that quantum mechanics can be correctly applied to all systems. However, I think the question of measurement is still with us. For example; it is not clear whether or not there is a limit to the size of objects that may be put into superposed states that have experimental consequences.

This thesis describes a collection of experiments demonstrating the interference of sodium atoms. In the context of the remarks made above, these experiments are tests of the quantum mechanical laws of motion applied to larger systems. Alternatively, the experiments may be viewed as an application of 1990's technology to make clear demonstrations of physics that was well understood in the 1930's.

The central result of my graduate work is the demonstration of an interferometer for atoms. However, this thesis is organized so as to present “atom optics” as if it was a distinct field, with the interferometer and various other work presented as examples. This somewhat artificial construction is intended to make two points: that atom optics *is* becoming a distinct subject, and that it should be seen as a collection of useful tricks to be applied to interesting problems rather than as an end in itself.

The description of the core experimental work is distributed throughout the thesis. The atom beam system is described in chapter 1.C, the grating fabrication in 1.D.ii, and the interferometer design in 3.B.ii. The data from the interferometer are presented in chapter 3B.iii. My discussion of the context and theory associated with the

experimental work is contained in chapter 2 and in the beginning of chapter 3. The details of the numeric modeling of the experiment are described in chapter 2.B. The papers included in the appendices contain significant information that is not discussed in the thesis body. I will now outline the thesis in more detail in order to assist the reader in locating material that may be useful.

I begin Chapter 1 with a summary of various existing particle beam sources—the context for atom optics. I then turn to the details of our atomic beam system, the most idiosyncratic part of the experiment. The chapter closes with the detailed recipe for making our transmission gratings.

Chapter 2 opens with some unfocused generalities regarding the difficulties of applying standard quantum mechanics to the the problems of atom optics. In the second section I cover the details of the numeric models we have constructed of our experiment.

Chapter 3 contains the details of the interferometer experiment. It starts with a brief outline of the historical context of atom interferometers. It then turns to a categorization of the applications of atom interferometers. Finally, the experimental design and data are covered in part B of the chapter.

Chapter 4 consists of an example of how our atom interferometer might be applied to making a simple measurement. I briefly examine how we could perform a simple equivalence principal test with our apparatus—the atom conterpart of the COW experiment.

Chapter 5 concludes the thesis by examining the status of this work as science.

1 Atom Optics: Beams and Gratings

1.A What is atom optics?

By atom optics we mean the expanding collection of techniques by which atoms may be manipulated in the manner of light in classical optics. Existing atom optical elements include mirrors, lenses, and diffraction gratings as well as dissipative elements such as slowers, 'coolers', and traps which have no analogue in classical optics. To date, these atom optical elements have mainly been realized as demonstrations of principal, we hope that we will soon see some of them used as tools in real experiments. My thesis work has centered around developing such demonstrations of atom optics: transmission gratings, reflection gratings (yet unrealized), zone-plate lenses, and an interferometer. In this chapter I will set specific discussion of our beam and gratings into the more general context of atom optics.

1.B Beams: Atoms and other particles

For a matter-wave optician, an ideal beam system has simple characteristics: a source with arbitrary brightness emitting particles of given mass and velocity distribution, which are detected by an infinitely-fast noiseless detector. The internal quantum state of each particle is relevant to experiments, but is conveniently ignored in this discussion. A key issue is the specification of the quantum state of the particles' external degrees of freedom. This is the question of whether the phase space density of a thermal-source particle beam fully determines its quantum state.

Beam	B cm^{-2} sec^{-1}	v m sec^{-1}	s $s=v/\Delta v$	m AMU	quantum density	det response sec	Reference
n	10^{14}	2.7×10^{5}	1	1	1.2×10^{-15}	10^{-6}	Shull, 1988
e	6×10^{20}	4×10^{9}	10^{3} (?)	5×10^{-4}	1.2×10^{-12}	10^{-9}	Standard text[1]
e	6×10^{26}	1.3×10^{10}	3×10^{5} (??)	5×10^{-4}	3.2×10^{-6}	10^{-9}	Field emmison[2]
He	10^{22}	10^{5}	200	4	2×10^{-5}	flux mode	Toenneies[3]
He^{*}	2×10^{15}	1.7×10^{5}	15	4	3.6×10^{-14}	10^{-8}	Faulstich, 1990
Na + ν	5×10^{15}	4.7×10^{-2}	100 (?)	23	5×10^{-5}	flux mode	Nellessen[4], 1990
Na	10^{19}	10^{5}	10	23	5.3×10^{-12}	10^{-2}	Our beam
ν	4×10^{26}	c	$5\ 10^{8}$	n.a.	5×10^{11}	10^{-9}	n.a.[5]

Quantity	Symbol	Notes
Source brightness	B	Detected brightness: str^{-1} cm^{-2} sec^{-1}
Mean velocity	v	m sec^{-1}.
Speed ratio	s	Just the inverse relative velocity width, $v/\Delta v$. Used extensively in the supersonic beam literature.
Mass	m	In AMU.
Quantum density		Also Known as the occupancy ratio.
Detector time response	τ	In particle counting mode.

Table 1. Properties of various low energy particle beams compared. By Na + ν I mean laser cooled Na, He^{*} is metastable He. For calculating wavelengths I find it most convenient to remember h=0.4 AMU μm^2 sec^{-1}.

[1] For an ideal Pierce diode at 10 keV; I used "Building scientific apparatus" by Moore (1983), p303 (an exceptionally useful book).

[2] This information is suspect, it is from Silverman (1987) who references a Tonomura paper that does not contain all the relevant facts. I suspect it may be inflated by as much as 10^3 in spectral brightness.

[3] There are many similar references, this is now standard beam technology.

[4] This is the Ertmer group, I assume that the transverse and longitudinal velocity widths are 0.5 m sec^{-1}, although this is not clearly stated in the paper. They used florescent detection but could use a hot wire detector like ours.

[5] This example is for a standard frequency stabilized dye laser (Coherent 699).

This is a non-trivial issue, which will be treated in the theory section below. For now, I will assume that the external quantum state is fully determined by the velocity distribution. In the table below I compare various existing particle beam systems on the basis of these characteristics.

A most important quantity is the spectral brightness which is

$$Bs = \sigma\left(\frac{p}{\Delta p}\right)^3 \tag{1.1}$$

where σ is the flux, and p is the momentum. From this we can calculate the phase space density

$$\rho_\Omega = \frac{Bs}{m^3 v^4} \tag{1.2}$$

which is important because, by Louville's theorem, it is a constant (along a particle's trajectory) for conservative systems. The phase space density is proportional to the quantum density or occupancy ratio: quantum density=$h^3 \rho_\Omega$, where h is Planck's quantum of action. The quantum density determines the extent to which quantum statistics are important.

1.C Our beam

The supersonic sodium beam source used in this research was constructed over a period of six years by at least four successive Phd students. It was last described in full by Gould in '86, and since then it has been treated only Incrementally in the theses of successive students. Because I have rebuilt and redesigned all of its major components, I think it is useful to attempt a complete description. In doing so I must make a few disclaimers. I know little of the physics of supersonic flows, or of the ionization of alkalis on metal surfaces. Although knowledge of these disciplines is necessary for a full understanding this device, they are sufficiently complex to make a virtue of an empirical approach.

I will start with a condensed description of the complete beam apparatus, followed by a detailed description moving from source to detector. Our atomic beam is a supersonic nozzle-beam of sodium in an argon carrier gas. Adiabatic expansion of the gas after it leaves the nozzle results in a fairly monochromatic beam: $\Delta v/v = 12\%$ with v

= 10^3 m/s. The sodium has the same velocity as the carrier gas, giving it a de Broglie wavelength of 16 pm. The beam is collimated by two 20 μm slits spaced 0.9 m apart to form a 1 mm × 20 μm ribbon-shaped beam with a divergence of 20 μrad. Individual sodium atoms are detected after surface ionization on a 25 μm-diameter hot wire (80% Pt, 20% Ir alloy) located 1.6 m downstream from the second slit. In order to achieve high ionization efficiency it is necessary to expose the wire to Oxygen at regular intervals: 10^{-3} torr O_2 for ~1 min every ~30 min usually proves to be sufficient. Under these conditions the detector's time response is ~15 msec and the average background is ~20 Hz. A key problem is that the background signal is dominated by highly non-Poissonian bursts (see example in Fig. 3.9). Although we cannot directly measure the ionization efficiency of the wire we believe that it is better than 10%. In any case, greater wire efficiency, combined with improvements to our vacuum system, and the sodium source, now allow us to achieve detected fluxes of >1 MHz through a 1 mm high slit. This corresponds to a detected source brightness of 10^{19} sec^{-1} cm^{-2} str^{-1}.

Supersonic-expansion molecular beams are treated in a number of comprehensive works, especially useful and comprehensive are Habetts (1977) and Comparge (1974), a useful short summary of seeded alkali beams is found in Serri (1974), . The basic physics of the gas expansion is clear. The flow through the nozzle is at high renolds number (>10^4) so that we can ignore the work done against viscosity, and calculate the final velocity using energy conservation in the form of Bernoulli's theorem. After leaving the nozzle a packet of gas continues to expand adiabatically, doing work on the surrounding packets, and thus decreasing local temperature while increasing the mean velocity. This expansion continues until the gas ceases to expand adiabatically because the mean free path gets longer than the length scale of the temperature change — that is until a particle experiences its last collision. As the gas expands the local sound velocity decreases with the root of the temperature so that the flow becomes hypersonic.

There are two distinctly different approaches to the placement of the skimmer. It can either be before or after the region in the undisturbed vacuum expansion of the beam in which the atoms undergo there last collision. In the "Comparge" type source that we use, the atoms last collision occurs after the skimmer orifice. The expanding gas forms a stationary shock front where it interacts with the background gas in the chamber (~10 μtorr). In theory the hypersonic flow ensures that the gas inside the shock front expands

as it would into vacuum. By placing the skimmer inside this shock front we are able to extract a small on axis portion (~1%)[6] of the mass flux, allowing the rest to be pumped away by high throughput pumps. A Comparge source uses the shock front to allow a higher source chamber pressure, and thus a less expensive pumping system, at the expense of more tricky optimization during operation.

Our source (Fig 2.1) consists of the pressurized sodium oven, and the beam extraction skimmer enclosed in a chamber evacuated with a high throughput vacuum pump (a stokes ring jet booster pump). It is important to consider the oven and beam extraction system as a unit, because their performance cannot be meaningfully measured in isolation. The oven is a small heated container containing a few grams of sodium pressurized with ~2 bar of Argon, see figure 1.1. Operating temperatures at the nozzle range from 590 to 730°C, the reservoir is kept about 30 to 60°C cooler. The nozzle is 70 μm in diameter, and is located ~1 cm from the skimmer.

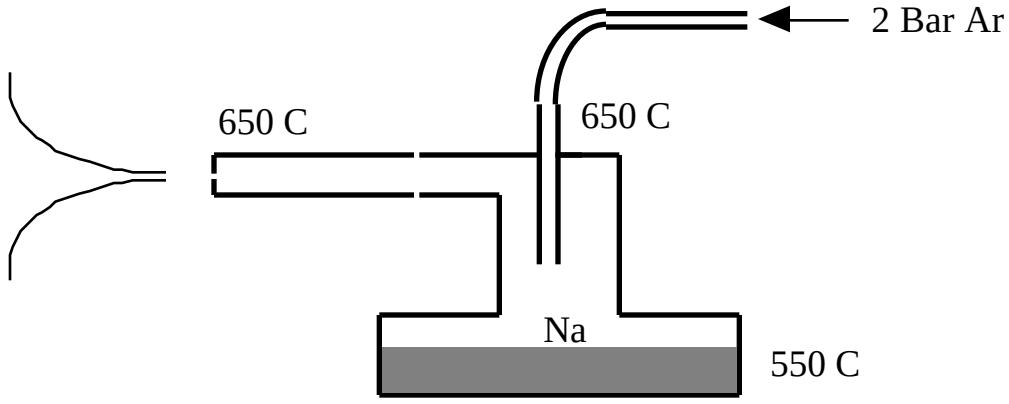

Figure 2.1. A schematic of our atom beam source.

On their flight from source to detector the atoms pass through a 30 cm-long differential pumping region, and a 1.7 m-long main chamber. The atom flux is monitored with a hot Iridium ribbon (current from surface ionization is measured) at the exit from the differential chamber. There are several mysteries associated with understanding the measured fluxes. The first concerns the flux from the oven; it is ~10 times less than we predict using the vapor pressure for Na and the measured fluxes. The second is the attenuation of the beam in the main chamber. At a pressure of ~10^{-6}

[6] Measured by us, using ion gauges to and assumed pumping speeds, we get a ratio of 0.003.

torr the mean free path of sodium in the main chamber should be ~10 m if we use the total quantum mechanical cross section of 500 A^2. There should be no significant absorption, but we have evidence gathered by varying the pressure with a leak (when the vacuum system was working very well), that indicates the absorption may be as large as a factor of ten. Presumably, the discrepancy is because the atoms are lost from the beam if they are scattered by more than ~3×10^{-5} rad.

The sodium atoms are detected by ionization on a high work-function metal surface, the ions are then counted using a channel electron multiplier (CEM). The surface ionization process requires that the work function of the metal be larger than the ionization potential of the atom. Surface ionization occurs when an electron bound to an atom in contact with the surface may tunnel through the potential barrier to attain a lower energy state in the metal leaving the free ion. In practice, both the efficiency of ionization, and the mean residence time before ionization occurs depends on the wire's temperature and surface chemistry. The residence times are surprisingly long, for our Pt/Ir alloy at 700 °C typical[7] residence times are 3-100 msec, and efficiencies are between unity and 1%. We assume that the long residence times (as compared with the quantum tunneling time) is due to non uniformity of the surface work function, the atom diffuses over the surface until it arrives at a region of high work function.

In general the efficiency, background rate, and detection speed increase with the temperature, the rate of increase rises dramatically at 600-800 °C. However, we often see a small region in which the efficiency and background *decrease* with temperature at 700 °C, this is our ideal operating point. We have been able to achieve a ~10 fold increase in sensitivity by periodically oxygenating the hot wire. I believe that the oxygen acts by burning off carbon deposits formed by hydrocarbon contamination of the vacuum system. This hypotheses is supported by the fact that the effect of oxygenation persists longer when the vacuum is cyropumped with a small LN_2 trap. At best we are able to achieve efficiencies of over 10%, and time responses of ~5 msec with background rates of ~50 Hz. Hot wire ionization is extremely selective for weekly bound alkalis with respect to the constituents of the background molecular gas (H_2O, N_2,

---

[7] We have determined the temperature from the measured (I^2R) power dissipated. In order to do this accurately we made a simple numerical model of the temperature profile in the wire which is necessary because conduction to the ends is important.

etc). At the operating pressure of our detector chamber (~10^{-7} torr) the flux of background gas is as much as 10^9 times that of the detected sodium.

As compared to other available methods, detection by surface ionization has two wonderful properties: it is both efficient and highly selective. Other detection methods commonly considered are, florescence detection, and electron bombardment ionization followed by mass spectrometry. Both of these methods are difficult to implement because of the low fluxes involved, typically 10^5 to 10^7 cm^{-2} sec^{-1}. Florescence detection is extremely selective (even isotopically) but it entails considerable technical difficulties, it requires a dedicated frequency-stabilized laser system, and makes extreme demands on the efficiency of the scattered light rejection system. Impact ionization has poor efficiency due to limitations on the electron fluxes available, and mass spectrometry is insufficiently selective (at rejecting background gas ions).

A detection method that would be extremely selective, efficient, and fast is optical pumping to a rydberg state followed by field ionization. This method does require a complex laser system, but it should afford near unity efficiency (>90 %), near zero background rate (~0.2 Hz), and time response in the order of 10^{-7} seconds. In short — a nearly perfect detection system. With the advent of inexpensive diode laser systems, such a detector may become easily realizable for many atomic species.

1.D Gratings for atoms

1.D.i Gratings as beam splitters.

Diffraction gratings for atoms a interesting chiefly for their application as coherent beam splitters. This is true despite the disadvantages of gratings, and is a consequence of the difficulty of realizing any non dispersive alternatives. Solid beam splitters, such as are available for neutrons and photons, are impossible for atoms; this is due to the large potential energy of atoms in solids which makes the tunnelling depth of a free atom with thermal energy is much less than atomic dimensions. Atoms may be partially reflected from spatial discontinuities in their potential energy. In principal, static or near resonant electromagnetic fields could be used to make a beam splitter of this type. This is difficult because for efficient reflection the potential energies must be of order the atoms kinetic

energy, and the potentials must change over length scales not much larger that the atom's de Broglie wavelength. Three types of diffraction gratings for atoms have been realized: reflection from the atomic planes of a crystal surface, transmission through the periodic potential formed by a standing wave of near resonant light, and transmission through a free-standing periodic structure. I will discuss these examples in some detail, with reference to their possible application to atom interferometry. I will then argue that a forth type of diffraction grating is both feasible and useful.

Although it was not recognized as such, the first atomic beam splitter was demonstrated in 1929; it was the diffraction of atoms by reflection from the surface of an ionic crystal. Esterman and Stern (1930) observed diffraction of He from the cleaved face of a LiF crystal. This technique has since been refined through its extensive application to the study of the phonon structure of crystal surfaces. Constructing an interferometer from these crystal surface beam technique would be exceptionally challenging. This is because the interatomic spacing in a crystal surface is of the same order as the de Broglie wavelength of thermal atomic beams, and so the angular separation of the diffracted beams is of order unity (i.e., ~rad). The near normal incidence of the beam on the crystals of such an interferometer would require relative flatness, rigidity, and overall alignment of separate surfaces to tolerances smaller than atomic dimensions.

In 1983 our group (Gould et al, 83) demonstrated the atomic version of the Kapitza-Dirac effect, in which atoms are diffracted from a standing wave of near resonant light. The grating period in the standing wave is 1/2 the optical wavelength, thus the angular separation of the diffracted orders is $\lambda_{db}/\lambda_{light}$ which is ~60 μrad for a thermal sodium beam. This effect has subsequently been demonstrated using a beam of metastable Helium. In addition, a novel laser cooling technique which has the property of trapping atoms in a superposition of two momentum states differing by two units of photon momentum has been demonstrated. Interferometers based on this technique have been proposed, and will be discussed in detail in part two, but have not yet been realized. This method is limited to atoms that have accessible laser transitions (frequently requiring optical state preparation of the atoms), which are not the atomic species most suitable for the production of intense atomic beams (e.g. He).

In 1988 we demonstrated the diffraction of atoms by transmission through a fabricated periodic structure. The work is described in detail in Keith, 88 which is appendix 1 of this thesis. The

methods of fabricating such grating are described below. The advantage of these gratings is that they are work for any atom (or molecule), and that there is a practical possibility of reducing their period below 0.1 μm. Compared to the light gratings discussed above, the chief disadvantage of these gratings is that they are amplitude gratings, and so must necessarily absorb about half of the incident beam.

If atoms could be reflected from the surface of a conventional diffraction grating, a useful new class of atom beam splitters would result. This is because reflection gratings can be used at grazing incidence which makes the period appear foreshortened; resulting in large angular separation of the diffracted beams. Such a fabricated reflection grating would fill the gap between the 0.1 nm-period of crystal surfaces, and the 100 nm-period fabricated transmission gratings. This might prove ideal for a next generation of atom interferometers. However, such gratings depend on the specular reflection of atoms from smooth surfaces.

Atoms may be specularly reflected from surfaces when the de Broglie wavelength corresponding to their momentum perpendicular to the surface is much larger than the scale of surface roughness. For a smooth surface, the reflectivity is determined by the one dimensional atom wall potential. Theoretical predictions of reflectivity are difficult, but they indicate that reflection should only occur at transverse temperatures in the sub μK range. Despite this, Anderson, etal (1986) demonstrated efficient specular reflection of a thermal Cesium incident at angles of up to 40 mrad on a quartz surface. In this experiment the perpendicular temperature was a few mK, far larger than the theoretical predictions. Given this contradiction, it seems prudent to temporarily disregard theoretical questions, and attempt to gather more experimental data. Square profile quartz diffraction gratings are commercially available with rms roughness as small as 20 Å.

1.D.ii Fabrication of transmission gratings.

The gratings used in our '88 demonstration of the diffraction of atoms, were made by the sub-micron structures laboratory (SμSL) at MIT. They were large area (~1 cm^2) 0.2 μm-period gold gratings, which had been developed for use with soft x-rays. The grating fabrication method is described in brief in our '88 paper (appendix 1), related fabrication processes are detailed in papers published by our collaborators at the SμSL (Ceglio, Price et al. 1981; Schattenburg, Anderson et al. 1990). We originally intended to make the first

interferometer with these gratings, but unfortunately this proved to be impossible. Instead, we were forced to develop out own grating fabrication technology at the National Nanofabrication Facility (NNF) at Cornell.

The quality of gratings necessary for an interferometer is considerably higher than is needed to demonstrate diffraction of atoms. In particular, the gratings must be phase-coherent over their entire area. This implies that the grating lines must be straight to the order of their line width over the full height of the grating, and that the grating period be constant to the order of the grating period over the width of the grating. The transmission of the grating support structure (necessary to achieve the required line straightness) should be high since the final interference signal will be proportional to the third power of this transmission. In addition, the grating line to space ratio must be near 1:1, ideally the grating spaces should be 0.65 period for the first grating and 0.5 for the other two. The SμSL gratings were unusable because the grating lines were not sufficiently straight, and the grating transmission was too small.

The grating fabrication process which we developed at NNF will be described in three steps. First, tensile membrane windows of silicon nitride are formed in a silicon wafer. The windows are then coated with a plastic resist, which is exposed with the grating pattern using electron beam lithography. Finally, the pattern is transferred from the resist to the nitride by reactive ion etching (RIE). The chief difficulties are with distortions in the e-beam writing system, and the insufficient selectivity of the RIE process. Our process is similar to that developed by Lee (1984), who fabricated free-standing nitride wires using a direct write e-beam with a positive resist.

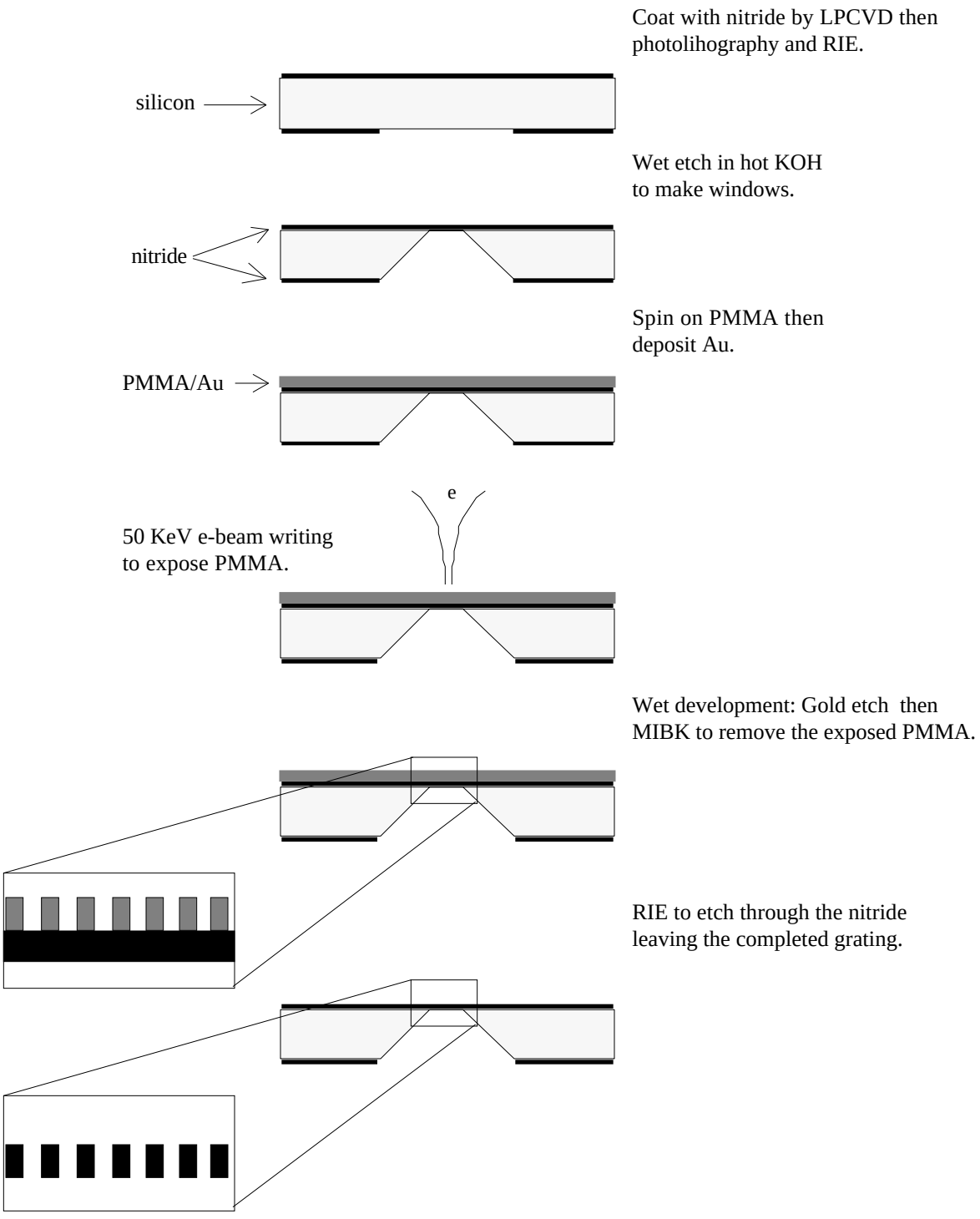

Figure 1.1. Schematic of the grating fabrication process. All text on the right describes the processes that transform the wafer between the states depicted above and below the text. Si, nitride and PMMA are indicated by the same patterns throughout.

I now turn to a detailed description of the fabrication process at a level intended for an experimental physicist with no experience with nanofabrication.

We start with a 250 μm-thick, 3"-diameter silicon wafer with a <100> orientation, which has been polished on both sides ("double polished"). The wafer it then coated on both sides with ~150 nm of amorphous silicon nitride (Si_3N_4), using low pressure chemical vapor depositor (LPCVD)[8]. When deposited in this manner, nitride is a hard, stiff (elastic modulus ~3×10^{11} Pa), and inert material. The nitride is formed with a tensile stress of ~ 6.5 GPa. Because this stress may be high enough to cause grating failure we also tried low-stress nitride. Low-stress or “Berkeley” nitride is grown with an excess of Si by a plasma enhanced LPCVD process. In this work we use two batches of films: a 160 nm-thick stoichiometric nitride, and a 210 nm low-stress nitride. The low stress nitride has about 1/10 the stress of the stoichiometric nitride, and about 1/2 the tensile strength (Koskinen and Johnson 1989).

The windows are made by first patterning the nitride on the back side of a wafer, and then using a directional etch to remove the exposed Si, leaving the membranes (fig. 1.1). In the first step of this process a 4" Chrome photomask is exposed using a computer aided design system to drive a 1 μm-resolution pattern generator. The exposed pattern is an array of ~20 identical chip patterns on a 12 × 7 mm grid. Each chip has seven rectangular holes[9] that define the windows, and ~70 μm-wide boundary lines that form cleave lines used to separate the chips. Next, the back side of the wafer is coated with 1 μm of photoresist which is then exposed with the Cr mask using contact photolithography. Great care must be taken to avoid scratching the front side of the wafer (which is the back side during these processes), and to align the mask with the crystal axis of the wafer. The nitride is then patterned by RIE using the photo resist as a mask. Finally, the wafer it etched in a hot KOH solution. The KOH etches about 50 times faster in the <100> direction than it does in the <111>. I found that at 93°C the 4 M KOH solution etched through the wafers in ~130 min. Surprisingly, overetching by as little as 10% may destroy the membranes even though the nitride thickness is reduced by less than 5% during the full etch time. We made windows in three

[8] nitride deposition was done by Robert Soave at NNF, it is the only process in which I did not do significant parts of the work.

[9] The holes must be larger than the intended window size by 180 μm on all sides (180=250/tan(54.7˚), where 54.7˚ is the angle between <100> and <111>).

sizes, 40 × 750, 120 × 500, and 500 × 500 μm in both high and low stress nitride.

The wafer is prepared for e-beam exposure by coating it with ~170 nm of polymethyl methacrylate (PMMA) film[10], and then with 15 nm of Gold. PMMA is the standard high-resolution e-beam or x-ray resist. Regions that are exposed to ionizing radiation are partially depolmerized allowing them to be removed by a methyl isobutyl ketone (MIBK) developer. The inherent resolution limit of PMMA/MIBK combination is about 10 nm. We found that the Gold was needed to reduce writing distortions caused by charging of the substrate during e-beam exposure. After exposure the Gold is removed with a standard 'Gold etch', and the exposed PMMA is removed with MIBK.

The performance of the electron beam writing system is the single most important factor determining the grating quality. We require that the e-beam system write patterns that are coherent over large areas, but care little about the quality (surface roughness) of the individual lines. These requirements on the e-beam system are significantly different from the tasks for which it is optimized. I will therefore discuss the detailed causes of writing errors which must be understood in order to optimize the system for our use.

An e-beam writer is similar to a scanning electron microscope in that it consists of a of a tightly focused electron beam which can be scanned over a small field on the target which is mounted on a micro positioning stage. In the JEOL JBX 5DII that we used, the 50 KeV beam is focused to a ~20 nm spot which is directed under computer control within a 80 × 80 μm 'U'-mode lens field. The translation stage position is controlled interferometricaly with a resolution of 2.5 nm. Thus, in order to write a large pattern the 80 × 80 μm fields must be written successively, and stitched together by repositioning the stage. We then have two sorts of errors, the error within a single writing field due to distortions in the lens or beam steering system, and field stitch errors due to stage repositioning. The combined error is estimated to be 30 nm rms, almost entirely due to field stitch error[11]. The field stitch error is due to two causes, thermal drifts in the work-piece dimensions, and variations in the height of the wafer

---

[10] Difficulties are encountered in spinning on the PMMA if the front of the wafer is not smooth enough or if there are any broken windows.

[11] Lense distortions are removed automatically by using the system in imaging mode to locate a spot on the stage which is moved through 64 subfields, generating a map of lense distortion which can then be corrected for.

relative to the focal plane of the lens. Thermal drift problems are significant because we require length stability of ~20 nm over lengths of ~20 cm (10^{-7}) during the ~10 min writing time for a single grating.

We attempted to mitigate the effects of e-beam writing errors using several methods. The thermal drift problems can be reduced by setting up the CAD package that drives the e-beam writer so that single gratings are written using successive fields in order to reduce the total writing time per grating. Distortions within a single field that are caused by electric fields due to the charging of the substrate during the writing process can not be removed by the automatic lens distortion corrections. This problem is not usually encountered for solid substrates, but we found that it caused ~50 nm sub-field stitching errors with our thin insulating membranes. We solved this problem by coating the PMMA with a thin layer of gold. We assessed the field stitch errors by writing small sections of grating at the field intersections, an then reading the relative errors with a SEM. Because the errors were almost exactly the same at each intersection independent of the time spend between patterns, we concluded that the residual errors are caused by wafer height variations rather than by thermal drifts. The effect of these errors on grating performance is much worse if the field stitched boundary is parallel to the grating lines than if it is perpendicular. Using this fact we were able to reduce the effect of the height variation errors by defining our patterns so that we never have to use an area of grating with a parallel stitch. In the future the errors caused by the tilt of the work piece could be reduced by sensing the position of markers on the wafer and using these positions to correct for wafer tilt and thermal drift under automatic control.

In the final step of the fabrication process, reactive ion etching is used to cut slots through the nitride that is exposed between the PMMA lines that have been formed by removal of the exposed PMMA[12]. This is not easy because RIE would usually be expected to etch PMMA considerably faster than the nitride. It is difficult to make the PMMA lines have a height/width aspect ratio of more than about two: so to make 200 nm-period gratings the PMMA lines must be about 200/100 nm. Therefore in order to RIE through 175 nm-

[12] If we had been unable to develop a selective RIE process our plan would have been to make metal gratings using a liftoff process (Kwong, 1989). We wanted to avoid this because of the higher resolution of the direct RIE process, as well as its simplicity. In addition, because of the relative brittleness of nitride, we think that gratings make out of it are less likely to distort than metal gratings when they are made freestanding.

thick nitride with out using up all of the PMMA it is necessary that the RIE etch the nitride at least as fast as the PMMA. In addition the etch must be directional, that is the etch rate normal to the surface must be a few times larger than the transverse rate so that the PMMA lines will not be undercut.

In essence an RIE machine consists of a reaction chamber in the from of a parallel plate capacitor, in which low pressure gases are exited by RF to form a plasma of reactive ions. The sample rests on the lower plate, and a DC bias of a few hundred volts is established so that the sample is bombarded by ions with velocity normal to the surface. In the 30 cm-diameter chamber that I used, the typical etch conditions are, 30 mtorr of CF_4 gas with a flow rate of 30 sccm, an RF power of 200 W, and a DC bias of 300 V. With the above requirements in mind I developed a more selective RIE chemistry by systematically measuring the etch rates for varying the gas mixtures. I finally settled on a 3:1 (by flow rate) mixture of H_2 to CF_4 at a pressure of 15 μtorr. With this method I measured etch rate ratios of PMMA vs nitride of 1:1.8, that is selective etching of *nitride*. Figure 2.3 shows a completed 0.2 μm period grating.

Figure 2.3 Gratings and zone plates made at NNF. The grating period is 0.2 μm, the zone plate is 130 μm wide and has a focal length of 0.6 m at λ=20 pm.

1.E Zone Plate lenses

Lenses for atom beams can be constructed by making gratings with a period that varies linearly with the distance from the beam's axis. Such lenses are called amplitude (as opposed to phase) zone plates.

Our lenses were made using methods nearly identical to those described above for gratings. We made cylindrical lenses in the 120 × 500 μm-windows using the same procedure as for gratings, changing only the CAD file sent to the e-beam machine (see Fig 2.3). Techniques similar to ours have been used to make zone plate lenses for X-rays (Ceglio, Hawryluk et al. 1983), although in this case they are phase lenses. Tennant, et al (1990) have constructed a spherical zone plate lens for atoms, but have not yet tested it. There fabrication method is similar to ours except that they used a Si membrane (rather than nitride) and a more complex etch process.

Our lenses were made with a focal length (f) of 60 cm for a wavelength of 16 pm by making holes in the membrane where the distance from the center line (d) satisfied the following formula.

$$2n\pi \leq \frac{2\pi}{\lambda}\frac{d^2}{2f} \leq (2n+1)\pi$$

We also made the complimentary structure, in which the lens has holes except where d is as above. A completed zone plate is shown in figure 2.3.

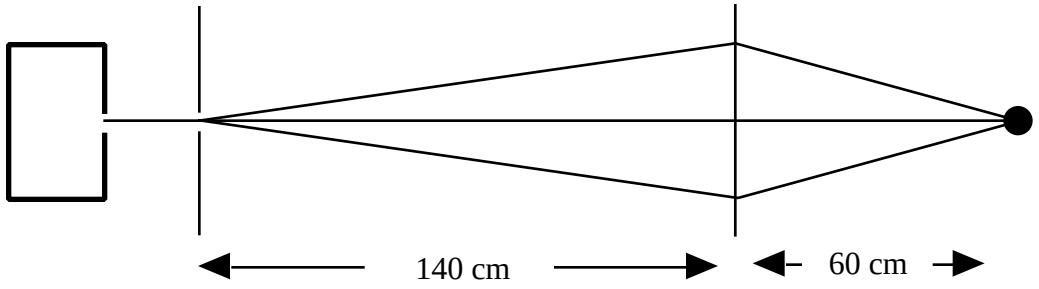

Figure 2.4. Schematic of the setup used for testing lenses.

The lenses were tested in our atom beam machine configured without the second slit, so that the lens formed an image of the first slit at the detector plane (Fig. 2.4). The results are disappointing (Fig. 2.5). We do not understand why the measured beam profile does not resolve the interesting structure of the focal spot. This structure is the sum of two components; the 0^{th} order transmission through the lens grating which forms a pattern of identical shape to that formed by a slit of the same width as the lens, and the focused spot. However, much of our disappointment with the results is due to the intrinsic limitations of amplitude type zone plates.

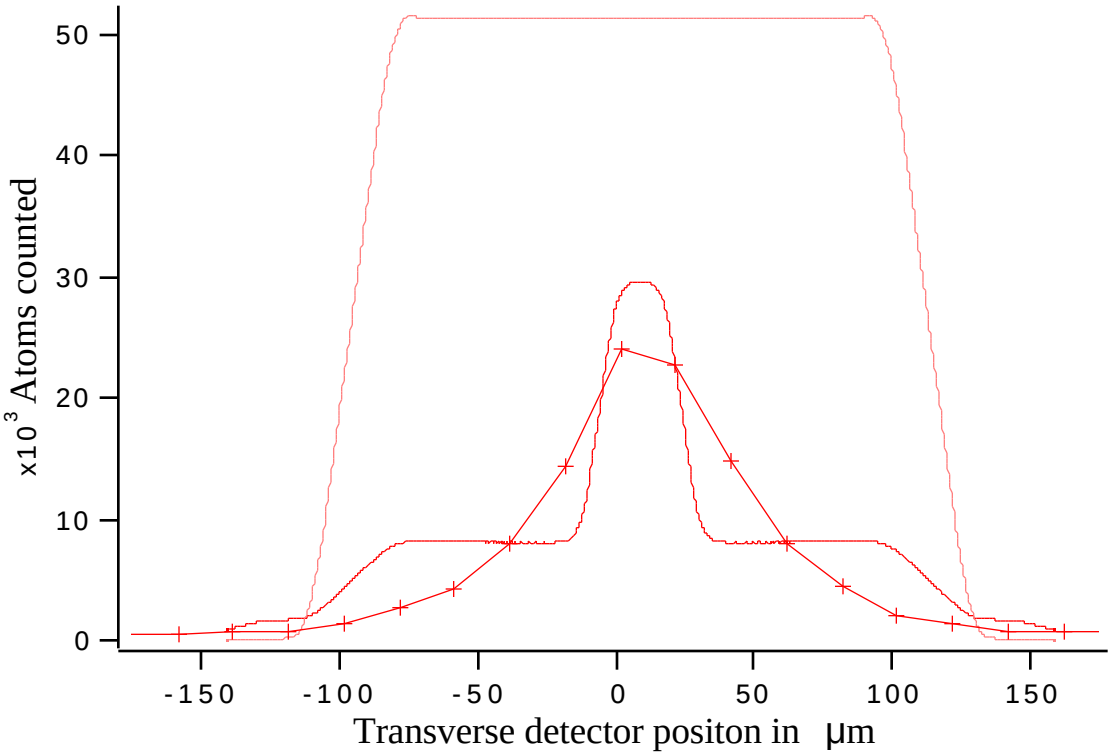

Figure 2.5. Data and and numerical model output showing the focused spot formed by a zone plate lens. The crosses are the experimental data (the line joining them is solely to guide the eye). The lines are theoretical, the lower curve is the pattern formed by the lense (assuming a 1/2 density support structure), the upper curve is the pattern formed when the lens is replaced by a slit of identical size. The model is fit to the data using only the mean position and integrated area of the beam.

2 Atom Optics: Theory

2.A General Quantum Mechanics

What is the correct quantum mechanical treatment of spatial interference phenomena in atom beams? At first glance the problem may seem trivial—thermal beams are nonrelativistic, and we are able to treat the atoms as point particles. It is reasonable to neglect the particle's internal structure because the potentials in the system are assumed to either be very smooth on the scale of atomic dimensions, or to be perfectly reflecting or absorbing walls. Thus we may neglect the atom's internal structure except for an adiabatic dependence of the internal energy on some external potential. Therefore it appears that we may just apply the Schrodinger equation for a single particle in a slowly varying potential. This presents no conceptual difficulties, only the technical difficulties of integrating the equation for given boundary conditions.

In fact the problem is not so easily solved, the difficulty is the specification of the initial state. This is the question alluded to in chapter 1.B: is the momentum distribution of a beam from a thermal source sufficient to determine the quantum state of the system? To further focus the question we may take "sufficient to determine the state" as determining the state well enough to predict the results of experiments. This is basically a question of the *a priori* existence of wave packets. That is; might a beam with a momentum distribution $\sigma(\mathbf{k})$ be composed of a statistical ensemble of wave packets with a different (narrower) momentum distribution?

These questions can be stated more formally in the following way. Consider a beam emitted by a thermal source propagating in one dimension. If we measure the wave vector distribution $\sigma(k)$, we are measuring the average value of $|\langle k|\psi|k\rangle|^2$, where ψ are the pure states in the ensemble. This is equivalent to a determination of the diagonal elements (populations) of the density matrix ρ in the $|k\rangle$ basis. Experimentally we might investigate this system by looking at interference in x, that is at the coherences of ρ in the $|x\rangle$ basis. If there are no coherences in the $|k\rangle$ basis then the populations in $|k\rangle$ determine the coherences in $|x\rangle$. The questions is: what are the coherences of ρ in the $|k\rangle$ basis?

I do not know the answers to these questions. In this experiment we have always assumed that the velocity distribution determines

the problem. We model our source as a luminous area which emits an ensemble of plane waves described only by their scalar velocity distribution and brightness. The beam is defined by the slits and the source. This assumption seems fully justified because the potentials in our interferometer are time independent, and because the quantum density is so small. I have no confidence that this assumption would be justified in cases where their are time dependant potentials inside an inerferometer. Time dependant potentials may probe the coherences in $\rho(k)$ by introducing phase shifts between different k's. These assumptions must fail if the quantum density approached or exceeds unity, or if one measures correlations between counting rates.

In this thesis I present two types of theoretical work. The first is detailed work on the solving the Schrodinger equation for the boundary conditions of our apparatus. This is handled in the section on numerics. I have also done less focused work on the question of how to treat the case where the quantum density in not small. This is treated in the section of correlation experiments.

2.B Numerics

In physics we consider an analytic knowledge of the fundamental equations to be both satisfying and necessary for a useful understanding of a system. However this is not sufficient; numeric modeling is a necessary basis for the precise prediction of experimental results. This is true because the boundary conditions of real world experiments seldom allow analytic solution of the fundamental equations of the theory. Thus, accurate prediction of experimental results, which is the basis for belief in the theory, must rest on numerics. For many real problems (e.g. fluid mechanics), an analytic knowledge of the theory may be insufficient to form even a rough understanding of the behavior of the system, let alone to make accurate predictions. In this light I find it somewhat disturbing how little numeric theory I was exposed to during my education; I suppose it lacks glamor.

2.B.i Motivation

In this experiment we modeled the two dimensional spatial interference patterns formed by systems of slits and gratings. We were motivated to construct a numeric model of our experiment because we were unable to answer certain basic questions

analytically. We are not yet concerned with making a quantitative comparison of experiment with theory (in this case the Schrodinger equation)[13]. Rather, we wish to make approximate predictions of the fringe contrast for various configurations of the interferometer, and we are unable to arrive at sufficiently unambiguous approximations by analytic means[14].

The original motivation for attempting a numeric simulation of our interferometer was simply to assure ourselves that it actually formed achromatic fringes. Later numeric work examined a number of more complex questions.

1. What is the contrast as a function of the inequality of the spacing of the three gratings?
2. How does the contrast vary with the width of the slits and is there any contrast with no slits?
3. How do zone plate lenses perform?

2.B.ii Stating the problem

The first step is to start with the basic theory, and to introduce sufficient simplifications of the physical system to generate a precise statement of the problem which can be solved numerically. We wish to solve the problem depicted in figure 2.1, a two dimensional model of our interferometer. In our notation the planes are named s, g_1 etc, and the x variables within the planes are x_s etc. We also use $g_n(x)$ to denote the transmission function of the grating or slit at the g_n plane. In the actual experiment the second slit and the first grating are separated by ~6 cm, in the model they are lumped together in the g_1 plane. Similarly for the source and the first slit which are separated by 21 cm.

---

[13] Such comparisons have been made for neutron interference patterns as a test of the linearity of quantum mechanics (Zeilinger, 1988).

[14] It is clear that no complete analytic solution exists because the gratings are in the near fields of the slits. The problem is to find analytic arguments that allow useful but incomplete prediction.

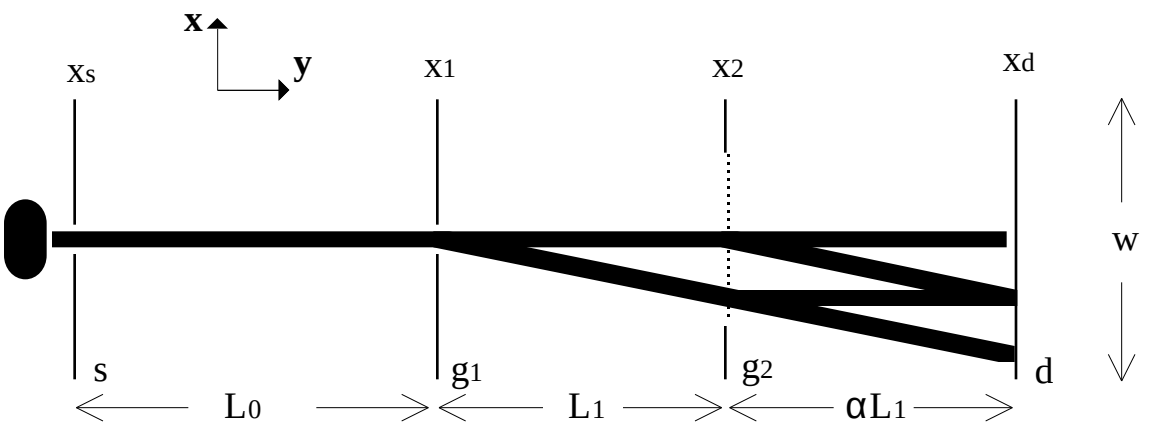

Figure 2.1. An idealized model of the interferometer showing selected beams. The planes are named s, g_1 etc, the variables within the planes are x_s etc. The actual dimensions are: lengths, L_0=.8 m, L_1=0.65 m, and $\alpha \sim 0.005$; wavelength $\lambda=2\times10^{-11}$ m; and period $d=2\times10^{-7}$ m. The diffraction angle is $\theta_{dif}=\lambda/p=10^{-4}$ rad. For the numeric model we define a maximum width w, and from that a maximum angle $\theta_{max}=w/L_0$.

The first approach is motivated by the Feynman treatment of quantum mechanics (Feynman and Hibbs). We wish to calculate <d|s> the amplitude for a particle to go from the source to detector. According to the basic principal of quantum mechanics this amplitude is *proportional* to the sum of amplitudes to go by all possible intermediate paths. This naturally leads to a discrete problem. We generate a set of paths by placing a grid of points in each grating slit and then forming the set of all connecting paths that go through one point on each plane. There are two problems with this approach. The first is with the normalization, which is trivial for finite sets of points. More serious is the question of what to use for the amplitude to go between points in free space. The correct Feynman picture is of course an integral of $e^{iA/h}$ over all paths in configuration space where A is the classical action. It is tempting to assume that we can just use $e^{iA/h}$, which in this case is just e^{ikr}, for propagator. As we will show in the next section this is incorrect, but turns out to be a good approximation for our problem.

A more rigorous approach is to start with the Schrodinger equation for a free particle

$$i\hbar\frac{\partial\psi(\mathbf{r}, t)}{\partial t} = \frac{-\hbar^2}{2m}\nabla^2\psi(\mathbf{r}, t) \quad . \tag{2.1}$$

The equation is trivially separated by taking $\psi(\mathbf{r}, t) = e^{-iEt/\hbar}\varphi(\mathbf{r})$ and $k^2=2mE/\hbar^2$ to get

$$\left(\nabla^2 + k^2\right)\varphi(\mathbf{r}) = 0 \quad . \tag{2.2}$$

This is just the Helmholtz equation, the basis of scalar diffraction theory, the theory of light propagation when the vector nature of the EM field is ignored (Marion and Heald 1980, chapter 12). Therefore we can use all the mathematical tools developed for the optical problem. We want to solve the Helmholtz equation under the boundary conditions of our interferometer: that is, wave propagation through a system of perfectly absorbing perforated screens. These boundary conditions are not easily incorporated into the Schrodinger equation because particle absorption is equivalent to a measurement. We will simply assume[15] the Kirchhoff boundary conditions for φ directly behind a thin adsorbing screen:

1. Behind a hole in the screen φ and $\nabla\varphi$ are the same as they would be if the entire screen were not present.
2. Behind a solid part φ and $\nabla\varphi$ are zero.

From the Helmholtz equation with the Kirchhoff boundary conditions we derive the usual Frensnel-Kirchhoff diffraction integral

$$\varphi(x_2) \quad k\int_{\sigma_1}\frac{e^{ik(r_1 + r_2)}}{r_1 r_2}(\mathbf{e}_1 + \mathbf{e}_2)\,\mathbf{n}_1\,da \tag{2.3}$$

where terms of $O(r^{-2})$ have been dropped, and the meaning of the symbols is indicated in figure 2.2. We note that the $(\mathbf{e} + \mathbf{e})\,\mathbf{n}$ terms make this is essentially different from what we would have derived by a naive application of the Feynman method (or Huggens principle).

---

[15] The Kirchhoff boundary conditions are rigorously *incorrect* even for the optical case, there only justification is that they seem reasonable and correctly predict experiment.

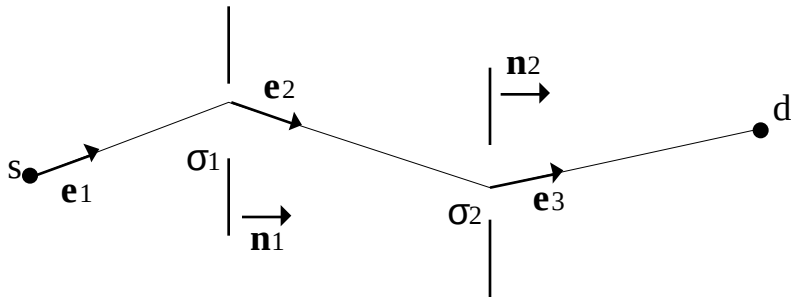

Figure 2.2. Notation for the multiple plane diffraction problem. r_1 is the length of the path along unit vector $\mathbf{e}_1$ etc, similarly x_1 is the position in the surface σ_1.

In our calculation we want to solve problems with two or more opaque screens as in fig 2.2. In general this results in a M-dimensional integral of the form

$$\varphi(s,d) \int_{M\ \text{screens}} \prod_{n=0}^{M} \frac{e^{ikr_{n+1}}}{r_{n+1}} \theta(x_n, x_{n+1}, x_{n+2})\,(dx)^M \qquad (2.4)$$

Where the θ functions are the Stokes inclination factors given by $\theta(x_n, x_{n+1}, x_{n+1}) = (\mathbf{e}_{n+1} + \mathbf{e}_{n+2})\,\mathbf{n}_{n+1}$, and $n \in \{s, x_1, x_2, \ldots d\}$. We want $\varphi(s, d)$ for a given source point s, so the computational difficulty for this problem scales as N^{M+1} where N is the number of discrete points in each surface, and M is the number of surfaces. Since we want to solve problems with up to three surfaces this is much too hard.

Because φ and $\varphi\,\mathbf{n}$ at a surface are sufficient to determine the φ and φ at the next plane (using the Helmholtz-Kirchhoff integral) we know that it must be possible to do the whole problem in $O(mN^2)$ time.

Instead of writing the integrals for φ at each plane we make the simplification by using the small angle θ_{max} to ignore all the inclination factors which are proportional to θ_{max}^2. We justify this approximation by noting that $\theta_{max} \approx 10^{-3}$, and the angles which contribute significantly to the sum are $\sim 10^{-4}$ radians.

With the further restriction that the surfaces are parallel planes we arrive at the following general form for two gratings:

$$\varphi_s(d) \quad \int_{g_1} g_1(x_1) \int_{g_2} g_2(x_2) f_{l_0}(s - x_1) f_{l_1}(x_1 - x_2) f_{\alpha l_1}(x_2 - d) dx_2 dx_1 \tag{2.5}$$

where $f_L(x)$ are the free space propagation factors

$$f_L(x) = e^{ik\sqrt{x^2 + L^2}} \tag{2.6}$$

The assumption that the planes are parallel simplifies Eq. 2.5 by allowing us two write the free space factors as $f_L(x_n - x_{n+1})$ rather than as $f_L(x_n, x_{n+1})$. This will be important later because it makes the integral look almost like a convolution. Our function $\varphi_s(d)$ is equivalent (ignoring normalization) to the amplitude to go from s to d, $<d|s>$. The intensity pattern at the detector plane is the usual $|\varphi(d)|^2$. To calculate the intensity distribution P(d) generated by an incoherent source with transverse profile $s(x_s)$ we repeat the calculation for many source points

$$P(d) = \int_{-\infty}^{\infty} dk \int_{-w/2}^{w/2} \sigma(k) s(x_s) |\varphi_s(d)|^2 dx_s \tag{2.7}$$

where $\sigma(k)$ is the velocity profile of the source and $s(x_s)$ is its transverse brightness distribution.

The sum of probability densities (Eq 2.7) seems to increase the computational difficulty of the problem by at least another factor of N. We cant simplify this sum, and tricks based on using random initial phases fail because the coherences are not removed. However, because there is no coherent addition it is not necessary to do the sums over a large number of points. We have found that a 100 source points is usually adequate as long as they are distributed in a non-periodic but reasonably even fashion. Our algorithm assigns nearly random values of position *and* momentum to each source point, while taking care that the final distributions are approximately correct[16].

2.B.iii Numerical method: how to do it fast

The naive way to integrate equation 2.5 would be to replace the continuous variables *x* with discrete variables x_n, and so to convert the integral into a sum.

---

[16] This elaborate procedure, and other tricks such a choosing not quite integer values for the constants, are designed to ensure that no unintentional symmetries are introduced into the problem.

The number of points required may be estimated by noting that the discrete grid acts just like an additional fine period grating. We must make the period of this imaginary grating fine enough that only its 0^{th} diffracted order contributes significantly to the sums. With the maximum angle in the problem $\theta_{max}=w/L$ as defined above, we must have

$$\frac{\lambda LN}{w^2} >> 1 \tag{2.8}$$

For our wide simulation $w=10^{-3}\mu m$, L=1 m, and $\lambda=2\times10^{-11}$ m we must have $N=10^6$ to get a product of 20. Therefore to integrate the problem for one source point will take about 10^{12} floating point operations which takes the CRAY-2 ($\sim10^8$ flops) about three hours. This is much too slow: we must find a more efficient algorithm.

We can reduce the difficulty of the computation to $O(mN\log(N))$ by writing the discrete sums as convolutions which can be done by the Fast Fourier Transform (FFT) algorithm in $N\log(N)$ time[17]. I will present this technique in detail because it does not seem to be known in the community of people solving similar problems of matter wave interference[18], although I strongly suspect that it must be common knowledge to experts in scalar diffraction theory.

We want to turn Eq. 2.5 into a convolution. We first go to the discrete case, taking φ_n and f_n as the discrete (N point) values of $\varphi_s(x)$ and $f_L(x)$. The problem[19] is to calculate φ', the amplitude at a given screen, from φ, the amplitude at the previous screen, and f by

$$\varphi'_i=\sum_{j=0}^{N-1} \varphi_j f_{j-i}, \quad \text{with } f_k=f_{-k} \tag{2.9}$$

If we break up the sum and use the symmetry property explicitly, this can be written as

---

[17] The germ of this idea was planted during a conversation with Michael Haggerty, who's help I gratefully acknowledge. Later development of the algorithms and and especially of the code was done as a collaboration with Quentin Turchette.

[18] Personal communications from Anton Zeilinger and John Clauser.

[19] My description of the this algorithm is partially copied from Quentins Turchette's undergraduate Thesis.

$$\varphi_i' = \sum_{j=0}^{i} \varphi_j f_{i-j} + \sum_{j=i+1}^{N-1} \varphi_j f_{j-i} \,. \tag{2.10}$$

We wish to write this as a discrete convolution, defined as:

$$(a \quad b)_i = \sum_{j=0}^{N-1} a_j b_{i-j} \tag{2.11}$$

where b must be periodic, that is $b_i = b_{i \pm nN}$ n=0, 1, 2, ... We can use the periodicity to break the sum as before

$$(a \quad b)_i = \sum_{j=0}^{i} a_j b_{i-j} + \sum_{j=i+1}^{N-1} a_j b_{i-j+N} \tag{2.12}$$

We want to demonstrate how equation (2.9) can be converted to convolutions of the form of equation (2.11). Since the discrepancy between the equations lies in the periodicity, we first attack this problem. Define vectors φ^{2N} and f^{2N} which have twice as many elements as their corresponding N-vectors. We choose φ^{2N} to be defined as:

$$\varphi_k^{2N} = \begin{cases} \varphi_k, & k \in [0,N-1] \\ 0, & k \in [N,2N-1] \end{cases} \tag{2.13}$$

and solve for the f^{2N} necessary to make a convolution of the 2N-vectors yield the results we want. The definition of the discrete convolution requires periodic symmetry of f^{2N}.

$$(\varphi^{2N} \quad f^{2N})_i \sum_{j=0}^{2N-1} \varphi_j^{2N} f_{i-j}^{2N}, \quad f_k^{2N} = f_{k \pm n2N}^{2N} \quad n=0,1,2,\ldots \tag{2.14}$$

We can once again split up this sum as:

$$(\varphi^{2N} \quad f^{2N})_i = \sum_{j=0}^{i} \varphi_j^{2N} f_{i-j}^{2N} + \sum_{j=i+1}^{N-1} \varphi_j^{2N} f_{i-j}^{2N} + \sum_{j=N}^{2N-1} \varphi_j^{2N} f_{i-j}^{2N} \tag{2.15}$$

Using the definition of φ^{2N} we see that the last term is identically zero and that the φ^{2N} in the first two terms is simply φ. Exploiting the periodicity of f^{2N} the convolution can be written

$$(\varphi^{2N} \quad f^{2N})_i = \sum_{j=0}^{i} \varphi_j f_{i-j}^{2N} + \sum_{j=i+1}^{N-1} \varphi_j f_{i-j+2N}^{2N} \tag{2.16}$$

Thus it is seen that with the proper definition of f^{2N} the sum in Equation (2.9) can be made to match that of Eq. (2.11). This forces f^{2N} to be defined as

$$f_k^{2N} = \begin{cases} f_k, & k \in [0,N-1] \\ f_{2N-k}, & k \in [N+1,2N-1] \end{cases} \tag{2.17}$$

With this, we see that

$$\varphi_i' = (\varphi^{2N} \quad f^{2N})_i \tag{2.18}$$

Thus we have transformed equation 2.9 into a convolution of vectors with 2N elements. We can now apply the discrete convolution theorem which transforms the Fourier transform of a convolution into the product of the Fourier transforms of its elements.

Because of the magic of the FFT algorithm this method represents an enormous simplification of the original problem. By the naive method our calculation took $O(mN^2)$ floating point operations, by the FFT method it only takes $O(3\times 2N\log(2N) + 2N)$ steps because one must do three 2N point FFTs and one 2N point product. For $N=10^6$ this represents a time saving of $\sim 10^4$, which allows us to do the calculation for a single source point and velocity in ~10 sec on the CRAY-2.

2.B.iv results

We first confirmed that an interferometer with ideal geometry will produce high contrast fringes from a source with a 12% FWHM velocity distribution. Figure 2.3 shows the calculated interference pattern at the plane of the third grating. The interferometer configuration was like that described in fig 2.1 except that L_0=1 m, and L_1=0.5 m, both slits were 20 μm-wide. This interference pattern was calculated by incoherently summing 100 source points in the pseudo random manner alluded to above. The calculation was done with $N=10^6$, that is 210 points per grating period, it takes ~20 min on the CRAY. From this pattern we then calculated the contrast measured by a detector masked with a square wave grating. Because the square wave grating is sampling a sinusoidal interference pattern, the measured contrast for is only $2/\pi$ (0.63) times the contrast of the interference pattern formed at the detector grating plane. When 25 μm-wide detector is located in the middle of the first order the contrast is 56%.

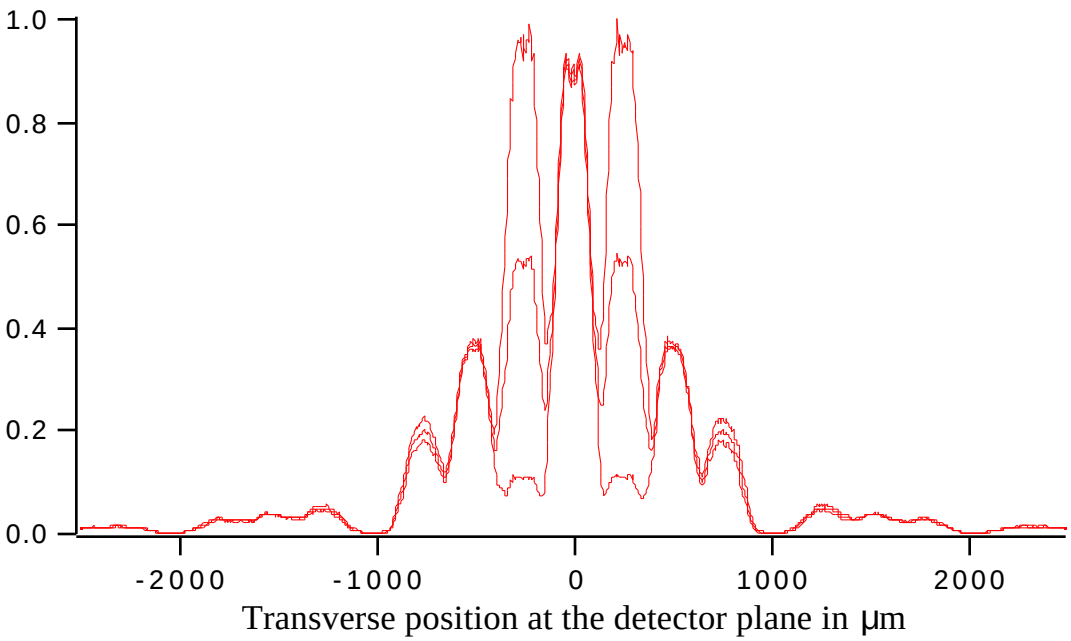

Figure 2.3. The calculated interference pattern formed at the position of the third grating. The three plotted lines are the average, local maximum, and local minimum. Note the large fringe contrast on the ±1 and ±3 orders. The horizontal scale is arbitrary. The faint asymmetry in the pattern is due to the random nature of the source.

The next question we addressed was the variation in fringe contrast as a function of the inequality in the spacing of the grating planes. We investigated this by calculating the interference pattern at various longitudinal positions of the detector plane (values of α in fig 2.2). In order to reduce numeric "noise" we then searched for the best contrast as a function of the transverse position of a 25 μm-wide detector. To save computation time we used the interference pattern from a point source to calculate the contrast at a wide range of misspacings. These data are plotted in figure 2.4. We then checked the dependence of these results on the fact that we that we used a point source by doing the full computation for a few values of α. With a configuration identical to that used for fig 2.3 the contrast was 56% for equal spacing and was degraded by 18% at a +2% misspacing. Since we can easily arrange the gratings to be equally spaced to better than 1% we predict that spacing errors will not significantly affect our contrast.

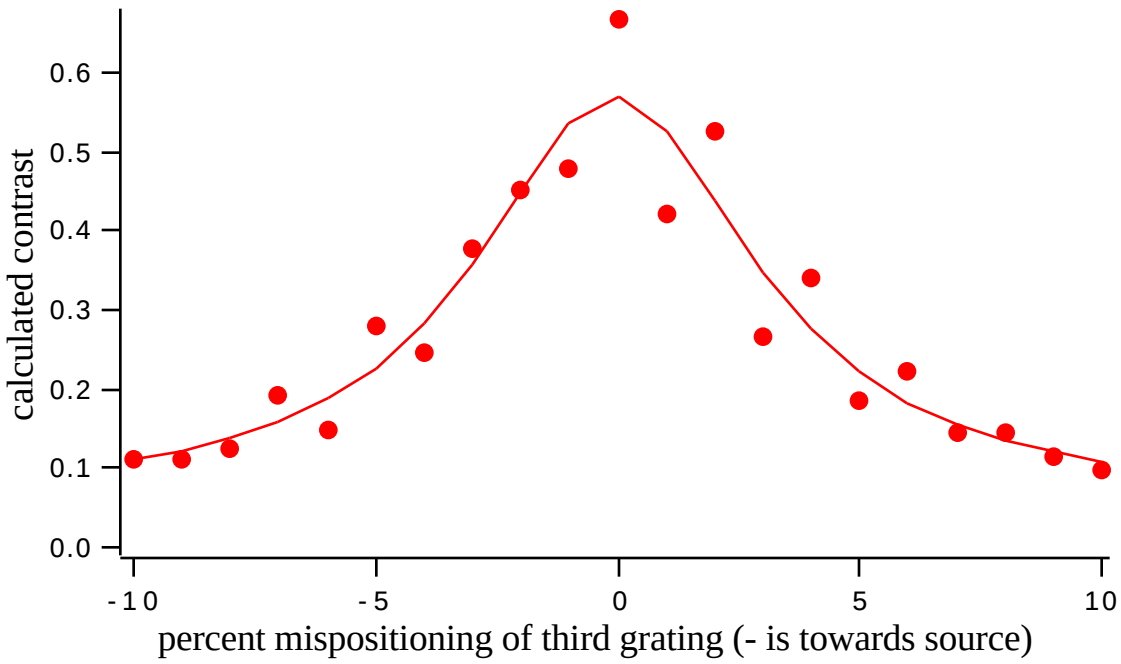

Figure 2.4. Calculated fringe contrast as a function of the position of the detector plane. The line is a Lorentzian fit, its only purpose is to guide the eye. Point source illumination with L_0=1 m, L_1=0.5 m, and a first grating width of 20 μm.

The most interesting question concerns the grating contrast as a function of the width of the collimating slits. The slits serve to define the beam so that the interfering orders are distinctly separated at the middle of the interferometer. This beam separation is necessary for many applications of atom interferometers (see chapter 3.A.2), in fact we have taken it to be implicit in the definition of an interferometer. However, if fringes of reasonable contrast were formed without collimating slits, this would be useful because of the greatly increased flux. The flux in a beam defined from a luminous source by two slits and a detector scales quadratically with the slit and detector widths, while the angular resolution decreases linearly. One practical application of operation with wide slits would be greatly facilitated alignment and testing of the gratings and of the vibration isolation systems. The gratings could be more quickly aligned by maximizing the detected fringe contrast, and when aligned, the comparison of measured and calculated contrasts would be a test of the coherence properties of the gratings.

We now[20] believe that interferometers with wide collimation slits, that is interferometers in which there is no spatial separation of the beams, do produce good fringe contrast. Figure 2.5 shows the results of a recent calculation in which both gratings had a width of 80 μm and the source slit was 200 μm. The calculated contrast is 35% when masked by the third grating. In this case the total flux is ~5 times that calculated for the case of 20 μm slits.

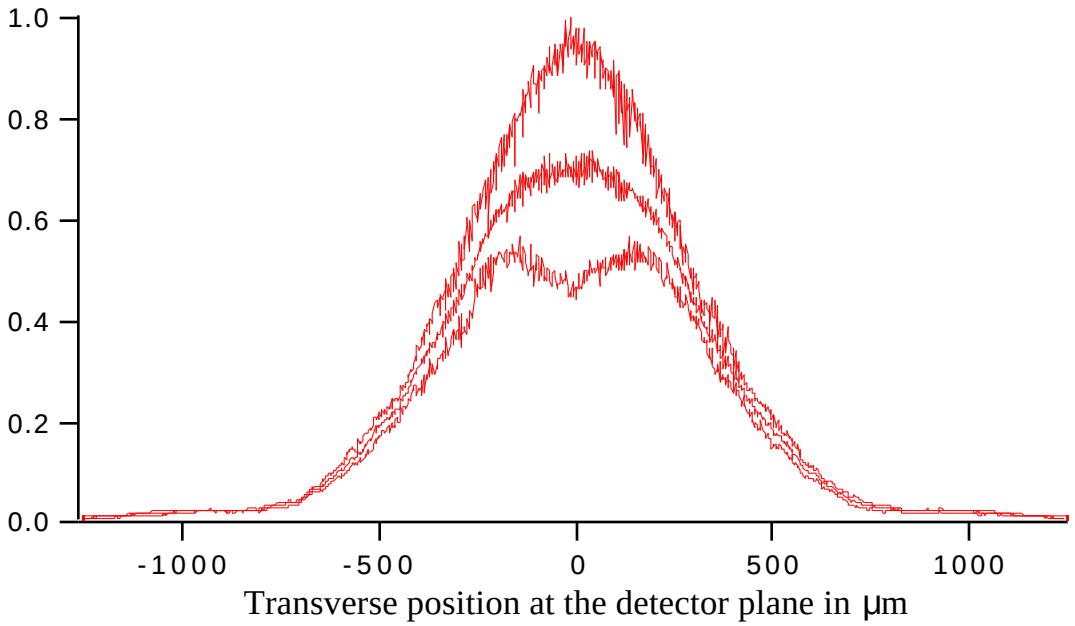

Figure 2.5. The interference pattern formed with 80 μm wide collimating slits. As in Fig 2.3 the three curves are the local maximum, minimum, and mean.

[20] Unfortunate we have only recently reached this conclusion. We had previously believed that such configurations did not produce high contrast fringes.

3 Atom Interferometers

3.A Introduction

3.A.i History of Matter wave interferometers

Optical interference phenomena were first described in Newton's day. Optical interferometers began to be used for measurement (that is other than as objects of study in them selves) at the end of the last century. A notable example is the Michelson-Morley experiment.

The first interferometers for material particles were realized in 1954 with the near simultaneous demonstration of two kinds of electron interferometer. Marton used a three crystal geometry, and required 1230 6 min exposures to find interference. Marton argues in the paper (1954) that a two slit geometry would be "almost impossible". A single wire (or double slit) biprisim was demonstrated by Mollenstedt in the same year.

In 1962 Maier-Leibnitz demonstrated the first neutron interferometer, a simple biprisim. It was 10 m long but was only able to separate the beams by 60 μm. Due to the low flux through this design, little was done with it. The first perfect crystal neutron interferometer was demonstrated by Rauch in 1974. Interferometers of this type use three crystalline diffraction gratings that are aligned by virtue of being cut from a single perfect crystal, and typically enclose an area of a few 10's of cm^2. Many such neutron interferometers have now been built, and a large body of work has been done, using them to study (or demonstrate?) basic quantum phenomena. Some highlights are; coherent spinor rotation (Rauch, Zeilinger et al. 1975), effect of the earths rotation (Sagnac effect) (Werner, Staudenmann et al. 1979), and the measurement of the phase shift due to the gravitational field (Colella, Overhauser et al. 1975, known as the COW experiment).

The first observation of diffraction for atoms was by Estermann and Stern in 1930. They observed diffraction peaks in the scattering of H_2 and He of a cleaved Li F surface. In the 1980's the advent of light force slowers for atom beams made atom interferometers seem more realizable. It is surprising that the first atom interferometers

were not demonstrated until 1991, and that none have yet used laser cooled atoms[21].

3.A.ii Applications of Atom Interferometers

Applications of atom interferometers, and indeed of matter wave interferometry in general, fall into three categories.

1. Measurement of inertial effects such as rotation, acceleration, and gravitational gradient.
2. Fundamental quantum mechanics and measurement theory.
3. Measurements of particle properties.

Discussion about which technologies are best for making atom interferometers are only fruitful in the context of the intended application.

In the measurement of inertial effects the one goal of interferometry is precision. Interferometers are only interesting in this application in so far as they out perform the alternative methods. An interferometer with simple geometry (separated beams are in a plane, and form only one loop) is sensitive to rotations in inertial space with sensitivity (rads of phase shift per unit of angular velocity) $4\pi Am/h$, where A is the area of the loop, and m is the particles mass. The equivalent sensitivity for an optical gyro is $\pi A/\lambda c$, the ratio is the rest mass of the particle to the energy of the photon, so this looks promising. If the interferometer made using diffraction gratings as beam splitters, and the angles of diffraction are less that a radian so that we can take $\sin(x)=x$, then the sensitivities can be expressed differently. The rotation sensitivity is $4\pi l^2/dv$, and for accelerations it is $2\pi l^2/v^2 d$, where d is the grating period, l the distance between gratings, and v the atom's velocity. These expressions are useful because they apply to all interferometer currently under construction, and they are expressed in terms of the quantities most directly controlled by experimentalists. The ultimate sensitivity of the device depends on the intrinsic phase shift due to the effect one wishes to measure and the flux of particles through the interferometer. The precision of fringe measurement is proportional to the square root of the total

[21] I assume that this is due to the generaly poor brightness of existing slow atom sources.

number of particles counted. A detailed and interesting discussion of atom interferometers as inertial sensors is found in Clauser (1988).

Many of the basic questions about the foundations of quantum mechanics, that is of measurement theory, are naturally posed as questions about interference experiments. Matter wave interferometers are fundamentally different from their optical cousins because there can be no correct nonrelativistic (single particle) analysis of optical interference.

> It is unfortunate that the interference phenomena most familiar to physicists occur for a system, light, for which there is no nonrelativistic approximation: one can introduce nonrelativistic wave functions $\psi(\mathbf{r})$ for a slow electron, but not for a photon, which is fundamentally relativistic. (Cohen-Tannoudji, Dupont-Roc et al. 1989, p205)

This fundamental simplicity of matter wave interference may allow cleaner tests of measurement theory. Compared to other massive particle interferometers, atom interferometer have many advantages for doing measurement theory experiments. These advantages rest on the ease of producing and manipulating intense atom beams (see chapter 1.1). Light beams can now be prepared in number states, coherent states, and mixed states. Existing particle beams are superpositions of number states with low occupancy numbers, in the near future atoms may be prepared in bose condensed, high-quantum density states (although I can not imagine how to produce a matter wave coherent state).

Atom interferometers may be used to probe the internal properties of atoms. Such experiments depend on the ability of interferometers to measure the phase shift due to a particle's interaction with a field that is localized on one side of the interferometer. Such probes of an atom's interaction with an external field are different from those done with conventional optical methods because they measure the energy shift of the whole atom (in whatever superposition of states) vs the undisturbed atom. In optical measurements it is always necessary to measure relative energy shifts by means of some interference of internal states. Possible measurements of atomic properties include, the measurement of ground state polarizabilities which is a useful test of atomic structure calculations.

3.B Our Interferometer

3.B.i Introduction

I now turn to a detailed description of our atom interferometer—the core of this thesis. I intend this description to include some of the dynamics of design, the reasons for decisions and the mistakes, in addition to the statics, the description of the device on the day it first worked. Initial design work began at the end of 1988, soon after our diffraction experiment (appendix 2). The basic mechanical design was completed in the first months of '89, and the whole experiment was first assembled in July of that year. Much of the next year and a half was spent attempting to solve problems with the SμSL gratings, and with improving the atom beam system. By the end of '90 we realized that it would be impossible to make the interferometer work with the SμSL grating technology, and so in early '91 we began fabricating our own gratings at NNF. This proved to be easier that we had expected, and we were able to use the new gratings to demonstrate the interferometer for the first time in late February '91.

The design work began with the boundary conditions that we use the SμSL 0.2 μm-period gratings, and make the minimum modifications to the existing atomic beam apparatus. Thus the goals were as follows.

1) The interferometer must be less than about 1.5 m long, so as to fit inside the existing beam tube while still permitting the machine to be used for light force experiments. The **x** position[22] of the gratings must be controlled so that they can be individually moved in and out of the beam line in vacuum, and repositioned with a accuracy of ~10 μm. This is because the good areas of the gratings may be small and it is necessary to find them by looking at the diffraction patterns from one grating at a time.

---

[22] We use a coordinate system where **z** is along the direction of the atom's motion, and **y** is upwards along the grating lines.

2) The grating lines must be aligned parallel to each other to ~10^{-4} rad which is the ratio of the grating-period to the beam height.

3) Given the sensitivity to accelerations, displacements and rotations discussed above, the gratings must be stable with respect to vibrations such that the resulting interferometer phase noise be a small fraction of a fringe.

3.B.ii Plans: the details of experimental design

The interferometer is build on three translation stages that are attached to vacuum flanges which are mounted on existing ports along the main tube of our atomic beam machine. This is a key design compromise. The primary alternative is to mount the gratings on a single bar which can be removed from within the beam tube. Such a design would make both vibration isolation, and grating alignment easier. We did not take this route because of the extensive redesign of the beam tube that would have been necessary to make sufficient room for such an apparatus. Mounting the gratings on flanges necessitated an active-feedback vibration-isolation system, and the ability to align the gratings in situ. However, we have subsequently realized that the advantages of an active system, such as much reduced thermal drift and direct measurement of the relative grating motion, are large enough that it probably would be necessary to construct one even for the single bar design.

A schematic of the whole experiment is shown in figure 3.1. We use an optical interferometer to measure the relative transverse displacement of the gratings, and to generate an error signal for an active vibration isolation system. Figure 2.1 shows another idealization of the interferometer, in which the diffracted beams are more clearly indicated. For reference, the longitudinal (**x** axis) dimensions are; beam skimmer to first slit 21 cm, first to second slit 83 cm, first slit to first grating 89 cm, distance between gratings 66.3 cm, and finally the distance from the last grating to the detector is 29 cm.

We used commercial translation stages (NRC model 425) which were chosen so that the pitch error (in our case **z** axis rotation during **x** axis translation) is less than 10^{-4} rad over 1 cm. This pitch specification is necessary to allow grating translation after alignment. The stages are mounted on aluminum bars projecting down from the

flanges. Aluminum base plates mounted on each stage hold the home-made rotation stages for the gratings. Each base plate is different. On the first (nearest the source) the grating rotation stage is controlled by a encoder mike (see below) and there is one optical grating whose **z** axis rotation can be controlled by a hand micrometer. On the middle stage the grating rotation is effected by a PZT and there are two fixed optical gratings separated by ~12 cm. On the last stage the grating angle is controlled by a differential micrometer and there is one optical grating on a rotatable mounting. In addition the base plate on the last stage has a photodiode mounted ~2 cm behind the optical grating. The **x** axis position of each stage is controlled by a encoder mike, but the middle stage has a PZT in addition.

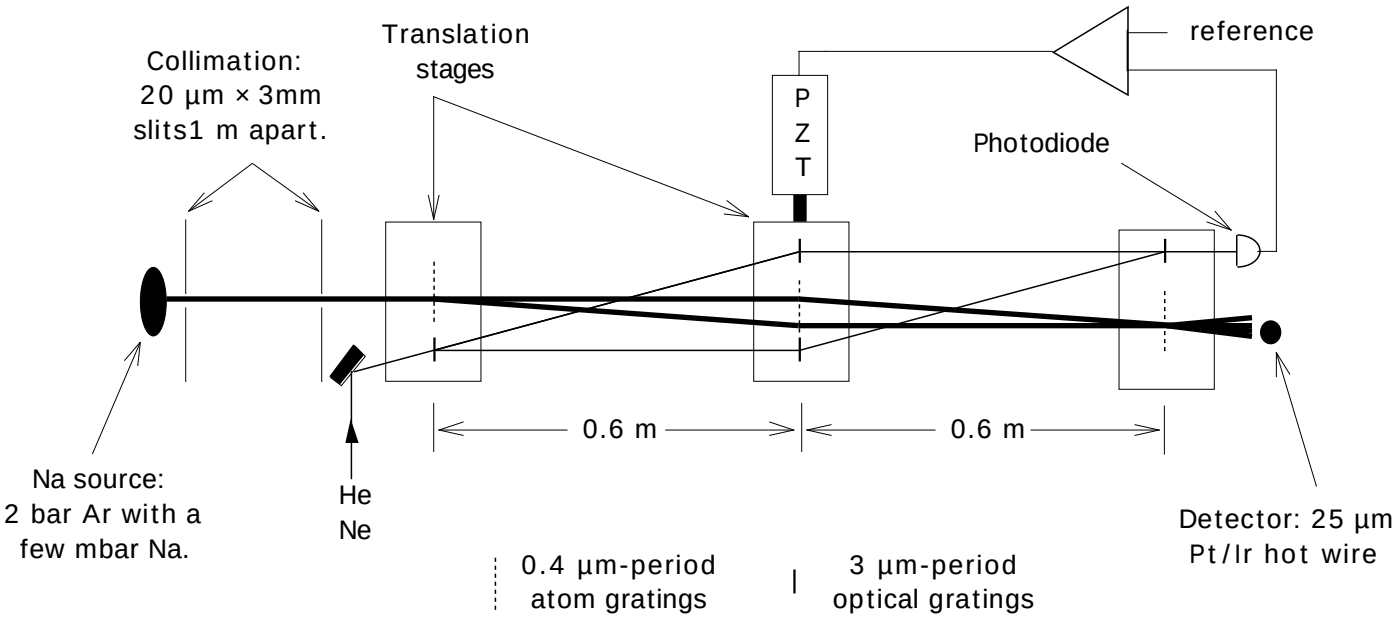

Figure 3.1 A schematic of our interferometer showing the active vibration isolation system. Not to scale

The gratings, slits, and detector are moved by micro-positioning motors under the control of an IBM PC-AT computer. We use DC-motor-driven micrometers with drive-shaft rotation encoders. The computer senses the shaft rotation and sets the voltage applied to the motor so as to control the micrometer positions[23] (i.e. a closed

[23] The motor control electronics were built by us as a cost saving measure (counting our cost as → zero). They consist of TTL circuitry to transform the quadrature output of the encoders into directional ('right' or 'left') pulses, and

loop control system). There are eight such micro-positioners. Five are needed to control the **x** positions of the gratings, second slit, and detector. Two more are used for rotation of the second slit, and of the first grating about the **z** axis. The final one is used to control a slit oriented along the **x** axis at the position of the second slit, which is used to control the height (**y** axis) of the beam. Most of the micro-positioners are "encoder mikes" made by Oriel, which combine in a single unit the micrometer, motor, and encoder. Two (on the second slit) are home-built combinations of a geared DC motor and encoder. A closed loop control system using DC motors was selected over an open loop system with stepping motors because of its ability to sense failures. In addition geared DC motors generally have smaller size, and lower stray-magnetic fields that do steppers.

In addition to controlling the motors, the computer records the atom flux on the wire by counting the pulses generated by the CEM in the detector, and can record the voltage from the photodiode sensing the intensity of the laser-interferometer signal. We have developed data taking software that keeps track of the motor positions and allows any motor to by moved while recording the atom-count rate so as to generate a profile of the beam. In addition the computer can simultaneously record the atom counts and the photodiode voltage (the only way we have taken interference data to date) or it can control the voltage input to the lock loop while recording the counts. In any data taking mode the computer can continuously record the atom counts in bins as small as ~1 msec in order to allow subsequent filtering of the noise bursts from the hot wire.

3.B.ii.1 Inertial noise

The interferometer is sensitive to inertial noise (vibration and rotation) which must be eliminated in order to observe stable fringes. I am concerned here with noise at frequencies above the reciprocal of the integration time used for phase measurement, so that it affects the experiment as a loss of fringe contrast rather than as a drift in the measured phase. Low frequency ($<10^{-2}$ Hz) phase noise is treated in the section on data analysis. The method for calculating contrast loss caused by any frequency of phase noise is

---

a multiplexing system so that seven motors can be under computer control at once. A "Scientific Solutions" data taking board in the PC-AT counts the directional pulses, and sets digital lines used by our electronics to select the multiplexer channel and to set the DC voltage applied to the motors.

outlined in Eq. 3.11. Here I deal with inertial noise at frequencies above 10^{-1} Hz.

Three kinds of inertial noise are relevant, and must be controlled in order not to loose fringe contrast. Numerical values are for the (yet unrealized) 0.2 μm-period interferometer except as indicated.

1. Acceleration. The interferometer has a sensitivity (radians of phase shift per unit of acceleration) given by

$$\varphi_a(\omega,a) = \frac{2\pi a\tau^2\sqrt{6-8\cos(\omega\tau)+2\cos(2\omega\tau)}}{p\qquad\qquad(\omega\tau)^2} \tag{3.1}$$

where τ is the transit time between gratings ~0.7 msec, p is the grating period, and I assume $a(t)=ae^{i\omega t}$. This gives a sensitivity of 260 rad m^{-1} sec^2 for $\mathbf{a}\cdot\mathbf{x}$ at zero frequency, which decreases roughly proportional to f^{-2} for frequencies over ~250 Hz, This equation (and 3.2) can be deduced by considering the acceleration sensitivity as being due to the motion of the gratings during the atom's transit through the interferometer.

2. Rotation. The sensitivity for rotation (Sagnac effect) normal to the plane of the interferometer (**y** axis) is given by.

$$\phi_\Omega(\omega,\Omega) = \frac{4\pi\Omega\tau L}{p}\frac{\sin(\omega/2)}{(\omega/2)} \tag{3.2}$$

where $\Omega(t)=\Omega e^{i\omega t}$ and τ and p are as in Eq. 3.1. This gives a sensitivity of 10^4 sec (that is rad/(rad sec^{-1}) at zero frequency.

3. Relative translations, while not truly an inertial effect, may be caused by the machine bending in response to inertial noise. The sensitivity to relative motions along the **x** axis is (2π/p) at all frequencies. The phase shift as a function of the **x** axis positions is

$$\phi = \frac{2\pi}{p}(x_1-2x_2+x_3) \tag{3.3}$$

Which can be deduced from simple symmetry arguments[24].

Inertial noise enters the machine through the floor or the vacuum hoses, and it is generated in the machine by vacuum pumps. We control the noise by isolating the machine from the floor, by reducing the effect of pumps, and by servoing out relative motion. A typical acceleration spectrum of the floor is shown in figure 3.2.

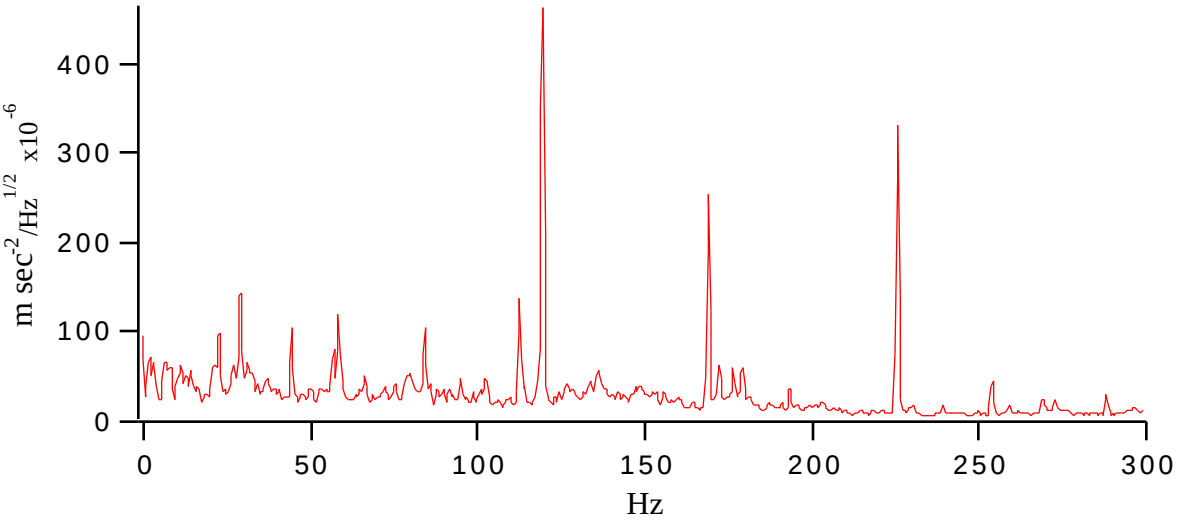

Figure 3.2 Acceleration spectrum of the floor near our experiment. Data are for transverse (**x** axis) motion. The rms acceleration is 0.8×10^{-3} m sec^{-2}, rms motion above 5 Hz is 50 nm.

We measure the acceleration with a accelerometer consisting of a peazo-electric force transducer attached to a free mass. We use Endevco model 7707-1000 accelerometers, which generate a charge proportional to **a**. These devices have no sensitivity at DC, and in practice[25] their low frequency response is determined by the amplifier, and the high frequency limit is determined by internal resonances at 8 kHz. After some effort designing low-noise, low leakage-current amplifiers we are currently able to achieve useful

[24] Symmetry argument: translation as a unit must give no phase shift, the effect of moving x_1 and x_3 must be equivalent since the wave equation is reversible. Because this argument applies to any three-grating interferometer (e.g. higher orders, multiple orders, phase gratings) it is also true for our optical interferometer.

[25] In theory, the low frequency limit is set by the internal series resistance of over 10 GΩ giving a 1/RC of 3×10^{-3} Hz.

data at frequencies as low a 0.1 Hz. Figure 3.3 shows a schematic of our accelerometer amplifier circuit. These accelerometers have very low intrinsic noise floor[26] of about 10^{-6} m sec^{-2}.

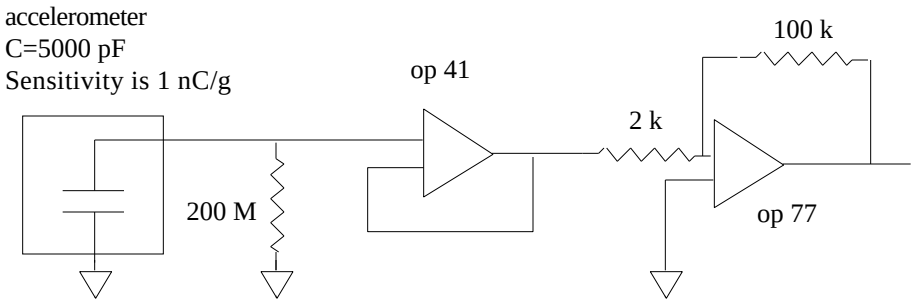

Figure 3.3 Schematic of our accelerometer amplifier. The value of the 200 MΩ resistor is chosen based on the input bias current of the op41 so as to minimize the total noise figure of the amplifier. This circuit produces a signal of 1 V per m sec^{-2} for the Endevco 7707-1000.

Angular acceleration can be measured by taking the difference signal between accelerometers mounted on opposite ends of a rigid bar. This difference signal $\Delta a(\omega)$ has magnitude $\omega\Omega l$ where l is the accelerometer separation and $\Omega(t)=\Omega e^{i\omega t}$. I have constructed such a sensor with a one meter long bar and a common mode rejection ratio (CMMR) of >100. By demanding that Δa due to rotation be 20 times larger that the background a_{rms}/CMMR we can derive the rotational noise floor for this device:

$$\Omega_{noise}=\frac{a_{noise}}{CMMR\times 10\times \omega l}\approx\frac{10^{-4}\ Sec^{-1}}{\omega} \qquad (3.4)$$

Thus with this device we can detect rotation noise at a level that would be relevant to the interferometer (10^{-4} sec^{-1}) at frequencies down to ~0.5 Hz. This means that it should be possible to detect any rotation noise that matters because the rotation noise is generated at ~5 Hz (see the last paragraph of this section).

The relative position of the three gratings is measured using a optical interferometer. The HeNe-laser interferometer uses the same transmission grating geometry as the atom interferometer. The 3.3

[26] This data was supplied to us by members of Rainer Weiss's laser-interferometer gravity-wave group at MIT. They are masters of vibration isolation who provided us with much valuable advice including recommending these accelerometers to us.

μm-period gratings for the optical interferometer are mounted on the same three translation stages as the matter wave gratings in order to record the relative alignment of the matter wave interferometer. We use a photodiode to sense the intensity of one of the interfering beams behind the third grating. The optical interferometer phase is given by Eq. 3.3 where p=3.3 μm, and the x's are the stage positions; the intensity is then proportional to $(1+c\sin(\phi))$ where c is the (experimentally determined) contrast. The "relative position" of the three gratings is calculated by inverting the intensity equation to find the phase (see Eq. 3.13) which is then multiplied by $p/2\pi$. Figure 3.4 shows a frequency spectrum of this position noise.

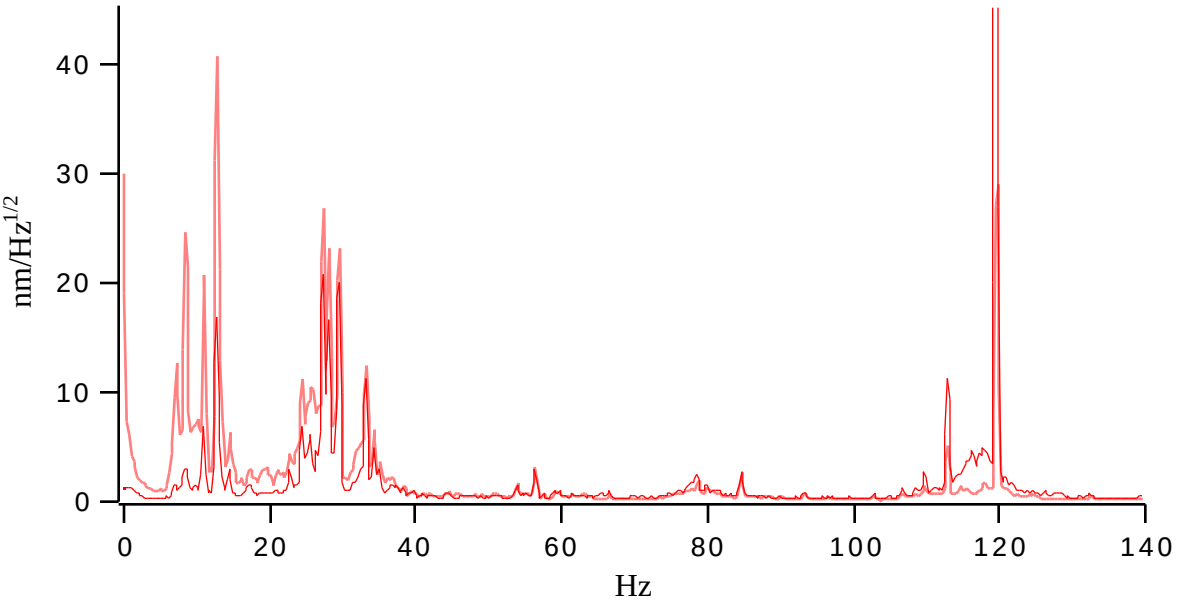

Figure 3.4. Position amplitude spectra showing the effect of the active vibration damping system. The dashed line shows the relative grating motion measured by the optical interferometer. The solid line is with the active servo on (120 Hz peak is 67 nm/Hz$^{-1/2}$). In both cases the rms motion is 60 nm. Note the dramatic reduction in the low frequency noise with the servo on (a factor of 10 at 1 HZ).

We have controlled the effect of inertial noise by reducing its sources, and by vibration isolation. We remove the noise caused by the high vacuum pumps that must be attached to the machine by

turning off some of the worst offenders during data taking. Specifically, we turn off the water flow in the cooling baffle of the diffusion pump on the main chamber which is a major source of high-frequency (100 Hz) noise. It is possible to turn this water off for about 5 min without a significant pressure rise. The effect of mechanical main roughing pumps was limited by moving them ~4 m from the machine, at the end of flexible forelines. The remaining rough pump (on the detector chamber) is also shut down during data taking.

Vibration isolation systems are low-pass filters for inertial noise. Passive systems can be modeled as a mass attached to the noisy system by damped springs. Active systems sense absolute position and apply this signal through a feedback network to a position transducer[27]. In either case the noise is random motion specified by a generalized power spectrum (usually in position or acceleration). The response of the isolated mass can be predicted from the transfer function of the isolation system.

Figure 3.5 shows schematics of idealized passive and active systems. Typical passive systems for large masses (>100 kg) have a Q of 1.5-3 and a resonant frequency of 2-10 Hz. For small masses passive systems can easily be combined to get higher order inertial noise filters: lead and rubber stacks are commonly used[28]. A common difficulty with these passive systems is the nonlinearity (increasing k at low ω) of rubber springs for *small* displacements. The chief difficulty with passive systems is their performance near DC.

[27] More generally an active vibration isolation system may sense some other quantity such as acceleration, or relative position (our case), and may apply the feedback to a force transducer.

[28] I have constructed such systems to test for the noise floor of our accelerometer.

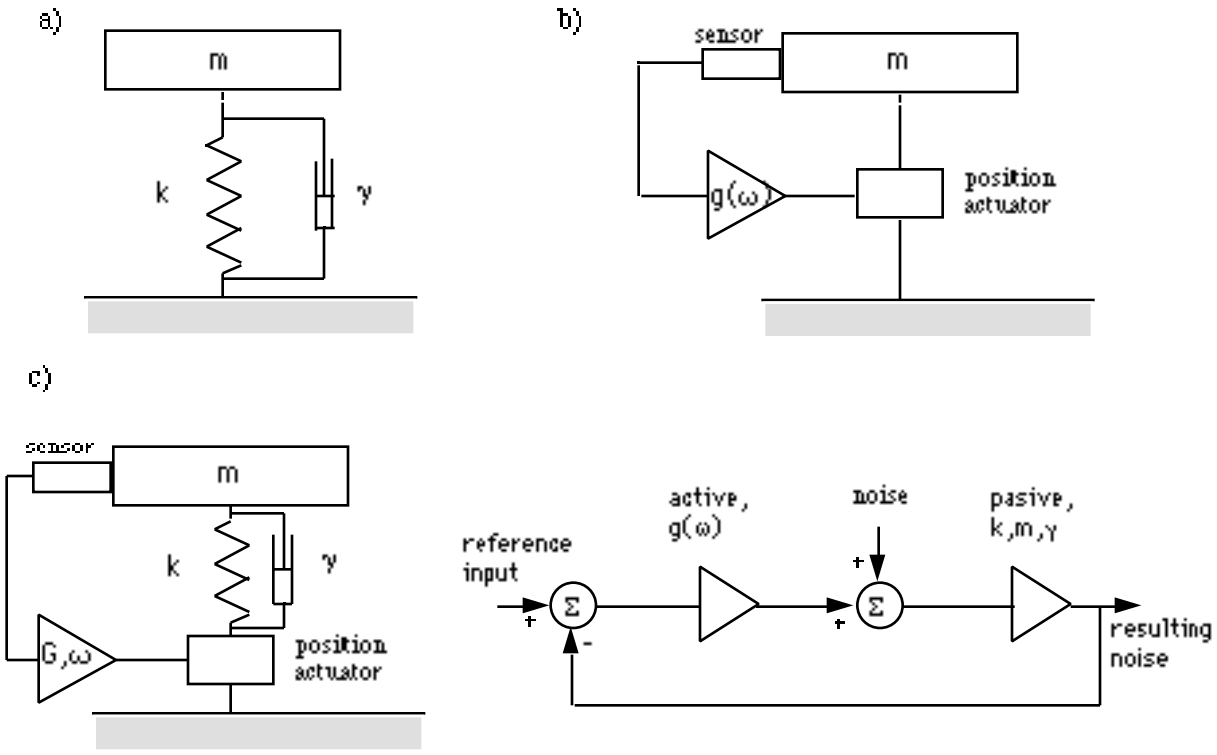

Figure 3.5. Schematics of vibration isolation systems: a) a simple passive system, b) an idealized active system, c) a simple (realistic) active system and its network diagram. In all cases the floor is modeled as a infinitely-massive source of position noise with amplitude spectrum $x_n(\omega)$.

For the ideal active system of fig 3.5-b the noise to position transfer function is given by $g(\omega)/(1+g(\omega))$ where $g(\omega)$ is the transfer function for the feedback network. In reality active systems are always coupled to passive resonances that set a limit to their performance. Figure 3.5-c shows the schematic and network diagram for a more realistic active system. In this system the resulting motion x_{out} is calculated from the position noise x_n, the reference position x_{ref}, and the passive and active-system gains:

$$x_{out} = \frac{g_p g_a x_{ref} + g_p x_n}{1 + g_a g_p} \tag{3.5}$$

At DC with $x_{ref}=0$ the noise-output transfer function is given by

$$\frac{x_{out}}{x_n} = \frac{g_p}{1 + g_a g_p} \tag{3.6}$$

The passive-system limits the performance of the active system by limiting the amount of gain that may be used in g_p before the combined system oscillates. The limit is simply the stability condition that the phase of $g_p(\omega)g_d(\omega)$ not be $-\pi$ when the amplitude is greater than unity.

We use an active system to remove the relative position noise from the translation stages. It uses the position sensed by the optical interferometer to apply feedback to a PZT on the **x** axis of the middle grating stage. This system is very similar to the "realistic" active system described above in the last paragraph. The key difference is that the position sensor in the real system is nonlinear—position is given as a function of optical fringe intensity in Eq. 3.12, it is only linear in position near the middle of a fringe. Figure 3.6 shows a simplified schematic of the feedback network. The gain of this system is limited in the manner described above by coupling to a resonance at about 130 Hz. Figure 3.4 shows the actual performance of the system as measured by the reduction in noise.

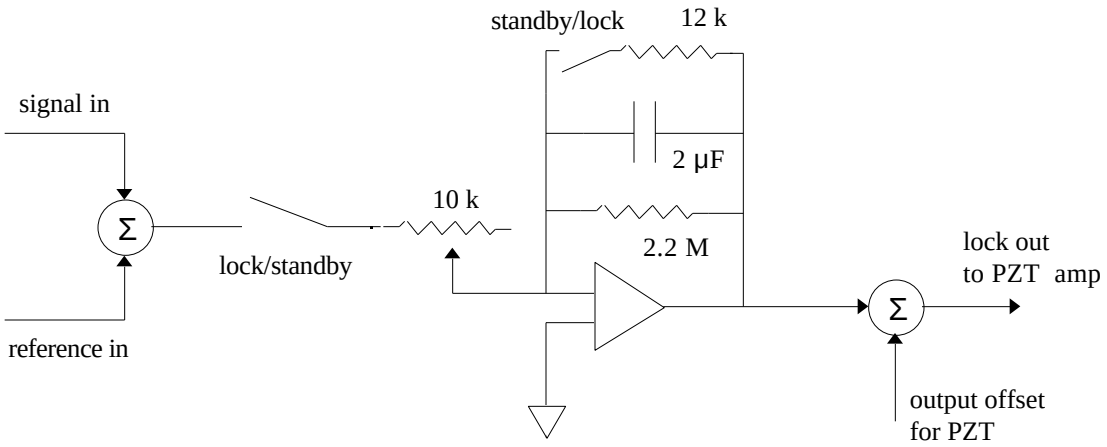

Figure 3.6 Schematic of the optical interferometer feedback circuit. The 3 dB point of the integrator is at a frequency of 0.04 Hz. We usually operate the circuit with a DC gain of a few hundred.

We have experimented with a number of passive isolation systems, two of which are permanently (ha!) incorporated into the machine. The turbo pump on the detector chamber makes a lot of noise at 1 kHz, about 50 nm on the accelerometer and 120 nm in relative grating motion measured with the optical interferometer. We

isolated this pump by hanging it on vacuum bellows which acts as a spring to support the weight of the pump with a resonant frequency of ~1 Hz. The bellows system reduced the acceleration noise by a factor of ~200, enough to make the relative motion noise undetectable. Another serious noise source was the two large mechanical rough pumps. We removed most of this noise by making "u"-shaped vacuum fore-lines with very low spring constants which act as two pole filters for noise coming from the wall mounted vacuum manifold.

The whole experimental apparatus may be isolated from floor noise by a passive system consisting of separate resilient feet. We have devised two such systems, one with ~10 cm-high pneumatic feet, and the other consisting simply of rubber pads. The pneumatic system has a resonant frequency of a few Hz for transverse (**x**) axis motion of the machine, and it successfully reduces the RMS acceleration by an order of magnitude (see figure 3.7). However such systems have an undesirable side effect; they translate transverse floor noise into rotational motion due to the nonsymmetric mass distribution of the machine. For this reason we have so far operated our interferometer without the floor noise isolation system. More work is necessary to determine the best compromise between transverse isolation and the generation of rotational noise.

3.B.ii.2 alignment

The fringe contrast of an interferometer depends on the alignment of it's beam splitters. In the three grating geometry that we use, there are four relevant kinds of alignment requirements.

1. Equality of the spacing of the three gratings along the (**z**) axis of the beam.
2. Alignment of the grating lines with the height axis of the beam, i.e. with the collimation slits.
3. Rotation of the gratings about the grating lines, the **y** axis. The gratings should be in a plane normal to **z** in order to prevent foreshortening of the grating periods.

4. Alignment of the gratings with respect to rotations about **z** (the beam axis). They must be precisely aligned with respect to each other, and roughly aligned to the slits (condition 2).

In addition, because of the limited height (along the grating lines) and width of the gratings we used, there are two requirements on the positions of the gratings:

5. Alignment with respect to translations along **x**.

6. Alignment w.r.t. translations along **y**.

It is difficult to calculate the effect on fringe contrast of unequal grating spacing (requirement 1). This problem was one of the motivations for attempting the numerical simulation of the experiment described in chapter 2, and it is the only method I know of for calculating the contrast as a function of grating spacing. The grating spacing is fixed by the positions of the flanges and the design of the translation stage assemblies. It is 0.663±0.003 m, with a relative spacing error of 0.7%. The calculated contrast loss for this spacing error is 3% (see fig 2.4).

The interference pattern formed by the first two gratings makes a moire pattern after transmission through the third grating. The period and direction of this moire pattern is a function of grating alignment errors of type 3 and 4, and of the differences in the grating periods. In our case the grating period and **y** axis (type 3) errors are insignificant. The contrast measured by the detector decreases with the number of periods of the moire pattern that it samples. The wave vector of the moire pattern, $\Delta\mathbf{k}$ is the difference between the $\mathbf{k}_{fringe}$ of the fringe pattern formed by the first two gratings and the wave vector of the last grating (fig 3.x).

$$\mathbf{k}_{fringe}=\mathbf{k}_1-2\mathbf{k}_2 \qquad \Delta\mathbf{k}=\mathbf{k}_{fringe}-\mathbf{k}_3=2\mathbf{k}_2-\mathbf{k}_1-\mathbf{k}_3 \tag{3.8}$$

Note the similarity of this formula to that of Eq. 3.3; both are based on similar symmetry arguments. The contrast reduction factor is calculated by finding the average of this moire pattern over the area of the detector[29].

[29] Note that this condition ignores the degree of overlap of the interfering spots. For our atom interferometer this requirement is trivial, but it is significant for the optical interferometer. Equation 3.9 is sufficient when the angle of diffraction is much less than the angular size of the beams, that is when $h/2l >> p/\lambda_{db}$. This means that we can align the atom interferometer by turning only one grating, but we must adjust two for the optical case.

$$\frac{\int_{det} e^{-i\,\mathbf{r}\cdot\Delta\mathbf{k}}\,dA}{A} \approx \frac{\sin^2(\Delta\mathbf{k}\,\mathbf{w})\sin^2(\Delta\mathbf{k}\,\mathbf{h})}{(\Delta\mathbf{k}\,\mathbf{w})^2\quad(\Delta\mathbf{k}\,\mathbf{h})^2} \tag{3.9}$$

A good approximation is to require that $\Delta\mathbf{k}\cdot\mathbf{w}$ and $\Delta\mathbf{k}\cdot\mathbf{h}$ be less that $\pi/2$, where **w** and **h** are the width and height of the detector. For the 0.2 μm-period gratings and a 1 mm × 25 μm-detector ("standard configuration") this requirement means that the gratings must be aligned about the **z** axis (requirement 4) to better than 10^{-3} radians. This is our most difficult alignment problem; its solution is detailed below.

a)

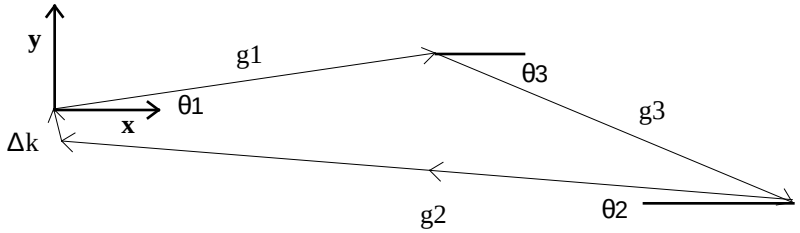

b)

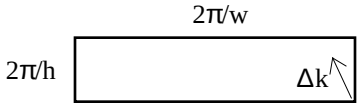

Figure 3.x: a) shows how the wave vector ($\Delta\mathbf{k}$) of the moire pattern sampled by the detector is derived from the **k**'s for the three gratings. b) shows how restrictions on $\Delta\mathbf{k}$ are imposed by the height and width of the detector.

The effect of rotations about the grating lines (requirement 3) can be calculated by considering it as a change in the effective grating period. In the momentum-space picture given above this is equivalent to taking $|\mathbf{k}_{eff}|=\mathbf{k}\cdot\mathbf{x}$ for each grating. Luckily this effect is

second order in the angular misalignment because $k_{eff}=k\cos(\theta_y)$. For the standard configuration all that is required is alignment to less than 3×10^{-2} radians. This precision is easily achieved by the original machining tolerances so that no alignment is needed during normal operation.

The vertical positions of the gratings must be collinear with the detector, vertical-slit, and beam skimmer. These adjustments are performed with a telescope when the oven is removed. With a light behind the detector the various elements are adjusted in turn by aligning them with the telescope cross-hairs. The estimated errors are ~100 μm, which is sufficient because the shortest grating (the middle one) is 500 μm-high. The skimmer is positioned last, and then the nozzle is aligned to it by maximizing the hissing sound heard when the argon jet strikes the skimmer (with the apparatus open to the air). During this process the horizontal positions (**x** axis) are roughly aligned, but they can only be accurately aligned with the atom beam during operation.

In addition to horizontal and vertical alignment, the telescope is also used to align the gratings with the slits, and to roughly align the slits with the detector. The first slit alignment is not critical because the beam is only 300 μm-high at its position, thus the angular tolerance is ~0.1 rad (20 μm-width over 300 μm). The second slit must be parallel to the detector wire to ~0.02 rad in order for the detected beam width to be a minimum. This alignment is done with the beam operating by repeatedly scanning the detector to measure the FWMH of the beam, which is then minimized by rotating the second slit under computer control. The gratings are aligned parallel to the second slit (requirement 2) by eye through the telescope. Our estimated error is ±0.05 rad.

The alignment of the grating lines to each other (requirement 4) is done using optical diffraction from the 4 μm-period support structure gratings[30]. This is possible because the fabrication method

---

[30] The experiment was originally planed with different alignment method (Anderson, 1988). I will describe it here because it has advantages that may make it preferable in the future (and because a great deal of time was spent developing it). The method is based on using the fine period gratings as optical polarizers. A beam polarized at ~45° to the grating axis is passed through a photoelastic modulator (PEM) with strain field perpendicular to the grating lines. The beam then passes through the grating and is detected. A lock-in amplifier is used to monitor the signal at twice the frequency with which the PEM is modulated (50 kHz in our case). For small angles the resulting signal is *linearly* proportional to the angle between the PEM and the grating. The precision of this method is very high, we routinely get 10^{-5} rad.

ensures that the support structure grid is perpendicular to the fine grating to the precision with which either is defined (see chapter 2.x). In the first step of the alignment procedure the three gratings are arranged collinearly along a HeNe laser (λ=0.63 μm) beam. Next the gratings are aligned normal to the laser beam using their back reflections, this can easily be done to better than 10^{-3} rad. A tensioned wire is used to define a line parallel to the laser beam but displaced from it by ~1 m, which is most simply accomplished with plumb lines hanging from the wire which is above the laser beam. Finally, the gratings are rotated so as to bring the high-order diffracted-spots from the support structure on to the wire. The precision with which this can be done is limited by the width of the gratings: they are only 40 (120) μm-wide[31] so the diffracted orders have a single slit pattern along **x** which is 16 (5) mrad wide. The accuracy is limited by the straightness of the wire, and by subtle diffraction effect which result in non-coplanar diffracted orders. Because of the dimness of the high-order diffracted-spots (we used 5^{th} or 6^{th} order) it is necessary that most of this operation be performed in near-total darkness (Plant 1973).

The alignment is performed with the flanges which hold the gratings flipped over (rotated 180° about **z**) and resting on their respective flange mounts[32] ("o"-rings removed). Because the gratings are rotated exactly 180° they maintain their relative alignment when they are flipped again to replace them inside the vacuum envelope. This is true *independent of the orientation of the flange mounts*, depending only on the top and bottom of the flange being coplanar. Our flanges are flat to 10^{-3} rad.

Using this method we are able to align the grating lines to ±1 mrad. The method has the advantage that it not only aligns the gratings to each other, but also aligns them to the vertical if the plumb lines are used. This is important because, due to the gravitational phase shift being proportional to v^2, the fringe contrast falls off steeply with tilt angle (see figure 4.x).

However, there are serious accuracy problems. We found angular offsets as high as 10^{-2} rad.

[31] We used two sizes of gratings (see chapter 1.x), the short wide one in the middle and the tall narrow ones at each end.

[32] It can not be too strongly recommended that this flipping task not be delegated to individuals prone to dyslexic fits.

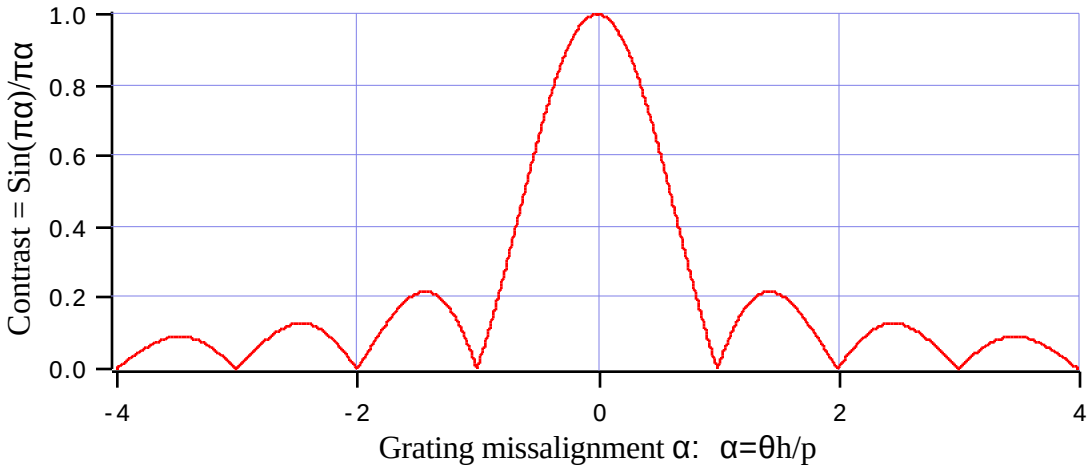

Figure 3.8: Contrast loss as a function of **z** axis misalignment of the gratings. The effective misalignment angle θ is given by $\theta_{g1}+\theta_{g3}-2\theta_{g2}$, h it the detector height and p is the grating period.

Final alignment of the gratings is done by maximizing the fringe contrast with the interferometer operating. The expected fringe contrast as a function of this alignment is shown in figure 3.8. The strategy for searching for interference (non-zero fringe contrast) must be carefully considered. It may be useful to reduce the effective height of the gratings using the vertical height slit. This has the effect of reducing the interference signal while increasing tolerance for grating misalignment. The signal to noise ratio is reduced with decreased slit height because of the reduction in total signal (gaussian statistics s/n $\sqrt{n}$) and because the hot-wire background remains the same. Because the contrast is so much higher when the misalignment angle is less 0.5 h/p, the reduction in signal to noise may be worthwhile.

3.B.iii Data

3.B.iii.1 Data collection

Data are collected with the object of determining if there is an interference signal, and if one is found, of measuring its phase. The method is to vary the interferometer phase while recording the atom count rate, and then to examine the record for a correlation between phase and rate.

In the analysis that follows I will assume that the interferometer signal S is determined by the controlled phase ϕ_c according to:

$$S=I(1+C\sin(\phi_c+\phi_n+\phi_v(\alpha))) \tag{3.10}$$

Where I is the total beam intensity transmitted through the three gratings, and C is the fringe contrast. Where ϕ_c is a known incremental phase applied by the experimenter for the purpose of measuring the other phases. If one wishes to measure the phase shift due to some applied potential, then ϕ_v is a phase shift and the potential is assumed to be controlled through a parameter α. In an experiment of this type one wants to measure the function $\phi_c(\alpha)$, e.g. if one desires to measure the effect of electric fields, α would be the voltage applied to the field plates. The phase due to all factors that are not deliberately controlled is ϕ_n, i.e. this is the rug under which all but α and the *intended* value of ϕ_c are swept. The measured count rate R is equal to S convolved with the detector time response $\rho(\tau)$, and added to the hot-wire background B:

$$R(t)=B(t)+\int_{-\infty}\rho(\tau)S(t+\tau)\,d\tau \tag{3.11}$$

I and $\bar{B}$ Are easily measured by using the beam blocking shutter to modulate I; typical values are $\bar{B}$=50 Hz and I=100 Hz. $\rho(\tau)$ can be determined by modulating the shutter and recording the time response when I is made large by removing the gratings, typical 20-80% response rise times are 5 to 50 msec.

In general it is advantageous to modulate ϕ_c in order to average out noise in I and B, and so reduce the error in the determination of C and $\phi_n+\phi_v$. We modulate ϕ_c by changing the relative positions of the three gratings. This is accomplished by modulating the reference voltage that is input to the lock loop; typically we use a triangle wave of amplitude ~1/3 of an optical fringe (~1 μm) at ~0.3 Hz. While we modulate the reference input we record $R(t)$ and the value of $\phi_c(t)$ measured by the optical interference signal.

The amplitude of the ϕ_c modulation is calibrated by the optical interferometer which in turn is calibrated by measuring the intensity limits of its interference signal. We turn off the lock loop and drive the optical interferometer through several fringes while the computer records the intensity with an Analog to Digital Convertor

(ADC). From a density histogram we derive the intensity limits in ADC counts. The phase ϕ_c is then calculated from the measured intensity and the ratio of optical- to atom-grating period by

$$\phi_c(v) = \frac{p_{\text{optical}}}{p_{\text{atom}}} \operatorname{asin}\left(\frac{v - \frac{1}{2}(v_{\max} - v_{\min})}{\frac{1}{2}(v_{\max} + v_{\min})} \right) \tag{3.12}$$

where v is the measured optical intensity. This procedure removes gain calibration as a source of error by comparing measured ADC counts, although ADC linearity may still be a problem. Thus, the measured $\phi_c(t)$ departs from the "intended" ϕ_c due only to these calibration questions.

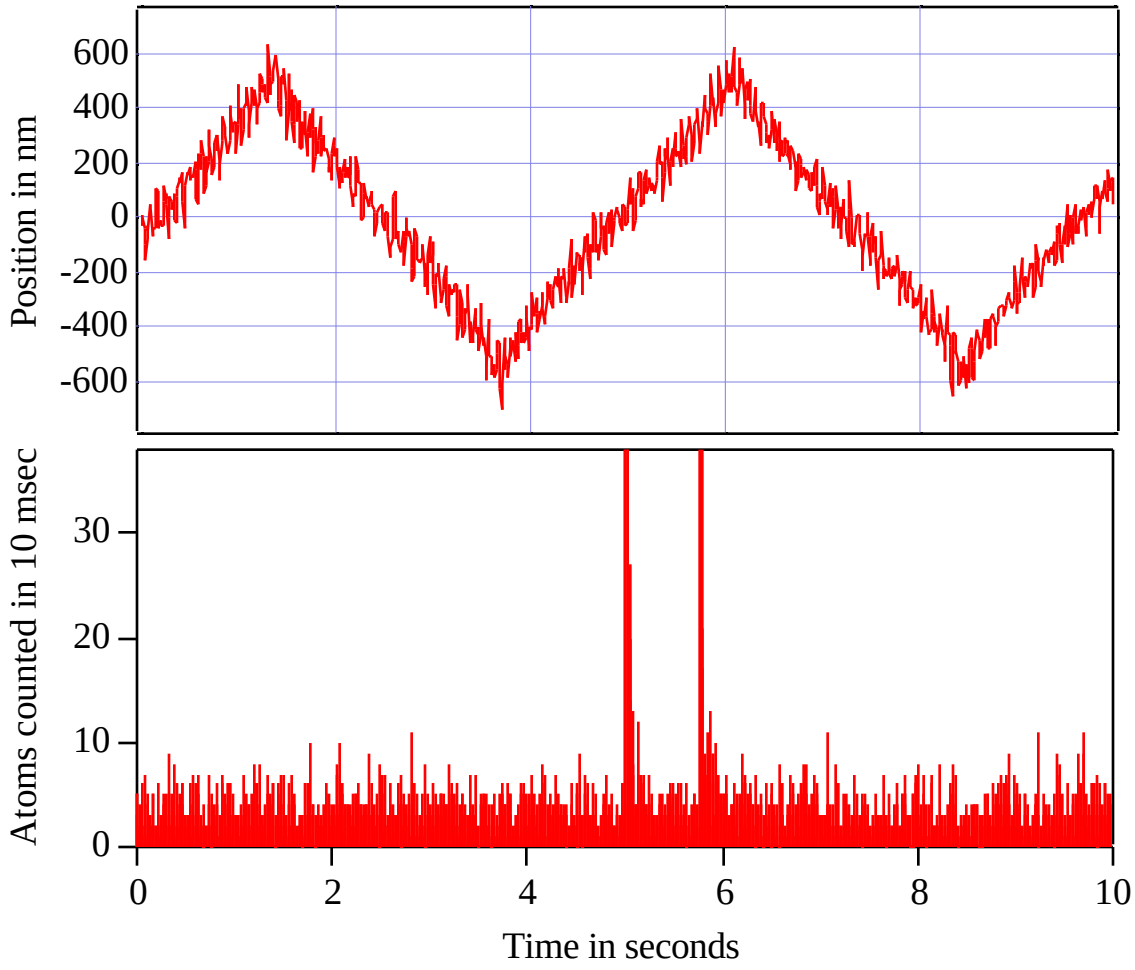

Figure 3.9: Ten seconds of raw data. The upper graph shows the relative transverse position of the interferometer gratings as measured by the optical interferometer. The lower graph shows the number of atoms per 10 msec bin. Peak heights of the off-scale hot wire noise bursts are 92 and 304 counts respectively.

The 0.3 Hz ϕ_c-modulation is very effective at removing the noise in I because measured beam intensity changes on 10's of minute time scales. However, the ϕ_c-modulation frequency is to low to remove much of the high-frequency burst noise in B. It is impossible to significantly increase the frequency because of the time response of the detector. The worst of the hot-wire noise is removed in the computer by an algorithm that detects and removes the bursts. The beginning of a burst is easily recognized because they typically have

rise times of ~10 msec and peaks of 100 $\bar{R}$, the algorithm removes all data from the start of the burst until the signal falls below $\bar{R} - 2\sqrt{\bar{R}}$.

We usually take data for 200 sec in 10 msec bins. During data collection we shut off the worst sources of vibration noise: the water flow through the cooling manifold of the main chamber diffusion pump, and the mechanical pump on the detector chamber. Shutting off these pumps currently limits our data taking intervals to about 7 minutes, but this problem could be easily solved.

3.B.iii.2 Data analysis: random errors

After taking a data set (200 sec is about 150 K Bytes) the data are transferred from the experiment control PC-AT to a faster computer (Mac IIci) for analysis. The data analysis program first determines the optical fringe limits by computing a histogram of a calibration data-set and allowing the user to indicate the fringe limits. The phase ϕ_c is then calculated for each data point using Eq. 3.x. Noise bursts are removed from the $R(t)$ record by the algorithm described above, with no reference is made to ϕ_c. A density histogram of ϕ_c is calculated from which we choose a section of the data that is an integral (m) number of grating periods wide ($2\pi m$ in ϕ_c). Ideally the modulation amplitude is adjusted so that the ϕ_c data spans an integral number of periods and no data are lost. However, because of the residual noise in the lock-loop and the consequent noise in the measured $\phi_c(t)$, the data density departs substantially from the square profile that would result from pure triangle wave modulation. Typically this noise results in about one third of the data being discarded.

The selected R datum then sorted and binned according to its corresponding ϕ_c value.

$$\text{bin}_n = \sum_{\frac{2\pi p}{4} n < \varphi_c \le \frac{2\pi p}{4}(n+1)} R(\varphi_c) \tag{3.13}$$

Where n {0, 1, ..., 4m-1}, that is four bins per period for an integral (m) number of periods. Each bin is then normalized by dividing it by the number of data points summed in that bin. Finally the signal amplitudes in the sine and cosine phases are calculated by multiplying the bin_n data by square waves of period 4 (in n). The amplitude in the sine phase A_s is given by

$$A_s=\frac{\pi}{8m}\sum_{n=0}^{4m-1} \mathrm{bin}_m \xi(\mathrm{floor}(n/4)) \tag{3.14}$$

where ξ is 1 for even integers and -1 for odd. Similarly, A_c is calculated by replacing n/4 with (n+1)/4. The amplitude is $A=\sqrt{A_s^2+A_c^2}$, and so the measured contrast is A/I, where I is the mean intensity. The measured phase is calculated from the amplitudes by

$$\phi_n+\phi_v=\mathrm{atan}\left(\frac{A_s}{A_c}\right) \tag{3.15}$$

Assuming that the data are evenly distributed over the bins and that the statistics in each bin are gaussian, the error in the phase is

$$\frac{1}{\sqrt{n\left(A_s^2+A_c^2\right)}}. \tag{3.16}$$

Where n is the mean number of points per bin.

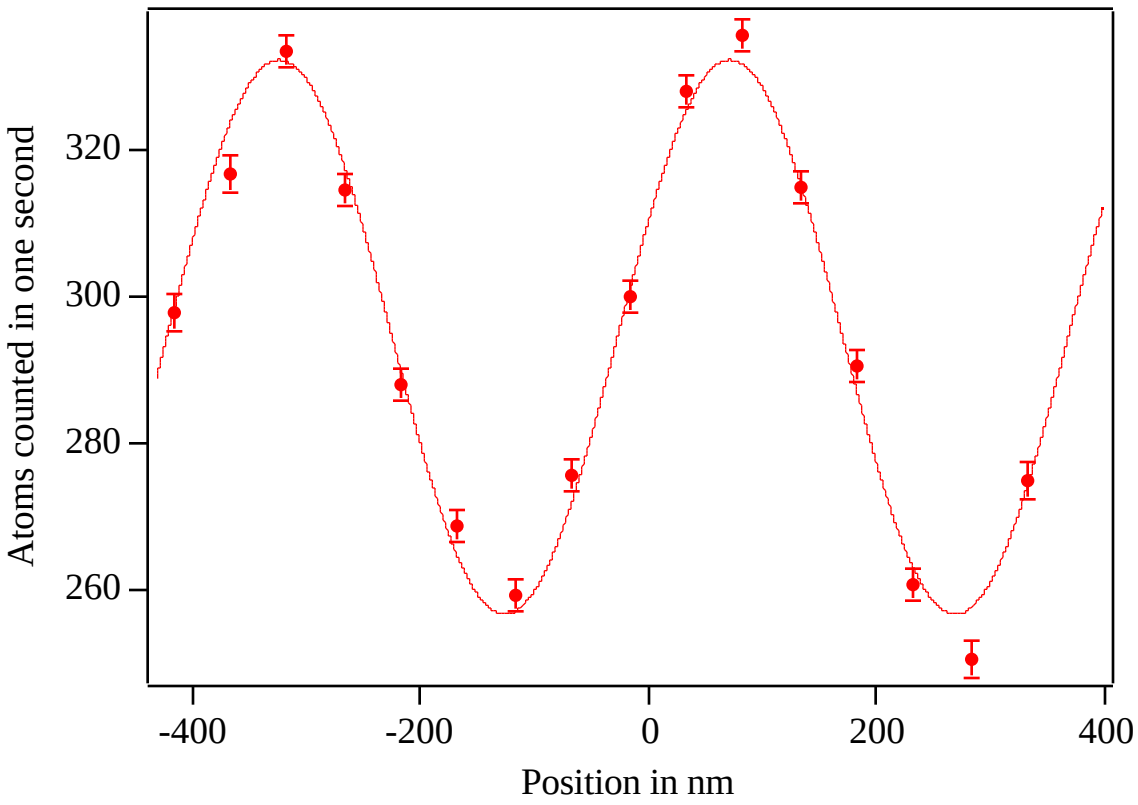

Figure 3.10. Interference signal from 400 seconds of data. Background hot wire noise of 40 Hz subtracted. Error bars are one standard deviation assuming Poissonian noise, and slightly underestimate the noise because of the super-Poissonian character of the hot wire background.

It is difficult to choose the optimal method for analyzing the $R(\phi_c)$ data because it is not equally spaced in ϕ_c. Standard Fourier transform techniques are inapplicable to unequally spaced data; instead one must resort to generalized periodigram methods or divide the data into equally spaced bins. Neither solution is very satisfactory because of the difficulty of assessing the expected noise power at each frequency. Because we already know the period to better accuracy than we can easily expect to measure it, our data analysis method is able to avoid these pitfalls. The method we use (square wave power in an integral number of periods) escapes from the difficulties by using the minimum number of bins. It has two disadvantages: the data wasted to keep the number of periods

integral and the loss of signal to noise ratio incurred by using a square wave.

3.B.iii.3 Systematic errors

We have no way of determining the absolute phase in the interferometer, so systematic errors in our phase measurements are caused by drifts in the noise phase ϕ_n. Assume that one wishes to measure the phase shift $\phi_v(\alpha)$ as a function of some applied potential parameterized by α. The method would be to set α and vary ϕ_c in order to measure $\phi_v+\phi_n$. Repeating this sequence for many values of α allows the determination of the combined phase as a function of α: $(\phi_v+\phi_n)(\alpha)$. Assuming that ϕ_n is independent of α this in principal allows the determination of $\phi_v(\alpha)$ with no error. In practice time limitations make is very hard to average out low frequency drifts in ϕ_n, so they become the limit on the accuracy with which $\phi_v(\alpha)$ can be measured. I now turn to a discussion of the causes of drift in ϕ_n.

The PZT which is mounted of the middle grating for fine rotation adjustment also translates it relative to the optical grating. PZTs suffer from "creep", a long time constant asymptotic approach to there equilibrium position after the control voltage is changed. This is the most easily controlled of the causes of ϕ_n drift, a wait of 1 hr will essentially remove it. However it causes significant difficulties in adjusting the grating angles for maximum contrast.

The optical interferometer removes all of the large 1-10 μm hr^{-1} thermal drifts in the positions of the translation stages. However, temperature changes acting over the short (~5 cm) lengths separating the optical from the atom gratings could still cause significant drifts. For 0.4 μm-period gratings the drift is ~100 rad $^{\circ}C^{-1}$ if you assume that the stages expand independently.

If the optical and atom interferometers are not coplanar then vertical **y** axis drifts in the translation stage positions will cause drift in ϕ_n. For small angles θ between the planes, the relative position drift will be the product of θ and the vertical drift. We estimate vertical drifts of 1-10 μm hr^{-1} from calculation of the thermal drifts and measurements of the **x** axis drift. Therefor, to achieve 0.1 rad hr^{-1} phase stability for 0.4 μm-period gratings θ must be less than 10^{-2} rad. At present we have only aligned θ to 0.1 rad, but 10^{-3} rad should be achievable with plumb line techniques.

Drifts in the calibration of the optical interferometer, that is in the fringe intensity limits, cause drifts in the effective ϕ_c. These drifts can be caused by bending of the laser beam optics relive to the optical gratings. We remove much of the effect of this drift by recalibrating the fringe limits for each data set we take. The residual drift could probably be reduced further by using a differential detection scheme instead of the current single detector, or by an improving the laser mounting scheme.

4 An application: the COW experiment

In this Chapter I briefly discuss the possibility of using our interferometer for a repetition of the COW equivalence principal experiment. I include this discussion both because we are actually in the process of doing the experiment, and because it is a good example of the applications of atom interferometers discused in 3.A and of the data analysis covered in section 3.B.iii.

The COW experiment takes its name from the authors of the original paper—Colella, Overhauser, and Werner (1975). The experiment is a test of the Einstein equivalence principal in a quantum system, it is simply the use of a matter wave interferometer to measure the local gravitational acceleration, little g. The experiment may be regarded as interesting because it is the only system in which we can directly test the use of the mgh form of the gravitational potential in the Schrodinger equation.

The experiment consists of measuring the phase shift in the interferometer as a function of the tipping angle (between vertical and a normal to the interferometer's enclosed area). One then compares the measured acceleration calculated from the phase shift by Eq. 3.1 with the known value of g. In the language of Chapter 3.B.iii the tilt angle is α and the phase φ_v is given by 3.1 where $a=g\sin(\alpha)$, that is we are testing whether

$$\varphi_v = \frac{2\pi\tau^2}{d} g\sin(\alpha) \tag{4.1}$$

where d is the grating period and τ is the atom's transit time (L/v). In our interferometer with 4 μm-period gratings this gives $\varphi_v = 69\,\alpha$ for small α.

The quadratic dependence of the phase shift on the atom's velocity means that the contrast decreases quickly with increasing α. In addition, the phase $\varphi_v(\alpha)$ that is measured by varying φ_c differs from the φ_v that would be measured if the velocity width was zero. This difference results from the integration of Eq. 4.1 over the velocity distribution. Figure 4.1 shows the contrast loss and the phase error calculated for a 10% velocity width.

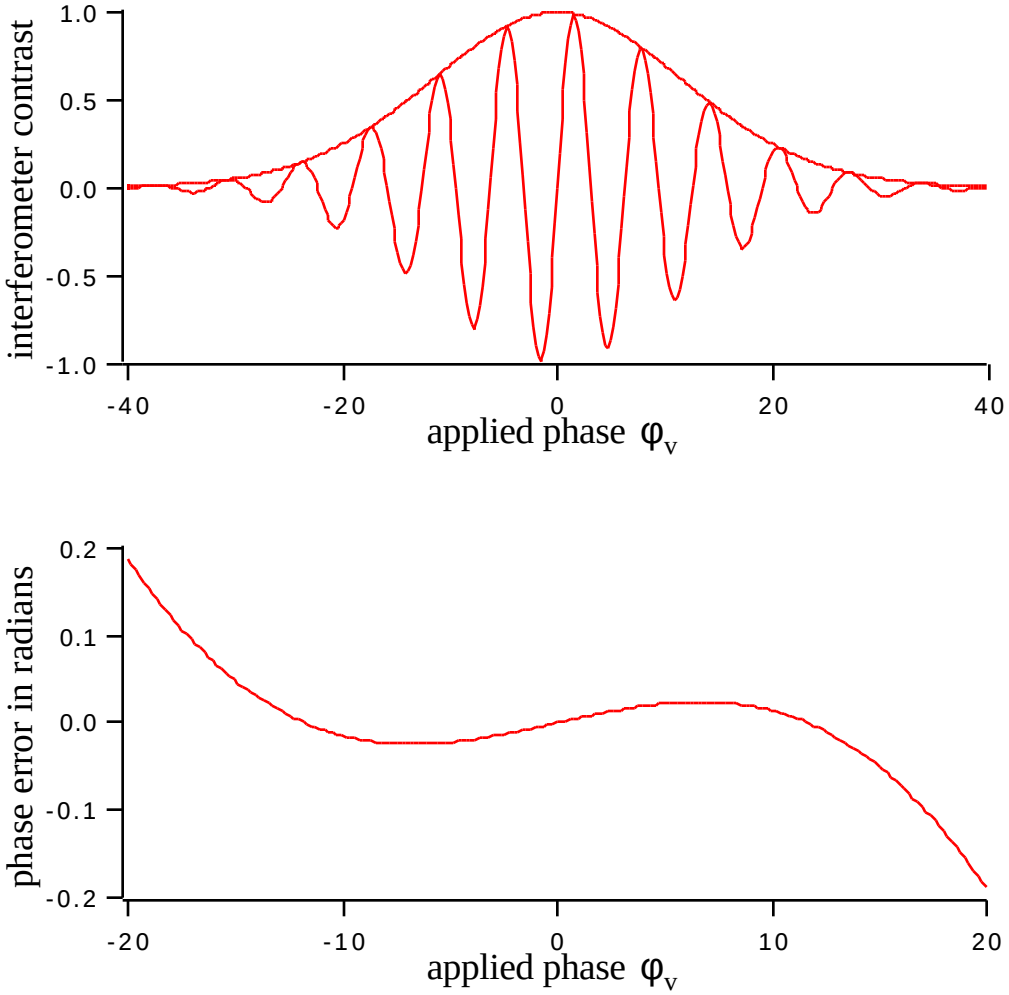

Figure 4.1. Calculated effect of phase shifts that are proportional to v^2 with a velocity width of 10%. The upper graph shows the contrast and the sine phase of the interferometer signal as a function of the applied phase. The lower graph shows the difference between the phase measured with a 10% velocity width, and with a single velocity.

It seems interesting[33] and feasible to measure g to a few parts in a thousand by this method. I expect this experiment to be limited by the following sources of error.

[33] Recent experimental tests with neutrons Werner (1988) show 0.8% (eight sigma) deviations from mgh. However, S. Chu (personal comunication with D. Pritchard) has recently done the experiment with atoms and found no deviation at the 10^{-5} level.

1. Motion of the optical gratings with respect to the atom gratings. If this relative motion is caused the by bending of the apparatus as it is tilted it represents a systematic error. The active position stabilization system should remove this, but only if the optical and atom interferometers are in the same plane.
2. Limitations in our knowledge of the of the mean velocity and velocity distribution. This can be measured either by diffraction from a grating of known period (difficult to get the distribution), or by laser florescence methods.

5 Conclusions

Is it reasonable to call the work described in this thesis science? This is a return to the issue raised in the introduction: are these experiments tests of theory or are they technologically novel demonstrations of well known facts. Unfortunately the reader is justified in assuming that no definitive answer will be given to this question.

The argument that the work is not science rests simply on the observation that no one is interested in the results as such. The considerable interest that these experiments have generated is due to their technological novelty, and to the simplicity with which they *illustrate* basic theory. Moreover, we do not think of ourselves as testing the theory. Had our atoms failed to show interference we would never have doubted the basic quantum mechanics, but rather would have used it to analyze what we were doing wrong.

It is argued that any confrontation of theory with fact constitutes science[34]. However, this argument is very unsatisfying. Historical study has clearly demonstrated that science does not proceed by blind testing of theory. For example, dropping stones to test Newton's theory cannot reasonably be called science. It is also argued that our work is science because it may make tests of interesting questions technologically possible (e.g. the Lense Thirring frame drag). This argument fails to make a distinction between science and technology, but perhaps this is unavoidable.

From a sociological standpoint the work is clearly science, because the community of people recognized as scientists are interested in it, and accept it as an appropriate endeavor. In the language of Lakatos (see below) it is part of an active research program.

Of course this discussion begs a definition of science, and unsurprisingly, I don't have a definitive one. For me, the scientific endeavor is the process of learning how to predict nature. That is, neither prediction or understanding alone are sufficient. This definition is motivated by the discussion in Lakatos (1970) from which I took the quote that opened this thesis. I think Lakatos is correct in rejecting Poppers' model in which science proceeds by the falsification of theoretical hypotheses; and in emphasizing the process, the dynamics of scientific research programs. In my words, the *process* of *learning*.

---

[34] This claim was recently made to me in a discussion of these issues with a number of respected profesionals in this field.

6 Acknowledgments

Any complex experiment is truly the work of many people, and this one is no exception. In the lab my most important coworkers were Chris Ekstrom, Bruce Oldaker, Quentin Turchette and Garth Zeglin. They provided much more than assistance, rather they were both collaborators and friends. I am lucky to have had opportunity to work with each of them.

The staff of the National NanoFabrication lab were an once friendly, helpful, and vital to the success of our experiment. It is a good place to work hard. Most of all I thank Mike Rooks the e-beam wizard.

Pritchard's group is an extraordinarily friendly place to work. Such a human environment is what keeps me coming in to face the monstrous grad school work load, an even makes it (usually) a pleasure. All members of the group have been consistently helpful and supportive, even in the face of my occasional turns to the "trail of destruction" school of science. A special award must go to Chris Helmerson, for his continual helpfulness far beyond the call of duty. It is also a pleasure to acknowledge quality help and friendly tolerance from the Klepner group.

Of course, Pritchard's group would be impossible without Dave Pritchard. I would like to thank him both as admissions officer, for helping to give me the chance to attend MIT (not a simple decision on my record), and as thesis advisor, for being such a stimulating and tolerant person to work for.

I owe a big debt to the people who got me into physics; most specially Paul Corkum, but also Marius Neimanis and Malcolm Graham.

Finally, I thank my parents for providing the support that makes it all possible.

7 References

Anderson, A., S. Haroche, et al. (1986). “Reflection of thermal Cs atoms grazing a polished galss surface.” Phys. Rev. A **34**: 3513.

Anderson, E. H., A. M. Levine, et al. (1988). Appl. Optics Lett. **27**: 3522.

Campargue, R., A. Lebehot, et al. (1974). Rarefied Gas Dynamics. Vol. X, (1974).

Ceglio, N. M., A. M. Hawryluk, et al. (1983). “X-ray phase lens design and fabrication.” J. Vac. Sci. B (4): 1285.

Ceglio, N. M., R. H. Price, et al. (1981). “Gold transmission gratings with submicrometer periods and thicknesses > 0.5 microns.” J. Vac. Sci. Technol. **19(4)**: 897.

Clauser, J. F. (1988). “Ultra-high sensitivity accelerometers and gyroscopes using neutral atom matter-wave interferometry.” Physica B **151**: 262-272.

Cohen-Tannoudji, C., J. Dupont-Roc, et al. (1989). Photons and Atoms. Wiley.

Colella, R., A. W. Overhauser, et al. (1975). “Observation of gravitationaly induced quantum interference.” Phys. Rev. Lett. **34**: 1472.

Estermann, I. and O. Stern (1930). “Beugung Von Molekularstrahlen.” Z Phys. **61**: 95.

Faulstich, A., O. Carnal, et al. (1990). Optics with a Supersonic Atomic Beam. In: International Workshop on Light Induced Kinetic Effects on Atoms, Ions, and Molecules, Elba (Italy), L. Moi et al, eds., (1990).

Feynman, R. P. and A. R. Hibbs (1965). Quantm mecanics and path integrals. McGraw-Hill.

Habets, A. H. M. (1977). Supersonic expansion of argon into vacuum. PhD thesis, Technische Hogeschool Eindhoven.

Koskinen, J. and H. H. Johnson (1989). “Silicon nitride fibers using microfabrication methods.” Mat. Res. Soc. Symp. Proc. **130**: 63.

Kwong, Y. K., K. Lin, et al. (1989). “The apliction of rective ion etching in producing free-standing microstructures and its effect on low-temperature electrical transport.” JVST-B **7**(Nov/Dec 89): 2020.

Lakatos, I. (1970). Falsification and the Methodology of Research Programmes. Criticism and the Growth of Knowledge. Cambridge, Cambridge University press. 91-196.

Lee, K. L., H. Ahmed, et al. (1984). “Fabrication of Ultra-Thin Free-Standing Wires of Silicon Nitride.” Electronics Lett. **20**(29 Mar 1984): 289-291.

Maier-Leibnitz, H. and T. Springer (1962). “Ein Interferometer fur langsame neutronen.” Zeitschrift. f. Phys. **167**: 368.

Marion, J. B. and M. A. Heald (1980). Clasical Electromagnetic Radiation. Academic Press.

Marton, L., J. A. Simson, et al. (1954). “An electron interferometer.” Rev. Sci. Inst. **25**: 1099. The original (but less complete paper is: Marton, L., J. A. Simpson, et al. (1953). “Electron beam interferometer.” Phys. Rev **90**: 490-491.

Mollenstedt, G. and H. Duker (1954). “Frensnelscher interferenzversuch mit einem biprisma fur elektronenwellen.” Naturwissenschaften **42**: 41.

Moore, J. H., C. C. Davis, et al. (1983). Building Scientific Apparatus. Addison-Wesley.

Nellessen, J., J. Werner, et al. (1990). “Magneto-optical compression of a monoenergetic sodium atomic beam.” Opt. Com **78**: 300-308.

Rauch, H., W. Treimer, et al. (1974). “Test of a single crystal neutron interferometer.” Phy. Lett. **47A**: 369.

Rauch, H., A. Zeilinger, et al. (1975). “Verification of coherent spinor rotation for fermions.” Phys. Lett. **54A**: 425.

Schattenburg, M. l., E. H. Anderson, et al. (1990). “x-ray/VUV transmission gratings for astrophysical and laboratory applications.” Phys. Scripta **41**: 13-20.

Serri, J. (1974). Angular distributions for rotational energy transfer: $Na_2(v''=0, j_i) + Ar -> N_2(v''=0, j_f) + Ar$. PhD thesis, MIT.

Shull, C. G. (1988). N beam brightness, personal comunication. The brightness of the best thermal n sources is about 10^{14} str^{-1} cm^{-2} sec^{-1}.

Silverman, M. P. (1987). “On the feasibility of observing electron antibunching in a field-emission beam.” Phys. Lett. A **120**: 442-446.

Tennant, D. M., J. E. Bjorkholm, et al. (1990). “Free standing silicon microstructures for soft x-ray masks and cold atom focusing.” JVST-B (Nov-Dec 90):

Werner, S. A., H. Kaiser, et al. (1988). Physica B **151**: 22-35.

Werner, S. A., J. Staudenmann, et al. (1979). “Effect of the Earths Rotation on the Quantum Mechanical phase of the Neutron.” Phys. Rev. Lett. **42**: 1103.

Zeilinger, A., R. Gahler, et al. (1988). “Single- and double-slit diffraction of neutrons.” Rev. Mod. Phys. **60**(4 oct 88): 1067-1073.

8 Appendices

Publications associated with this thesis work.

1. Pritchard, D. E. and D. W. Keith (1989). "Matter wave optical systems in which an atomic beam intersects a diffraction grating at grazing incidence". U. S. Patent 4,886,964.
2. Keith, D. W., M. L. Schattenburg, et al. (1988). “Diffraction of Atoms by a Transmission Grating.” Phys Rev Lett **61**(3 Oct 1988): 1580-1583.
3. Keith, D. W. and D. E. Pritchard (1989). "Atom Optics". New Frontiers in QED and Quantumoptics, Plenum Press.
4. Keith, D. W. and M. J. Rooks (1991). “Free-standing gratings and lenses for Atom optics.” accepted for JVST-B (Nov/Dec 1991). Still in progress.
5. Keith, David. W., Christopher. R. Ekstrom, Quentin A. Turchette, and David E. Pritchard. (1991). “An Interferometer For Atoms.” accepted for Phys. Rev. Lett.

Work that we are considering.

1. Quentin A. Turchette and David W. Keith concerning Numerical simulations of matter wave interferometers.

A1) Diffraction of Atoms by a Transmission Grating

Diffraction of Atoms by a Transmission Grating

D. W. Keith, M. L. Schattenburg, Henry I. Smith, and D. E. Pritchard
Massachusetts Institute of Technology, Cambridge, Massachusetts 02139

Abstract

We have demonstrated a novel diffraction grating for atoms. A collimated beam of sodium atoms with a de Broglie wavelength of 17 picometers was diffracted by transmission through an array of slits with a spatial period of 0.2 μm formed in a gold membrane. This is the first reported diffraction of atoms by a fabricated periodic structure. Our transmission diffraction grating for atoms can divide or recombine an atomic beam coherently, and may provide the easiest route to the realization of an atom wave interferometer.

We report the first observation of the diffraction of atoms from a fabricated diffraction grating. More specifically, we observed diffraction of a highly collimated beam of atomic Na from a transmission grating of narrow slits in a gold foil. We note that the diffraction of atoms by an edge has been previously observed[35], as well as the diffraction of atoms reflected from the periodic potential of a crystal surface[36], and the diffraction of atoms by a standing wave of light[37]. Our observation seems significant because these transmission diffraction gratings, when used as beam splitters and combiners, may be the best technology for the construction of an atom interferometer. We discuss this application at the end of this paper.

Our diffraction gratings, which were developed for soft x-ray spectroscopy, consist of a 0.5 μm thick, 9 × 4 mm array of gold bars each about 0.1 μm wide with 0.1 μm slits in between. The grating fabrication process is described in detail elsewhere[38]. The grating periodicity is established by exposing a photoresist film to a UV optical interference pattern (so-called holographic lithography). Subsequent processing yields a mask suitable for x-ray lithography which is used to form a relief grating in a 0.5 μm thick polymethyl methacrylate (PMMA) film. The substrate for the PMMA is a Si wafer coated with ~ 5 nm of chromium and ~10 nm of gold (the 'plating base'). Gold is electroplated to fill the slots in the relief grating, and then the PMMA is removed leaving the gold bars on the thin plating base supported by the silicon wafer. Because such a structure would be too weak to stand on its own, a 4 μm-period grating, formed by gold electroplating, is superimposed orthogonally onto the 0.2 μm-period grating, and a 150 μm-period grating is superimposed orthogonal to the 4 μm-period grating to form a support grid. Finally, the silicon is dissolved and the plating base is removed by ion beam bombardment leaving a free standing grating. Figure 1 shows

---

[35] J.A. Leavitt and F.A. Bills, Am. J. Phys. **37**, 905 (1969).

[36] I. Estermann and O. Stern, Z. Physik **61**, 95 (1930).

[37] P. E. Moskowitz, P.L. Gould, S. R. Atlas, and D.E. Pritchard, Phys. Rev. Lett. **51**, 370 (1983); P. J. Martin, B. G. Oldaker, A. H. Miklich, and D. E. Pritchard, Phys. Rev. Lett. **60**, 515 (1988).

[38] A. M. Hawryluk, N. M. Ceglio, R. H. Price, J. Melngailis, and H. I. Smith, J. Vac. Sci. Technol. **19**(4), 897 (1981); N.M. Ceglio, A.M. Hawryluk, and R.H. Price., Proc. S.P.I.E. **316** (*High Resolution Soft X-ray Optics*), 134 (1981); E. H. Anderson, C. M. Horwitz, and H. I.Smith, Appl. Phys. Lett. **49**, 874 (1983); H. I. Smith, E. H. Anderson, A. M. Hawryluk, and M. L. Schattenburg, in *X-Ray Microscopy*, (Springer Series in Optical Sciences, vol 43), eds. D. Rudolph and G. Schmahl, (Springer-Verlag), Berlin, Heidelberg, 1984.

scanning electron microscope (SEM) micrographs of a completed grating.

The atomic beam system, described elsewhere[3], is a supersonic nozzle beam of sodium in argon carrier gas. Adiabatic expansion of the gas after it leaves the nozzle results in a fairly monochromatic beam; $\Delta v/v = 12\%$ with $v = 10^3$ m/s. The sodium has the same velocity as the carrier gas giving it a de Broglie wavelength (λ_{db}) of 17 pm. The beam is collimated by two 10 μm slits spaced 1 m apart to form a 2 mm × 10 μm ribbon-shaped beam with a divergence of 10 μrad. Individual atoms are detected after surface ionization on a 25 μm-diameter hot wire (Pt/W alloy) located 1.5 m downstream from the second slit. The detector can be moved perpendicularly to the beam in 10 μm (7 μrad in angle) steps to measure the profile of the beam. The resulting angular resolution is ~25 μrad as can be seen in Figure 2a.

Figure 2b shows the profile of the atomic beam diffracted by the grating which is placed ~1 cm on the detector side of the second collimating slit. The positions of the diffracted orders are given by the usual grating equation for small angles, $\theta_n = n\lambda_{db}/d$ where d is the grating period, which gives $\theta_{\pm}$=85 μrad for our standard case. The second order peaks are suppressed because the slit width is half the grating period. The higher orders are lost in the noise (e.g., the intensity of the n = \(+-3 orders should be only 4.5% of n = 0).

In order to increase the separation of the diffracted beams it is possible to lower the velocity of the sodium, and hence increase its de Broglie wavelength, by using a heavier carrier gas. This is because the gas velocity after expansion is inversely proportional to the square root of the mass. It is helpful to use a noble gas in order to suppress the formation of molecules and clusters; we chose xenon. Figure 2c shows the diffraction of the slow beam by the grating. The separation of the first order peaks is 240 μrad, which is 1.5 times the separation for argon carrier gas. This indicates that we did not realize the full slowing predicted by the mass ratio, $\sqrt{m_{Xe}/m_{Ar}} = 1.8$. We presume that this is due to residual argon in the reservoir or to velocity slip of the two components.

The strong intermediate peaks visible in Figure 2c must be caused by a grating aberration with a period twice the fundamental. The deformation responsible is clearly evident in Figure 3. This aberration is only present in isolated regions of the grating; it is caused by uneven tension in the grating membrane. Figure 2d shows the beam seeded with argon diffracted by a region of the grating

with the same aberration. The variation in total signal strength between the data sets is due to long time scale fluctuations in the raw beam intensity.

The diffraction gratings demonstrated here offer significant advantages over existing beam splitters which might be used to construct an atom interferometer. We first present some reasons for our interest in an atom interferometer, followed by a discussion of the relative merits of beam splitters which could be used to build one.

Interferometers measure the difference in phase accumulated by a particle while travelling between two points over different paths. The phase of the quantum mechanical amplitude for a particle to go between two points over a given path is proportional to the classical action for that path. Thus, an interferometer is sensitive to anything that affects the classical action, either changes in relative path length or any interaction (e.g., electromagnetic or gravitational) which changes the energy of the particles. To date matter wave interferometers have been realized for neutrons[39] and electrons[40].

An atom interferometer would allow a number of new experiments in atomic physics such as a measurement of the Casimir atom-wall potential, the phase shift on rotation of bosons, and various manifestations of Berry's phase (e.g., of atoms in spatially varying magnetic fields). Atom interferometers could lead to large improvements in the resolution of certain null searches such as the electron-proton charge difference.

For applications involving measurement of absolute rotation (Sagnac effect), relative translation, or gravitation, atoms appear to be better for matter wave interferometers than either electrons or neutrons. The neutrality of atoms means that they are far less sensitive to stray fields than electrons, allowing the operation of much larger area interferometers. Atoms are more useful than neutrons because they are available (at thermal energies) with 1 to 100 times shorter wavelengths, and are produced by cheap compact sources. More importantly, the detected spectral brightness (particles str^{-1} $time^{-1}$ $area^{-1}$ $v/\Delta v$) of available atomic beam sources is from 10^4 (our source) to 10^6 times brighter than the best neutron

---

[39]H. Maier-Leibnitz und T. Springer, Z. f. Phys. **167**, 368 (1962); The first 'perfect crystal' neutron interferometer reported was: H. Rauch, W. Treimer, and U. Bonse, Phy. Lett. **47A**, 369 (1974).

[40]L. Marton, J. Arol Simson, and J. A. Suddeth, Rev. Sci. Inst. **25**, 1099 (1954).

sources[41]. High fluxes should enable an atomic interferometer to make use of the fringe splitting techniques developed for optical interferometers (e.g., servo to the steepest point on a fringe and measure the error signal). Because the magnitude of the Sagnac effect scales with the rest energy (the energy for a photon) of the particles, the intrinsic sensitivity of atom interferometers to rotations is 10^{10} times greater than that of a geometrically similar laser gyro. It is possible that such a gyro could eventually be used to detect the dragging of inertial frames (Lense Thirring effect) predicted by General Relativity[42].

The key component necessary for an atom interferometer is a coherent beam splitter. Due to the large potential energy of atoms in solids the tunnelling depth of a free atom with thermal energy is less than atomic dimensions; thus, beam splitters based on partial transmission appear impossible. We envisage four types of beam splitters for atoms, all are based on diffraction by periodic media. Two involve reflection: diffraction from the atomic planes of a crystal surface and grazing incidence diffraction from a fabricated surface. The other two are diffraction by transmission through a fabricated structure or through a standing wave of light. All of these methods, except diffraction by a grazing incidence reflection from a fabricated surface, have now been demonstrated.

In addition to a beam splitter, one must be able to achieve sufficient mechanical rigidity, flatness, and alignment of the separate components of an interferometer to observe fringes. The required resistance to relative vibration scales with the de Broglie wavelength and the angle of incidence (the grazing angle θ_{gr} is the complement of the conventional angle of incidence). Specifically, for beam splitters involving a reflection the surface must be flat (over the area of the beam) and mechanically stable (during the detector response time) relative to other surfaces to order $\theta_{gr}\lambda_{db}$ For transmission gratings one requires stability to order $\theta_{gr}d$ (the 'effective' grating period), a less restrictive condition. For some, 'space-invariant' transmission grating interferometers the requirements are even weaker[43]. To build a successful interferometer one wants diffracted angles large enough for a useful separation of the beams, but not so large that the required alignment and stability are too difficult to

---

[41] C. G. Shull, personal communication. The best thermal neutron sources have a brightness of $\sim 10^{14}$ str^{-1} sec^{-1} cm^{-2}

[42] L. E. Stodolsky, Gen. Rel. and Gravitation. **11**, 391 (1979).

[43] B. J. Chang, R. Alferness, and E. N. Leith, Appl. Optics **14**, 1592 (1975).

achieve. With this condition in mind we will now discuss the merits of existing beam splitters.

Although it was not recognized as such, the first atomic beam splitter was demonstrated in 1929[2]; it was the diffraction of atoms from the surface of ionic crystals. Because the interatomic spacing in a crystal surface is of the same order as the de Broglie wavelength of typical atomic beams, the angular separation of the diffracted beams is of order unity (i.e., ~1rad). Constructing an interferometer from these crystal surface beam splitters would be exceptionally challenging because it requires relative flatness and rigidity of separate surfaces to less than atomic dimensions.

In 1983 our group demonstrated the Kapitza-Dirac effect in which atoms are diffracted from a standing wave of near resonant light[3]. The grating period in the standing wave is 1/2 the optical wavelength, thus the angular separation of the diffracted orders is $\lambda_{db}/\lambda_{light}$ which is ~60 μrad for a thermal sodium beam. Interferometers based on this technique have been proposed[44], but the diffracted angles are frustratingly small. In addition, this method is limited to atoms that have accessible laser transitions (frequently requiring optical state preparation of the atoms), which are not the atomic species most suitable for the production of intense atomic beams (e.g. He).

The reflection[45], focusing[46], and diffraction of atoms have been realized using their interaction with intense near-resonant laser light. We believe that it will be fruitful to look for alternative atomic optical elements based on the technology developed for x-ray optics. It should be possible to adopt grazing incidence x-ray mirrors, lenses, and diffraction gratings for use with atom beams. These techniques would be based on the specular reflection of atoms from smooth surfaces, which occurs when the surface roughness is much less than the wavelength corresponding to the momentum of the atom perpendicular to the surface. For example, efficient specular reflection of reactive atoms with thermal velocity at angles θ_{gr} of up to 40 mrad has recently been reported by Haroche et al[47]. A disadvantage of these methods is that they are critically sensitive to

---

[44] V.P. Chebotayev et al., J. Opt. Soc. Am. B **2** (11), 1791 (1985).

[45] V. I. Balykin, V. S. Letokhov, et al., JETP Lett. **45**, 353 (1987); V. I. Balykin, V. S. Letokhov, et al., Phys. Rev. Lett. **60**, 2137 (1988).

[46] J.E. Bjorkholm, R.R. Freeman, A. Ashkin, and D.B. Pearson, Phys. Rev. Lett. **41**, 1361 (1978); V.I. Balykin and V.S. Letokhov, Opt. Com. **64**(2), 151 (1987).

[47] A. Anderson, S. Haroche, E. A. Hinds, W. Jhe, D. Mexchede, and L. Moi, Phys. Rev. A **34**, 3513 (1986).

contamination of the reflecting surface. Another class of x-ray optical elements that could be adapted for use with atoms are based on transmission through microfabricated structures. In addition to the diffraction gratings described in this paper we believe that similar methods could be used to produce zone-plates and eventually wave guide arrays, for atoms.

In conclusion, the transmission diffraction grating reported here has many advantages over a Kapitza-Dirac grating which has been suggested as a beam splitter for an atom interferometer. It has 2/3 the period, will work with any atomic species, and requires neither a frequency stabilized laser nor optical preparation of the atoms. In the near future we hope to achieve diffracted angles more than an order of magnitude larger than are demonstrated here. We expect to do this by halfing the grating period and by using the gratings at grazing incidence. The effective spatial period of the gold foil grating can be varied by changing its orientation with respect to the beam. We expect that it will be possible to reduce the thickness of the gratings so that the ratio of slit depth to separation is 1/10 instead of the current 5/1. This would allow the grating to be used at a grazing angle of ~ 1/5 rad giving a five-fold increase in effective line density and thus in the beam separation. Such a grating would be ideal for the construction of the first atom interferometer.

This work was supported by the National Science Foundation (PHY86-05893).

Figure Captions

Figure 1. SEM micrographs of the completed grating at two different scales. Part A shows the 0.2 μm-period grating overlaid with the 4 μm-period grating. Part B shows the 150×4 μm support grid on a larger scale.

Figure 2. Experimental profile of the Na beam. The y axes are the number of detected atoms, the counting time at each point is ~1 sec. The line through the points is only for visual effect. As explained in the text, part A is the undiffracted beam, and parts B, C, and D show the beam diffracted by transmission through the grating. In C the carrier gas is Xe, in the other cases it is Ar.

Figure 3. SEM micrograph of a portion of the grating that was damaged during mounting.

Figures from “Diffraction of atoms by a transmission grating”

A2) Atom Optics

ATOM OPTICS

David W. Keith and David E. Pritchard

Physics department and Research Laboratory of Electronics
Massachusetts Institute of Technology
Cambridge, M.A. 02139

INTRODUCTION

By atom optics we mean the rich collection of emerging techniques by which atoms may be manipulated in the manner of light in classical optics. Existing atom optical elements include mirrors, lenses, and diffractive optics including beam splitters as well as dissipative elements such as slowers, 'coolers', and traps which have no analogue in classical optics. To date, these atom optical elements have been realized as demonstrations of principal, we hope that we will soon see some of them used as tools in real experiments. We must caution the reader that this paper is intended as a introduction and enticement to atom optics, not as an exhaustive survey. Most of the paper will be devoted to atom

interferometers; first general comments on beam splitters and interferometer geometries, then a detailed look at the one we are currently constructing, and finally a discussion of a few possible experiments with atom interferometers. The final section of the paper will describe an assortment of atom optical elements, concluding with a return to nearer term experimental realities — the need for the rapid development of atom sources that are both slow *and* bright.

ATOM INTERFEROMETERS

Gratings

The key component necessary for the construction of an atom interferometer is a coherent beam splitter. Therefore we will first discuss the available atom beam splitters with special regard to their suitability for constructing an atom interferometer.

Due to the large potential energy of atoms in solids the tunnelling depth of a free atom with thermal energy is less than atomic dimensions; thus, beam splitters based on partial transmission appear impossible. We now list three general classes of beam splitters for atoms.

1) Reflective diffraction gratings. Although it was not perceived as such, the first atomic beam splitter was demonstrated in 1929[48]; it was the diffraction of atoms from the surface of ionic crystals. Because the interatomic spacing in a crystal surface is of the same order as the de Broglie wavelength (λ_{dB}) of typical atomic beams, the angular separation of the diffracted beams is of order unity (i.e. ~1 rad). Atoms may be specularly reflected by surfaces when the de Broglie wavelength corresponding to the momentum perpendicular to the surface is much lager than the surface roughness. It should be possible to use this effect to diffract

[48]I. Estermann and O. Stern, *Z. Physik* **61**, 95 (1930).

atoms by grazing incidence reflection from a high quality laminar grating. We are currently trying to demonstrate this type of atom diffraction grating.

2) Transmission diffraction gratings. In 1983 our group demonstrated the Kapitza-Dirac effect in which atoms are diffracted from a standing wave of near resonant light[49]. The grating period in the standing wave is 1/2 the optical wavelength, thus the angular separation of the diffracted orders is $2\lambda_{dB}/\lambda_{light}$ which is ~60 μrad for a thermal sodium beam. In 1988 we demonstrated the diffraction of atoms by transmission through a fabricated periodic structure[50]. The transmission gratings are arrays of slits with a spatial period of 0.2 μm in a 0.5 μm-thick gold membrane.

3) Conventional beam splitters. If one could make a transmission grating micro structure with a surface sufficiently smooth to reflect atoms incident at some grazing angle while still transmitting atoms through the slits then one would have a near analog to the half silver beam splitter used in conventional optics. Unless the grating period is sufficiently small, such a device will still waste about 1/2 of the flux by scattering atoms into orders other than the desired 0^{th} order reflected and transmitted beams.

Interferometer Geometries

Interferometers have different geometries and properties depending on what class of grating is used. Irrespective of the class of grating used, the poor velocity width of existing atom beam sources ($\Delta v/v \sim 1\text{-}10^{-3}$) force one to design a white fringe interferometer in which an achromatic central fringe is assured by using

---

[49] P. E. Moskowitz, P.L. Gould, S. R. Atlas, and D.E. Pritchard, *Phys. Rev. Lett.* **51**, 370 (1983); P. J. Martin, B. G. Oldaker, A. H. Miklich, and D. E. Pritchard, *Phys. Rev. Lett.* **60**, 515 (1988).

[50] D. W. Keith, M. L. Schattenburg, Henry I. Smith, and D. E. Pritchard, *Phys. Rev. Lett.* **61**, 1580 (1988).

equal path lengths on either side of the interferometer. We now define various quantities needed for the discussion of interferometer properties; the atom de Broglie wavelength (λ_{dB}), the angle of incidence of the atom beam on the grating measured with respect to the grating surface (θ), and the grating period p. The height (h) (measured along the grating lines) and width (w) of the beam are also needed to determine the requirements on flatness and alignment. The various requirements on relative alignment of the gratings are of two types. The first is on the flatness of the gratings and the relative alignment of the grating surfaces, that is the collinearity of the vectors normal to the grating surfaces. The second is the alignment of the grating lines, that is the relative alignment of the gratings with respect to rotations about the surface normals.

For transmission gratings it is well known that an arrangement of three equally spaced gratings has may desirable properties[51]. This (Fig. 1a) is the same geometry as is used for neutron interferometers. This type of interferometer is completely insensitive to the incident angle and is achromatic, all requirements on relative alignment are on the scale of the grating period — independent of , and much smaller than, λ_{dB}. The grating lines must be parallel to $\sim p\sin(\theta)/h$, and the requirement on grating surface alignment expressed as a requirement on $\Delta\theta$ is that $\Delta\theta < p\sin^2(\theta)/w\cos(\theta)$.

[51] B. J. Chang, R. Alferness, and E. N. Leith, *Appl. Optics,* **14**, 1592 (1975). For the specific case of atom interferometers see V.P. Chebotayev et al., *J. Opt. Soc. Am. B* , **2**(11), 1791 (1985).

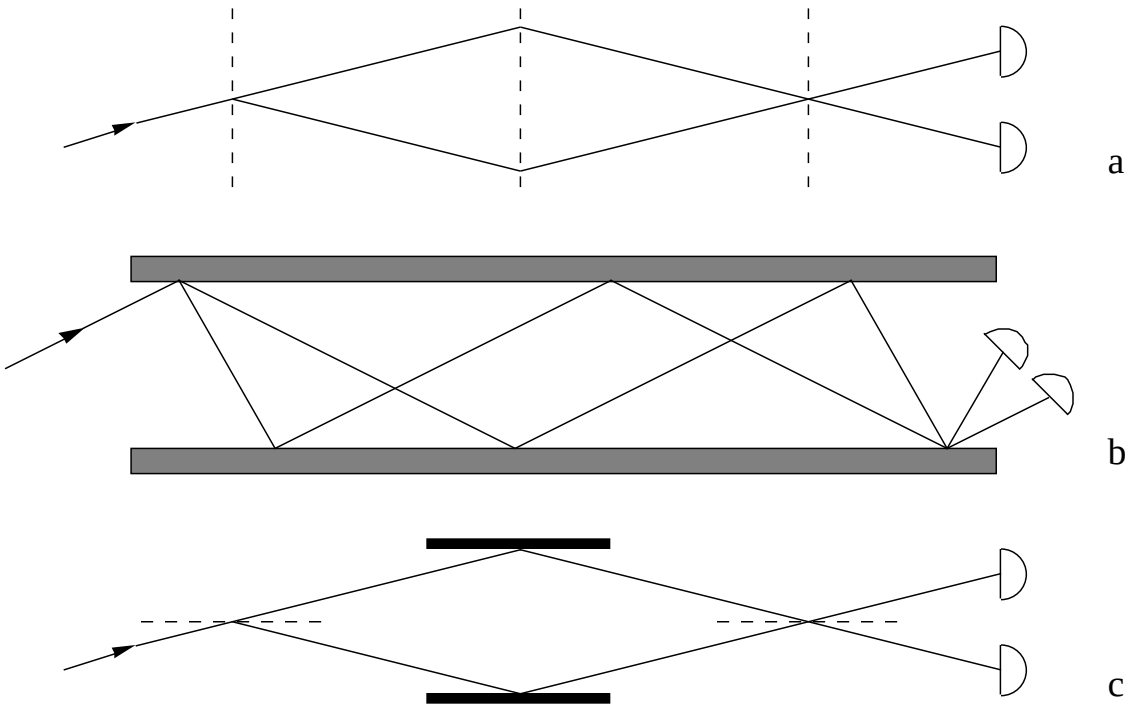

Figure 1: Three different interferometer geometries, transmission gratings (a), reflection gratings (b), and thin reflective gratings (c). In all cases angles are greatly exaggerated and diffracted beams that do not end at one of the detectors are not shown.

For reflection gratings the dependance of the separation of the 0^{th} and 1^{st} order diffracted beams on the angle of the incident beam make it harder to find geometries which are white fringe[52]. Figure 1b shows an example of a white fringe geometry for reflection gratings. The requirement on surface alignment is λ_{dB}/d where d is the larger of h and w. The conditions on line alignment are the same as for transmission gratings, $\sim p\sin(\theta)/h$.

The properties of an atom interferometer made with 'conventional' beam splitters (fig. 1c) are different in several important respects. The requirement on

[52] Steven J. Wark, William A. Hamilton and Goffrey I. Opat, *J. Modern Optics.*, **34**, 1375 (1987); D. E. Pritchard and D. W. Keith, U.S. Patent pending.

grating surface alignment is λ_{dB}/d where d is as above, this is independent of the grating period. There is no requirement on the grating line alignment. Unlike the two previous cases the area of a conventional beam splitter interferometer is independent of λ_{dB}, which is important when one considers using atom interferometers as rotation sensors.

Our Interferometer

We are currently constructing a three transmission grating interferometer for sodium atoms. We now turn to a detailed description of this interferometer with the hope that the problems involved have some general interest. The present (late October 1989) state of this experiment is that all of its components have worked once, and we are hard at work. Our interferometer differs from the design described above only in that the the interference is detected as a spatial variation of particle density at the third grating, rather than by the variation in intensity in two beams with different directions of propagation in the far field. This detection scheme is of course only possible with amplitude gratings, it has the advantage that it requires only 2/3 the length of the separated beam method which gives us 3/2 greater separation of the beams in the interferometer for the fixed length of our beam tube.

The interferometer is built with a grating spacing of 60 cm giving us a 60 μm beam separation at the middle grating. This allows us to completely separate a 30 μm wide beam which would have an intensity of ~10^6 sec^{-1} using our existing apparatus with no gratings in place. A realistic estimate of our anticipated final signal strength may therefor be obtained from the properties of the individual gratings. Attenuation caused by the primary grating and the grating support structure gives an intensity in the 0^{th} order of 1/8 of the incident intensity, and of 1/16 in each of the $\pm 1^{st}$ orders. These factors combine to give an intensity at the

maximum of a fringe after transmission through all three gratings of only 0.005 of the incident intensity. The near field detection scheme limits the theoretical fringe contrast to 4:1, resulting in a final interference signal of ~0.004 of the incident intensity. Thus, the final interference signal through the interferometer is anticipated to be at most ~4×10^3 sec^{-1}: this signal will be reduced by any misalignment of the gratings. This signal greatly exceeds the noise of the detector ~10 sec^{-1}, allowing us in principal to see the fringes with a S/N of ~4 after a 0.01 sec averaging time.

There are a variety of experimental complications not mentioned in this description of our interferometer. We will now discuss the two of these which appear the most problematical and which are likely to be problems in any atom interferometer: vibration isolation and grating alignment.

We begin our discussion of vibration isolation with a review of the vibration problems relevant to our interferometer. There are two requirements, the first is that the three gratings are stationary relative to each other to within ~1/4 period (50 nm) during the time the final grating integrates the intensity at a given position. Thus, the rms amplitude of relative vibrations integrated over all frequencies greater than the reciprocal of the integration time must be less than ~50 nm. The second requirement is on motion of the gratings as a unit due to acceleration of the center of mass of the grating system during the time it takes for the atoms to traverse the interferometer, the motion due to this acceleration must also be less than ~1/4 period. In our interferometer the transit time is 1.3 msec which implies that the rms acceleration below ~900 Hz must be less than 10^{-2} ms^{-2}.

We have attacked our vibration problem using a combination of passive isolation and active feedback. The passive isolation system consists of small pneumatic feet which support the apparatus and act like damped springs with a 2

Hz resonant frequency. This simple isolation system reduced the rms motion due mainly to building noise by an order of magnitude to ~ 0.5 μm. The active feedback system is used to stabilize the relative positions of the three gratings at frequencies below ~150 Hz. This system works best at low frequencies (< 10 Hz) where the passive system is least effective. The reduction of relative motion provided by the active system will allow us to use much longer integration times when we are looking for the interference signal. The active feedback system uses a laser interferometer which has the same transmission grating geometry as the atom interferometer. The gratings for the optical interferometer are mounted on the same three translation stages as the matter wave gratings in order to record the exact relative alignment of the matter wave interferometer. The error signal from the optical interferometer provides a measure of the relative alignment of the three grating platforms, it is applied to a Peazo-electric translator (PZT) through a feedback network in order to stabilize the platforms. Using this system we have reduced the relative rms motion of the gratings from ~1500 to 40 nm.

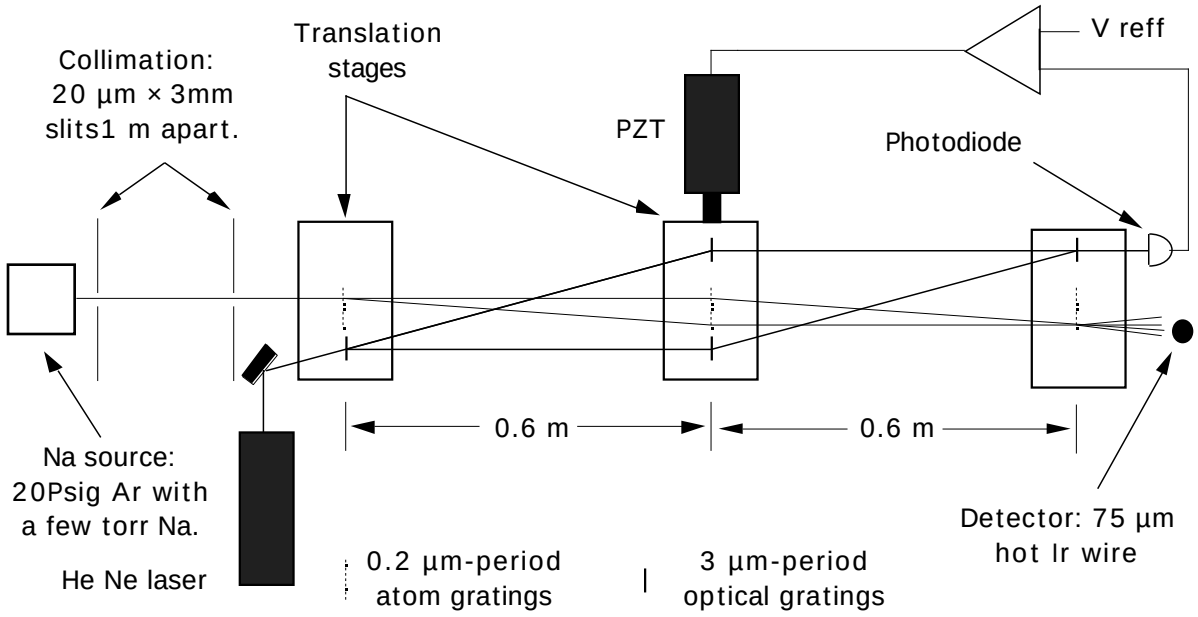

Figure 2: A schematic of our interferometer showing the active vibration isolation system. Not to scale.

In order that all points along the height (3 mm) of our ribbon shaped beam have the same phase of interference signal it is necessary that the gratings be aligned with respect to rotations about the beam axis to an angle of ~10^{-5} rad. We have accomplished this by using a technique based on the optical polarizing properties of the gratings. The 0.2 µm-period grating lines act as wire grid polarizers for light. In principal, it would be possible to align two gratings by rotating them so as to maximize the amount of light transmitted through the pair. This is not practical because the transmitted intensity is proportional to the square of the relative angle between the gratings (for small angles), requiring intensity comparisons to a part in 10^{10}. However, if the polarization of the incident light is modulated about some center angle at frequency f, the amount of light transmitted with modulation frequency 2f, is linearly proportional to the angle

between the grating and the center angle. We have used this technique[53] to align the gratings inside our machine to better than 10^{-4} rad, which will be sufficient for our purposes since we can afford to search through the final range of ~10 possible angles.

ATOM INTERFEROMETER EXPERIMENTS

We expect the atom interferometers will one day prove useful in the study of a number of problems in precision metrology, fundamental quantum mechanics, and atomic physics.

Metrology, especially General Relativity

In principal atom interferometers could be used in the manner of optical interferometers to measure fundamental quantities such as acceleration, length, and angular velocity. In practice, atom interferometers are very unlikely to be useful in the measurement of length or acceleration. This is because their advantages over optical interferometers are only due to the ratio of optical to atom de Broglie wavelength in the case of reflective interferometers (not likely to work for small λ_{db}), or on the ratio of optical wavelength to grating period in the case of diffractive interferometers. In either case these advantages will be outweighed by the superior fringe resolution and response time available from optical interferometers. In the area of basic metrology the promise of atom interferometers is in the sensing of inertial rotations, in this case both the low speed (compared to light) and the short wavelength of atoms are advantageous. The Sagnac effect sensitivity measured in radians of interferometer phase shift per unit of angular rotation frequency is $4\pi mA/h$ for a matter wave interferometer of

[53] E. H. Anderson, A. M. Levine, and M. L. Schattenburg, *Appl. Optics Lett.*, **27**, 3522 (1988).

area A, whereas it is $4\pi A / c\lambda$ for an optical interferometer operating at wavelength λ. For example, in order for rotation at one earth rate $\Omega_e \approx 10^{-5}$ sec^{-1} to cause a shift of one fringe in an interferometer using Xe atoms, it would need to have an enclosed area of 10^{-4} m^2, to achieve the same sensitivity in an interferometer using 0.5 μm light would require an area of 10^6 m^2. Of course, optical interferometers have the advantage that is is easy to fold the beam path so that the light makes many trips around the enclosed area effectively multiplying the sensitivity (and decreasing the frequency response) by the number of round trips. However, even if it were possible to build an optical ring cavity that had decay times equal to the millisecond transit times typical of atom interferometers, it would still be less sensitive by the wavelength ratio. It is worth noting that for interferometers using diffractive beam splitters at small incident angles (the simplest technology), the fact that A λ_{dB} means that the rotation sensitivity of the interferometer is inversely proportional to the atoms velocity; independent of the mass.

The obvious use for such precise rotation sensors is for tests of general relativity such as the search for the relativistic frame drag. The relativistic effects which might be observable with these techniques are as follows[54]: new limits on the preferred frame parameter in the PPN formalism (~$10^{-8}\ \Omega_e$)[55], the velocity dependant frame drag (~$10^{-9}\ \Omega_e$)[56], and the true Lense Thirring effect (~$10^{-10}\ \Omega_e$)[9]. The second two of these effects are most easily measured by comparing an orbiting gyroscope to the position of the fixed stars as measured from a platform fixed to the gyro. The difficulty of measuring the frame drag can be appreciated

---

[54] L. E. Stodolsky, Gen. Rel. and Gravitation. **11**, 391 (1979).

[55] M. O. Scully, M. S. Zubairy, and M. P. Haugan, *Phys. Rev. A*, **24**, 2009 (1981).

[56] C. W. Misner, K. S. Thorne, and J. A. Wheeler, *Gravitation* (Freeman, San Francisco, 1973), p. 1117.

when one considers that Everitt et al at Stanford[57] have been developing an experiment of this type (which employes a magnetically levitated spinning superconducting sphere as the gyro) for the last twenty years.

Fundamental Tests of Quantum Mechanics

Most of the experiments in fundamental quantum mechanics that have been performed using neutron interferometers could be improved by using atom interferometers. This is due both to the range of atomic properties potentially available and to the high brightness of atom sources as compared to neutron sources. We will consider two experiments that have not been performed with neutrons; an atom Hanbury Brown and Twiss experiment and a Berry's phase experiment with electric fields and integer spin particles.

Although not an interferometer in the same sense as described above, a conceptually simple application of atom beam splitters is the possibility of experimentally measuring the atom atom correlation functions in atom beams. The general picture of such experiments is shown is Figure 3, it is closely analogous the the Hanbury Brown and Twiss[58] experiment that measured second order correlations in photon counting. When performed using a 'classical' light source this experiment gives a coincidence rate at t=0 which is twice the rate at $t \rightarrow \pm\infty$. This may be interpreted as photon bunching due to the Bose statistics of the electromagnetic field. There has been much recent interest in this phenomena which has centered around the production of anti-bunched states of the of the electromagnetic field in which the coincidence rate goes to zero at t=0. Correlation experiments with atoms would give access to quantum counting

[57] J. D. Fairbank, B. S. Deaver Jr, C. F. W. Everitt, and P.F. Michelson eds., *Near Zero* (W. H. Freeman and company, New York, 1988) VI.3.

[58] R. Hanbury Brown and R. Q. Twiss, *Nature*, **177**, 27 (1956).

statistics in a fundamentally different regime: unlike photons, atoms are either bosons or fermions and is possible to define a positional wave function for atoms. One expect that given Δt (defined below) small enough the coincidence rate at t=0 will be zero for a beam of fermions and will be twice the rate at $t \rightarrow \pm\infty$ for a beam of Bosons from a thermal source.

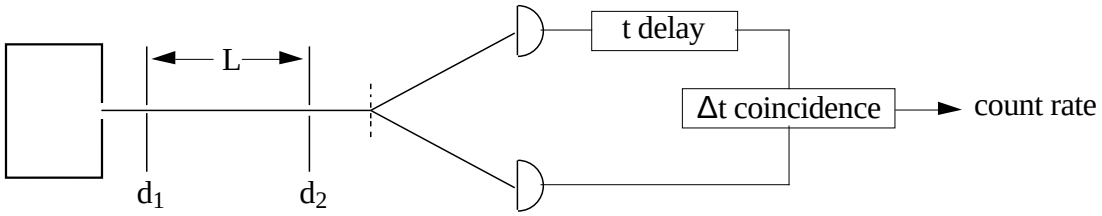

Figure 4. Schematic of an atom Hanbury Brown and Twiss experiment. d_1 and d_2 are the diameters of the collimation pin-holes.

The practical possibility of performing such an atom correlation experiment depends on the expected counting rate. We will calculate the coincidence counting rate as a function of the following beam parameters. At first we will assume that the experimental parameter Δt, the time window within which counts are registered as coincident can be chosen as small as is necessary.

Quantity	Symbol	Typical value
source brightness	B	10^{17}-10^{21} sr^{-1} sec^{-1} cm^{-2}
speed ratio	$s=v/\Delta v$	1-10^{-3}
mass	m	1-100 AMU
mean velocity	v	10^{2}-10^{5} cm sec^{-1}

We want the detectors to sample the same single transverse mode of the atom wave function. Therefore, the second aperture must fit within the diffraction

pattern of the first i.e. $d_2=L\,\lambda_{dB}/d_1$, which implies that the flux through the second slit is given by (ignoring factors of $\pi/4$)

$$f=Bd_1^2\left(\frac{d_2^2}{L^2}\right)=B\lambda_{dB}^2$$

In addition to requiring that the detectors sample the same transverse mode we will also choose Δt to be equal to the atom coherence time τ so that the detectors sample a single longitudinal mode.

$$\tau=\frac{\lambda_{dB}}{v}s$$

If we assume that the counting rate is low, i.e. that the number of counts in Δt is small;

$$f\Delta t=\frac{\lambda_{dB}^3 s}{v}\ll 1$$

then the coincidence rate given by Poisson statistics is

$$f^2\Delta t=\frac{B^2Sh^5}{m^5v^6}\rightarrow\frac{10^{-12}B^2S}{m^5v^6}\ \text{(cgs with m in AMU)}$$

We believe that it will soon become experimentally feasible to measure the effects of atom-atom correlation in beams. An ideal system would be metastable He for which laser slowing techniques and fast detectors are readily available. For example; a laser slowed He^* source with a final velocity of 100 cm sec^{-1} and a brightness of 10^{13} sr^{-1} sec^{-1} cm^{-2} seems experimentally realizable, and would give a coincidence counting rate of 1 Hz. In this case the coherence time is $\tau=10^{-7}$ sec, and one can make Δt equal to (or even less than) τ by counting the He^* directly on electron multipliers.

Atom interferometers are an ideal system in which to investigate the predictions by M. V. Berry[59], Aharonov, and Anandan[60] regarding modifications to the adiabatic theorem. Despite the numerous recent tests of Berry's phase, atom interferometers allow a test of the theory which is novel in several respects. A

---

[59] M. V. Berry, *Proc R. Soc. Lond. A*, **392**, 45 (1984).
[60] Y. Aharonov and J. Anandan, *Phys. Rev. Lett.*, **58**, 1593 (1987).

Berry phase experiment involving the effect of electric fields on Na would be the first such experiment involving non-zero mass bosons and the first where the perturbing field appeared quadratically in the hamiltonian. It should also be possible to test the Aharonov-Anandan geometrical phase in the case of non-adiabatic change.

Atomic Physics

An atom interferometer measures any interaction which differentially affects the energies of particles traveling along separate paths through the interferometer. Thus, atom interferometers could be used to measure such quantities as the electric polarizability or magnetic susceptibility of atomic ground states, or to measure a basic null effect such as the charge neutrality of atoms. In order to determine what problems atom interferometers are most suitable for we must consider the factors which limit the precision of interferometric measurements. The relative precision with which a white fringe interferometer can be used to measure a differential energy shift ΔE is limited by the number of visible fringes, which is approximately given by the speed ratio (S) of the atom beam. The relative precision of energy measurement, $\Delta E/E$ is limited to $\Delta f/S$ where Δf is the fractional accuracy of fringe resolution. If the interferometer is shot noise limited $\Delta f \quad 1/\sqrt{n}$ where n is the total number of atoms counted to determine the phase of the interferometer fringe. These considerations suggest that atom interferometers may be most profitably employed as balance (null) meters i.e., when used to balance the effects of two different interactions applied to opposite sides of the interferometer. For example, an interferometer only slightly more advanced than our first device should be able to measure the ground state polarizability of sodium to $\sim 10^{-2}$ but, its ability to measure the ratio of polarizability to magnetic susceptibility would be limited only by the precision

with which the strength of the individual fields could be controlled — perhaps two orders of magnitude better.

ATOM OPTICAL ELEMENTS

Most of the recent work in atom optics has involved the use of light pressure forces to manipulate the atom beams. Mirrors[61], lenses[62], and gratings for atoms have been demonstrated using the stimulated gradient forces on atoms in near-resonant optical radiation. We will not discuss these developments, instead we will review atom optical elements that do not involve light forces. we ignore light force atom optics both to contain the discussion and because of the obvious advantages of developing atom optical elements that are independent of laser technology. It is interesting to note that all the grating types (except the Kapitza-Dirac effect and the reflection/transmission grating) described above have been realized for neutrons and for X-rays. It is fruitful to look for alternative atomic optical elements based on the technology developed for x-ray optics. It should be possible to adopt grazing incidence x-ray mirrors, lenses, and diffraction gratings for use with atom beams. These techniques are based on the specular reflection of atoms from smooth surfaces, which may occur when the surface roughness is much less than the wavelength corresponding to the momentum of the atom perpendicular to the surface. For example, efficient specular reflection of reactive alkali atoms with thermal velocity at angles of up to 40 mrad has recently been reported by Haroche et al[63]. At least two reflective lenses for atoms have recently been demonstrated. Doak has made a cylindrical lens for a He beam by reflecting

---

[61] V. I. Balykin, V. S. Letokhov, et al., *JETP Lett.* **45**, 353 (1987); V. I. Balykin, V. S. Letokhov, et al., Phys. Rev. Lett. **60**, 2137 (1988).

[62] J.E. Bjorkholm, R.R. Freeman, A. Ashkin, and D.B. Pearson, *Phys. Rev. Lett.* **41**, 1361 (1978); V.I. Balykin and V.S. Letokhov, Opt. Com. **64**(2),151 (1987)

[63] A. Anderson, S. Haroche, E. A. Hinds, W. Jhe, D. Mexchede, and L. Moi, *Phys. Rev. A* , **34**, 3513 (1986).

it off an Au coating on a bowed mica wafer at angles of about 30 degrees[64]. A most favorable system for demonstrating atomic reflection is the reflection of H off of films of He at cryogenic temperatures. Berkhout et al[65] have made a spherical mirror coated with liquid He that focuses an 18 mm diameter beam of H-atoms down to 0.5 mm. Further progress in reflective atom optics is hampered by the deficiency of theoretical or empirical knowledge of the necessary conditions for the reflection of atoms, especially slow atoms, from surfaces.

Another class of x-ray optical elements that could be adapted for use with atoms is based on transmission through micro-fabricated structures. Atom optical elements based on transmission have the advantage that they work for any atomic species independent of surface physics or laser technology. Since our demonstration of transmission diffraction gratings for atoms we have used similar methods[66] to produce 200 nm-period gratings as thin as 5 nm. These gratings can be tilted so as to increase their effective dispersive power, in addition they are a first step towards the reflection/transmission gratings described above. Fabrication methods similar to ours have been used to produce free standing zone-plates which should work as lenses for atom beams.

Slow sources

---

[64] Bruce Doak (AT&T), personal communication.

[65] J. J. Berkhout, O. J. Luiten, I. D. Setija, T. W. Hijmans, T. Mizusaki, and J. T. M. Walraven, *Phys. Rev. Lett.*, **63**, 1689 (1989).

[66] A. M. Hawryluk, N. M. Ceglio, R. H. Price, J. Melngailis, and H. I. Smith, *J. Vac. Sci. Technol.*, **19**(4), 897 (1981); N.M. Ceglio, A.M. Hawryluk, and R.H. Price., Proc. S.P.I.E. **316** *(High Resolution Soft X-ray Optics)*, 134 (1981); E. H. Anderson, C. M. Horwitz, and H. I.Smith, *Appl. Phys. Lett.* , **49**, 874 (1983); H. I. Smith, E. H. Anderson, A. M. Hawryluk, and M. L. Schattenburg, in *X-Ray Microscopy*, (Springer Series in Optical Sciences, vol 43), eds. D. Rudolph and G. Schmahl,
(Springer-Verlag), Berlin, Heidelberg, 1984.

A key barrier to practical use of most of the atom optical devices discussed above is the poor brightness of existing slow atom sources. A number of radiation pressure atom slowers[67] have been demonstrated. They all work by arranging that an atom decelerating in the slower is continually exposed to radiation that is tuned slightly to the red of the atomic resonance and is directed opposite to the atomic velocity. This Doppler tuning condition may be met either by frequency chirping the laser or by Zeeman tuning the atom's resonance. In either case the atoms accumulate random transverse momentum due to the scattering of the incident photons, the rms transverse momentum is proportional to the square root of the number of photons needed to slow the atom times the total change in atom momentum.

The tools necessary to increase the brightness of slowed beams are available, but they have not as yet been assembled into a bright slow source. The simplest way to increase brightness is to apply transverse cooling in the form of 'red molasses' to the atoms emerging from the end of the slower. A more powerful general method for increasing brightness is to first apply transverse cooling followed by a lens (which alone, increases flux but not brightness), followed by a second region of transverse cooling at the focus of the lens. Another possibility would be to replace the cooler-lens-cooler combination with a single two dimensional spontaneous force optical trap. It is clear that there are no theoretical barriers to the development of laser slowed and intensified atom sources — the development of such sources is a worth while challenge for experimentalists in atom optics.The work on beam splitters was funded by the National Science Foundation (PHY86-05893) with help from the Joint Services Electronics Program (DAAL03-86-K-0002) which supports the M.I.T. Submicron Structures

[67] William D. Phillips, John V. Prodan, and Harold J. Metcalf, *JOSA-B*, **2**, 1751 (1985).

Laboratory. Work on the Atom interferometer is supported by O.N.R. (N0001489-J-1207) and A.R.O. (DAA L03-89-K-0082).

A3) An Interferometer for Atoms

An Interferometer For Atoms

David W. Keith, Christopher R. Ekstrom, Quentin A. Turchette,
and David E. Pritchard

Massachusetts Institute of Technology, Cambridge,
Massachusetts 02139

ABSTRACT

We have demonstrated an interferometer for atoms. A three grating geometry is used, in which the interfering beams are distinctly separated in both position and momentum. We used a highly collimated beam of sodium atoms with a de Broglie wavelength of 16 pm and high-quality 0.4 μm-period free-standing gratings which we fabricated using a novel method. The interference signal is 70 cps, which allows us to determine the phase to 0.1 rad in 1 min. Applications of atom interferometers are briefly discussed.

There have been several recent proposals for the realization of an atom interferometer[68], and a number of experiments have demonstrated interference of atoms[69]. In addition to the work reported here, several other groups have recently demonstrated interference fringes for atoms[70]. We report the demonstration of the first interferometer for atoms in the sense that it uses amplitude division to separate the beams in momentum and distinctly separates the beams in space[71]. We note that mater wave interferometers have been previously demonstrated for electrons and neutrons[72]

We used a three grating white fringe geometry in which the phase of the interference fringes is independent of incident wavelength and angle[73]. Such a geometry allows the largest interference signal for a given beam brightness. Figure 1 shows a

---

[68] S. Altshuler and L. M. Frantz, U. S. Patent 3,761,721 (1973); V. P. Chebotayev et al., J. Opt. Soc. Am. B **2**, 1791 (1987); D. W. Keith, D. E. Pritchard, in *New Frontiers in QED and Quantum Optics*, A. O. Barut, ed., (Plenum Press, 1990); Ch. J. Borde, Phys. Lett. A **140**, 10 (1989).

[69] I. Estermann, and O. Stern Z Phys. **61**: 95 (1930); D. W. Keith, M. L. Shattenburg, H. I. Smith, D. E. Pritchard, Phys. Rev. Lett. **61**, 1580 (1988); A. Faulstich, O. Carnal, J. Mlynek, in: Proc. Int. Workshop on Light Induced Kinetic Effects, Elba (Italy), L. Moi et al, eds., (1990).

[70] O. Carnal, J. Mlynek, preceding paper in this Phys. Rev. Lett; F. Riehle, T. Kisters, et al. submitted to Phys. Rev Lett.; S. Chu personal communication.

[71] Devices such as the one presented here in which wave-fronts are divided (using either wave-front or amplitude division), spatially separated, and purposefully recombined (e.g. using reflection or refraction) are universally referred to as interferometers. When all of these conditions are not met, there is a division of opinion. In particular, Young's experiment is not generally classed as an interferometer (e.g. Born and Wolf, *Principals of Optics*, (Pergamon press, sixth ed. 1980), chapter VII).

[72] Neutrons: H. Maier-Leibnitz and T. Springer, Z. Phys. **167**, 368 (1962); The first "perfect-crystal" neutron interferometer reported was by H. Rauch, W. Treimer, and U. Bonse, Phys. Lett. **47A**, 369 (1974); Electrons: L. Marton, J. Arol Simson, and J. A. Suddeth, Phys. Rev. **90**, 490 (1954).

[73] B. J. Chang, R. Alferness, and E. N. Leith, Appl. Opt. **14**, 1592 (1975). Our geometry is identical to that used in a three diffraction grating interferometer for neutrons: M. Gruber, K. Eder, A. Zeilinger, R. Gahler, W. Mampe, Phys. Lett. A **140**, 363 (1989).

schematic of our experiment which we will describe in four parts: the atomic beam system, the gratings, the interferometer system, and the data analysis method.

Our atomic beam system has been considerably improved since it was last described[74]. It is a supersonic nozzle beam of sodium in an argon carrier gas. Adiabatic expansion of the gas after it leaves the nozzle results in a fairly monochromatic beam: $\Delta v/v = 12\%$ with $v = 10^3$ m/s. The sodium has the same velocity as the carrier gas giving it a de Broglie wavelength of 16 pm. The beam is collimated by two 20 μm slits spaced 0.9 m apart to form a 1 mm × 20 μm ribbon-shaped beam with a divergence of 20 μrad. Individual sodium atoms are detected after surface ionization on a 25 μm-diameter hot wire (80% Pt, 20% Ir alloy) located 1.6 m downstream from the second slit. In order to achieve high ionization efficiency it was necessary to expose the wire to oxygen at regular intervals: 10^{-3} torr O_2 for ~1 min every ~30 min proved to be sufficient. Under these conditions the detector's time response was ~15 msec and the average background was ~20 cps. A key problem is that the background signal is dominated by highly non-Poissonian bursts (see example in fig. 3). Although we cannot directly measure the efficiency we believe that it is better than 10%. In any case, greater wire efficiency, combined with improvements to our vacuum system, and the sodium source, now allow us to achieve detected fluxes of >1 MHz through a 1 mm high slit. This corresponds to a detected source brightness of 10^{19} sec^{-1} cm^{-2} str^{-1}.

---

[74] P. L. Gould, MIT PhD thesis; D. W. Keith, M. L. Shattenburg, H. I. Smith, D. E. Pritchard, Phys. Rev. Lett. **61**, 1580 (1988); most recently in: D. W. Keith, MIT PhD thesis.

The quality of gratings necessary for an interferometer is considerably higher than is needed to demonstrate diffraction of atoms. In particular, the gratings must be phase-coherent over their entire area. This implies that the grating lines must be straight to the order of their line width over the full height of the grating. The transmission of each grating support structure (necessary to achieve the required line straightness) should be high since the final interference signal will be proportional to the third power of this transmission. In addition, the grating line to space ratio must be near 1:1; ideally the grating spaces should be 0.65 period for the first grating and 0.5 for the other two.

Our diffraction gratings consist of arrays of slots in a tensile silicon nitride membrane. Several membranes are formed on a 12 × 7 mm Si chip. The gratings we used were made in two sizes; 750 × 40 μm and 500 × 140 μm with periods of 400 and 200 nm. The grating fabrication process, described briefly below, will be detailed elsewhere[75]. First a double polished, <100> Si wafer (250 μm thick) is coated on both sides with 200 nm of low-stress nitride (Si_3N_4) by plasma-enhanced low-pressure chemical vapor deposition. Conventional photolithography is used to pattern the nitride on the back side of the wafer with small rectangles which are aligned to the crystal axis. The Si under these rectangles is etched along the <111> planes using a hot KOH solution, leaving the nitride windows on the front side. The front side of the wafer is then coated with 150 nm of polymethyl methacrylate (PMMA) film and then with 15 nm of Au.

---

[75] D. W. Keith and M. J. Rooks, forthcoming in: J. Vac. Sci. Technol. (Nov/Dec 1991)

Electron-beam lithography is used to expose the grating patterns in the PMMA. We used a JEOL JBX 5DII(U) e-beam writer, and took care to minimize the effects of field stitching. The Au is needed to reduce charging of the substrate which can cause writing distortions. The exposed PMMA and the Au are then removed leaving a direct mask for reactive-ion etching (RIE) of the nitride. It was necessary to develop a highly directional RIE process, which was able to selectively etch nitride using PMMA as a mask. By this method we have made high-quality 200 and 400 nm-period gratings; figure 2 shows a completed example.

The interferometer consists of three 400 nm-period gratings mounted 0.663±0.003 m apart on separate translation stages inside the vacuum envelope. During operation, the 0^{th} and 1^{st} order beams from the first grating strike the middle grating (which is 140 μm wide) where they are diffracted in the 1^{st} and -1^{st} orders so that they converge at the third grating. At the second (middle) grating the beams have widths of 30 μm (FWHM) and are separated by 27 μm. The first two gratings form an interference pattern in the plane of the third grating, which acts as a mask to sample this pattern. The detector, located 0.30 m beyond the third grating, records the flux transmitted by the third grating.

In order to observe stable fringes, various requirements on mechanical stability and alignment must be met. These requirements are a consequence of the sensitivity of the interferometer to the rotation, acceleration and translation of the gratings. We now describe these problems, and our solutions to them.

The gratings must be aligned with respect to rotations about the beam axis to angular tolerance given by the beam height over the period (10^{-3} rad). We aligned the gratings by using the 4 μm-period support structures as diffraction gratings for a Helium-Neon laser. Our grating fabrication method ensures that the support structure grating is orthogonal to the primary fine-period grating to an accuracy equal to the line straightness of either grating. The primary limitation of this technique is that the grating windows are only 40 μm wide, so that the diffracted laser spots have an angular width of 10^{-2} rad. In practice we were able to achieve alignment to about 2×10^{-3} rad. The final grating alignment is performed while the experiment is operating, by rotating the middle grating so as to maximize the interferometer fringe contrast.

The interferometer is sensitive to accelerations of the three gratings as a unit. The sensitivity in radians per unit of acceleration is given by $2\pi l^2/v^2p$ where l is the distance between gratings, v the atom's velocity, and p the grating period. In our interferometer this is 13 rad m^{-1} sec^2, which can be understood as the phase change due to the translation of the gratings during the atoms 1.3 msec transit through the interferometer. Rotation of the interferometer about the axis perpendicular to its enclosed area causes a phase shift (the Sagnac effect) proportional to the rotational velocity which is given by $4\pi l^2/pv$. In our interferometer this sensitivity is 1.4×10^4 sec. Thus, rotation at one earth rate produces a phase shift of one radian. In addition to the phase shifts caused by motion of the three gratings as a unit, the interferometer is sensitive to the relative position of the gratings. In order to observe any fringe contrast, it is necessary

that the relative positions of the three gratings be stationary to within ~1/4 period (100 nm) during the time the final grating samples the fringe pattern.

We have solved these problems using a combination of passive isolation and active feedback. The passive isolation system consists of small rubber feet which support the apparatus. This simple isolation system reduced the rms motion, due mainly to building noise, by an order of magnitude to ~ 0.5 μm. It is difficult to improve this further by using more sophisticated pneumatic supports because such systems have unacceptably high levels of low-frequency rotational noise. The active feedback system uses a laser interferometer which has the same transmission grating geometry as the atom interferometer. The 3.3 μm-period gratings for the optical interferometer are mounted on the same three translation stages as the matter wave gratings in order to record the relative alignment of the matter wave interferometer. The error signal from the optical interferometer measures the relative alignment of the three grating platforms; it is applied to a piezo-electric translator (PZT) through a feedback network in order to stabilize the platforms. Using this system we have reduced the relative rms motion of the gratings from ~500 to 40 nm. The active feedback system is used to stabilize the relative positions of the three gratings at frequencies below ~100 Hz. This system works best at low frequencies (< 10 Hz) where the passive system is least effective. The reduction of relative motion provided by the active system allows us to use long integration times when we are looking for the interference signal.

The data necessary to determine the interferometer phase and fringe contrast is acquired as follows. A triangle wave at ~0.2 Hz is applied to the reference port of the optical interferometer feedback network with the amplitude of the reference wave chosen so that the optical interferometer is driven through 1/3 of an optical fringe. The raw signal from the optical interferometer is then recorded simultaneously with the signal from the atom counting electronics. Both signals are sampled at 10 msec intervals for a total time of ~2 min.

The data are then analyzed by first calculating the optical interferometer's relative position from the measured intensity, the optical fringe limits, and the known 3.3 μm-period of the gratings. Figure 3 shows an example of these data. Next, the data obscured by noise spikes from the hot wire are discarded (typically about 2% of the total samples). This is done automatically, without reference to the position information. Finally, the atom count data are summed into bins according to the position at which they were taken and the result is then divided by the time spent taking samples at that position. Figure 4 shows the measured interference signal.

We have performed extensive numerical simulations of this experiment. The simulations were two dimensional with a transverse resolution of 1 nm, and included an incoherent sum over source points with the experimentally measured velocity distribution. The calculated contrast in this configuration is 25%; our measured contrast is 13%. We ascribe the discrepancy to a number of small effects including grating imperfections and creep in the alignment PZT.

The peak to peak amplitude of our interference signal is 70 cps, which enables us to determine the interferometer phase to a precision of 0.1 rad in 1 min. The large low-frequency gain of our position stabilization system provides measured atom-interferometer phase drift of less than 0.1 rad over 10 min.

In the near future we plan to insert a septum between the beams of our interferometer. If needed, we can increase the beam separation by using 0.2 μm-period gratings and by using Xenon as a carrier gas in our source. We should then be able to make accurate measurements of the Aharonov-Casher[76] phase, and the polarizability of sodium.

Atom interferometers may also be used for tests of basic quantum mechanics and perhaps for tests of general relativity[77].

We would like to thank Mike Rooks and other staff at the National Nanofabrication Facility. Bruce Oldaker and Garth Zeglin provided valuable technical assistance during the early phases of this work. We gratefully acknowledge funding from: ONR contract N0014-89-J-1207, ARO contract DAAL03-89-K-0082, and JSEP contract DAAL03-89-C-0001.

[76] Y. Aharonov, A. Casher, Phys. Rev. Lett. 53, 319 (1984).
[77] L. E. Stodolsky, Gen. Rel. and Gravitation **11**, 391(1979)

Figure captions

Figure 1. (thesis Fig. 3.1) A schematic of our interferometer showing the active vibration isolation system. Not to scale. The 0.4 μm-period atom gratings are indicated by a vertical dashed line, the 3.3 μm-period optical gratings by a vertical solid line.

Figure 2 (left half of thesis Fig. 2.3) A Scanning Electron Micrograph of a completed 200 nm-period grating.

Figure 3. (thesis Fig. 3.9) Ten seconds of raw data. The upper graph shows the relative transverse position of the interferometer gratings as measured by the optical interferometer. The lower graph shows the number of atoms per 10 msec bin. Peak heights of the off-scale hot wire noise bursts are 92 and 304 counts respectively.

Figure 4. (thesis Fig. 3.10) Interference signal from 400 seconds of data (~23 seconds per point). Background hot wire noise of 40 cps subtracted. The solid line is a least square fit to a sine function with 400 nm period. Error bars are one standard deviation assuming Poissonian noise, and slightly underestimate the noise because of the super-Poissonian character of the hot wire background.

A4) Free-standing gratings and lenses for atom optics (abstract)